FUNCTIONAL GENOMIC STUDIES TO IDENTIFY THERAPEUTIC TARGETS IN CLONAL HEMATOPOIESIS

by

Michael Robert Waarts

A dissertation

Presented to the Faculty of Louis V. Gerstner, Jr.

Graduate School of Biomedical Sciences,

Memorial Sloan Kettering Cancer Center

in Partial Fulfillment of the Requirements of the Degree of

Doctor of Philosophy

New York, NY

September 2024

_____ _____

Ross L. Levine, MD Date
Dissertation Mentor

DEDICATION

I would like to dedicate this thesis to my parents, Orli and Robert Waarts, for their unconditional support, and for inspiring me to pursue a career in science.

ABSTRACT

Clonal hematopoiesis (CH) is a common premalignant state in the blood and confers an increased risk of blood cancers and all-cause mortality. Genomic studies have identified the chromatin modifiers *DNMT3A*, *TET2*, *ASXL1*, and *IDH2* as recurrently mutated in CH and these same mutations occur in acute myeloid leukemia (AML) at high variant allele frequencies, suggestive of their roles as leukemia initiating mutations[1-4]. While prior murine and human studies have demonstrated that CH mutations induce functional changes in hematopoietic stem and progenitor cells (HSPCs) including an increase in self-renewal activity, the specific mechanisms underlying these alterations have not been delineated[5-10]. Moreover, genotype-specific therapies for *DNMT3A*, *TET2*, and *ASXL1* mutations have not been reported in CH or AML. While IDH2 inhibitors are used clinically in AML, they are unable to induce durable responses in the vast majority of patients with *IDH2*-mutant disease and their efficacy in CH has not been demonstrated[11]. Given the broad prevalence and risk of malignant transformation associated with CH, there is an unmet need to identify novel therapies that can suppress clonal expansion and prevent evolution to malignancy.

The lack of an *ex vivo* platform for culturing primary genetically defined murine hematopoietic stem and progenitor cells (HSPCs) has proved a significant technical challenge preventing the application of unbiased screens to identify therapeutic targets. Recently, approaches that enable long-term *ex vivo* maintenance of HSPCs have been reported, including co-culture of HSPCs with bone marrow endothelial cells[12]. In Chapter Two, we utilize this system to establish a platform to study CH that yields rapid *ex vivo*

phenotypes of HSPCs with CH-associated mutations. We then apply this system for genetic/chemical perturbation studies and for unbiased high-throughput screens. We identify a catalogue of genetic vulnerabilities in wild-type HSPCs and in HSPCs harboring mutations in the four genes most recurrently mutated in CH.

Next, in Chapter Three, we investigated the function and mechanism of the *KDM3* histone lysine demethylase family members, which we found were strong dependencies in *IDH2*- and *TET2*-mutant HSPCs. Our data suggest that the *KDM3B* mutation cooperates with the *IDH2* mutation to rewire the epigenome and downstream transcriptome. Specifically, we observed that *KDM3B* loss in mutant cells led to decreased expression of critical cytokine receptors upstream of JAK/STAT signaling that are dysregulated in CH-mutant HSPCs, rendering mutant HSPCs preferentially susceptible to inhibition of downstream JAK2 signaling. Altogether, these findings nominate an epigenetic regulator and an epigenetically regulated receptor signaling pathway as genotype-specific therapeutic targets and provide a scalable platform to identify genetic dependencies in mutant HSPCs.

BIOGRAPHICAL SKETCH

Michael Waarts was born and raised in California before attending the University of Chicago for his undergraduate studies, where he graduated with degrees in Biology, Chemistry, and Biochemistry. During his time at the University of Chicago, Michael was part of the biology research honors program, under the mentorship of Dr. Stephen Kron. He wrote his undergraduate dissertation on work done under the mentorship of Dr. Jill de Jong investigating the genetic underpinnings of cancer stem cells in a zebrafish model of leukemia. Upon graduating, Michael began his PhD training at the Louis V. Gerstner, Jr. Graduate School of Biomedical Sciences at Memorial Sloan Kettering Cancer Center, where he worked under the mentorship of Dr. Ross Levine.

ACKNOWLEDGEMENTS

Most importantly, I would like to thank my mentor, Dr. Ross Levine, for his unwavering support throughout my PhD. I am very grateful for his constant presence and mentorship at every stage of this process. I am also thankful that he established a knowledgeable, supportive, and friendly laboratory that is such an excellent training environment. My experience in his laboratory during this transformative time has provided with me with fundamental lessons that I will bring into my future career. The work presented in this thesis is only made possible by his support.

I would like to thank my thesis committee, Drs. Omar Abdel-Wahab and Michael Kharas for their invaluable feedback and guidance. Their expertise in stem cells and hematological malignancies has been very important, and their continued support has allowed a timely completion of this dissertation.

The Levine lab has been a highly energetic and motivating environment to pursue graduate school, and I am thankful to each of the fantastic lab members over the past five years who have made this a very enjoyable time both in and out of the lab. In particular, I would like to thank Drs. Xiaodi Wu, Aaron Stonestrom, Robert Bowman, Sheng Cai, and Linde Miles for taking the time to provide me with both hands-on experimental training and insightful feedback on the work presented in this thesis. I am also grateful to my fellow graduate students, Rebecca Gelfer, Ines Fernandez-Maestre, and Troy Robinson for taking this journey with me. Finally, I would also like to thank Anthony Benitez-Martinez, Young Park, Isabelle Cseste, and Shoron Mowla for their critical technical support for the work presented in this thesis.

Lastly, I would like to thank the Gerstner Sloan Kettering Graduate School administration team, including Ken Marians, Michael Overholtzer, Linda Burnley, Thomas Magaldi, David McDonough, Stacy De La Cruz, and Julie Mason for going above and beyond to ensure that the PhD students had everything they needed to be successful. I am also thankful to all the past and present GSK students for enabling such a friendly and supportive community. A particular thank you to my fellow classmate Chi Nguyen for your love and support.

TABLE OF CONTENTS

LIST OF TABLES

LIST OF FIGURES

LIST OF ABBREVIATIONS

2-HG	2-hydroxygluturate
5-hmC	5-hydroxymethylcytosine
5-mC	5-methylcytosine
α-KG	Alpha-ketogluturate
ADCC	Antibody dependent cellular cytotoxicity
AML	Acute myeloid leukemia
ATAC	Assay for transposable accessibility of chromatin
BC	Breast cancer
BMEC	Bone marrow endothelial cell
CCUS	Clonal cytopenia of unknown significance
CH	Clonal hematopoiesis
CML	Chronic myeloid leukemia
CVD	Cardiovascular disease
DSB	Double-stranded break
GMP	Granulocyte-macrophage progenitor
HSPC	Hematopoietic stem and progenitor cell
KD	Knockdown
LSK	$Lineage^{-}Sca^{+}cKit^{+}$

LT-HSC	Long-term hematopoietic stem cell
mAb	Monoclonal antibody
MDS	Myelodysplastic syndrome
MEP	Megakaryocyte-erythroid progenitor
MOI	Multiplicity of infection
MPN	Myeloproliferative neoplasm
NGS	Next generation sequencing
NSCLC	Non-small cell lung cancer
PAR	Poly(ADP-ribose)
PRC2	Polycomb repressive complex 2
PROTAC	Proteolysis targeting chimera
RNP	Ribonucleoprotein
RTK	Receptor tyrosine kinase
sgRNA	Single guide RNA
ssGSEA	Single sample gene set enrichment analysis
tdT	tdTomato
TKI	Tyrosine kinase inhibitor
VAF	Variant allele frequency

CHAPTER ONE

INTRODUCTION*

Targeted therapies have come to play an increasingly important role in cancer therapy over the past two decades, in part due to advances in sequencing that have greatly improved our understanding of the genetic drivers present in individual tumors. Different classes of genetic drivers have been identified, including mutations/alterations affecting kinases, downstream signaling effectors, tumor suppressors, and chromatin modifiers. In light of these discoveries, different strategies and modalities for the development of targeted therapies have been explored. More recently, the presence and significance of premalignant conditions, including clonal hematopoiesis in the blood, have also been appreciated. An enhanced understanding of clonal hematopoiesis and its clinical consequences has initiated a search for targeted therapies in this indication. In turn, the application of targeted therapies in clonal hematopoiesis has been informed by the successes and challenges with regards to the prior development of targeted therapies against targets in cancer.

* Waarts, M.R., Stonestrom, A.J., Park, Y.C., Levine, R.L. (2022). Targeting mutations in cancer. JCI 132 (8)

Development of targeted therapies in cancer

Advances in the classical cancer treatment modalities of standard cytotoxic chemotherapy, radiotherapy, and surgery have led to reductions in cancer mortality rates over the last several decades; however, major challenges remain that often lead to tumor recurrence and death. These challenges have led to the exploration of mutation-targeted therapies for cancer. While standard chemotherapy uses cytotoxic agents that kill rapidly dividing malignant and normal cells, targeted therapies act on abnormal proteins encoded by mutated genes. Since normal cells lack the tumorigenic mutations that are exploited for drug targeting, there is often high differential sensitivity of malignant and nonmalignant cells to targeted therapies. As a result, targeted therapy frequently produces rapid and dramatic tumor regression while limiting the potential for off-target toxicities that are a hallmark of conventional chemotherapy. The overall drug discovery strategy for cancer has thus shifted away from cytotoxic agents and toward the identification of tumor-specific actionable mutations and the development of molecularly targeted agents.

Progress in targeted therapies is closely tied to technological advancements in sequencing made over the past two decades, including the revolutionary development of massively paralleled next-generation sequencing (NGS)[13]. The discovery of both common and rare genetic aberrations has launched research investigations into targeted therapies against resultant mutant proteins and exploration of downstream aberrant molecular signaling pathways that can be therapeutically exploited[14]. Additionally, NGS has proved critical to the clinical application of targeted therapies. Mutational evaluation by sequential oligonucleotide capture, amplification, and NGS has become a standard-of-care diagnostic tool in many cancers[15,16]. These tests are used to identify

actionable genetic mutations that are then used for selection of an appropriate targeted therapy, for prognostication, or as biomarkers for other clinical endpoints.

The discovery of the *BCR-ABL* fusion gene as the hallmark of chronic myelogenous leukemia (CML) and the development of the BCR-ABL inhibitor imatinib marked a pivotal moment in drug development. Since then, numerous targeted therapies have been approved by the US FDA, with many more agents under investigation (**Figure 1.1**). Oncogenic gene mutations may be druggable in several different ways: (a) they can encode a protein that can be targeted in a manner distinct from the WT protein; (b) they can cause abnormal activation of a protein (e.g., through a gain-of-function mutation or amplification) that is druggable but for which mutant-specific targeting has not been achieved; or (c) they can create novel molecular dependencies that are druggable ("actionable mutations"). Examples of truly druggable mutations in the first category are far less common than druggable mutations in the second category. However, excellent therapeutic indices are still achieved for many overactivated or amplified targets due to increased target expression and/or a high level of cancer-specific dependence on a specific protein. Additionally, other mutations that are not yet amenable to targeted therapy approaches are still useful as biomarkers that support selection of another appropriate therapy. Targetable genetic aberrations occur in a range of genes encoding kinases and their downstream signaling effectors, tumor suppressors, and chromatin modifiers (**Table 1.1**).

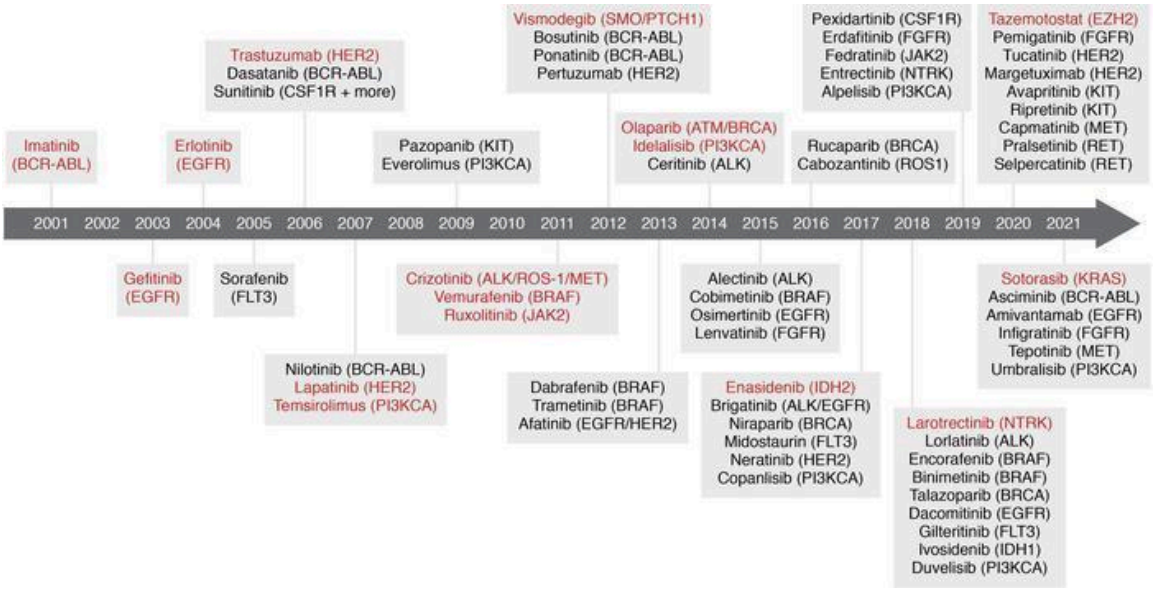

Figure 1.1: Timeline of FDA-approved targeted therapies in cancer. FDA-approved molecules with mutation-specific indications are depicted along with their associated mutation-specific indications. First-in-class molecules for novel targets are shown in red.

Table 1. Genetic indications for targeted therapy in cancer

Mutated gene	Common genetic alterations	Tumors implicated	Drugs
ALK	Mutation, fusion	Non–small cell lung cancer	Alectinib, brigatinib, ceritinib, crizotinib, lorlatinib
ATM	Mutation	Breast	Olaparib
BCR-ABL	Fusion	Chronic lymphocytic leukemia, acute lymphocytic leukemia	Bosutinib, dasatanib, imatinib, nilotinib, ponatinib, asciminib
BRAF	Mutation	Melanoma, colorectal, hairy cell leukemia, thyroid	Dabrafenib, encorafenib, vemurafenib, binimetinib, cobimetinib, trametinib
BRCA1/2	Mutation	Breast, ovarian, prostate	Olaparib, niraparib, rucaparib, talazoparib
CHEK2	Mutation	Breast, ovarian	Olaparib
CSF1R	Mutation, fusion	Giant cell tumor	Pexidartinib, sunitinib[A]
EGFR	Mutation, fusion, amplification	Non–small cell lung cancer	Afatinib, dacomitinib, erlotinib, gefitinib, osimertinib, brigatinib[A], amivantamab
ERBB2/3/4	Amplification, mutation	Breast	Afatinib[A], lapatinib, neratinib, tucatinib, trastuzumab[B], pertuzumab[B], margetuximab
EZH2	Mutation	Lymphoma	Tazemetostat
FGFR1/2/3	Mutation, fusion	Cholangiocarcinoma	Erdafitinib, lenvatinib[A], pemigatinib, infigratinib
FLT3	Mutation	Myeloid leukemia	Gilteritinib, midostaurin, sorafenib[A]
IDH1/2	Mutation	Myeloid leukemia, cholangiocarcinoma, glioblastoma	Ivosidenib, enasidenib
JAK2	Mutation	Myeloproliferative syndrome	Fedratinib, ruxolitinib
KIT	Mutation, fusion	Gastrointestinal stromal tumor, mastocytosis, melanoma	Avapritinib, imatinib, pazopanib[A], pexidartinib[A], ripretinib, sorafenib, nilotinib[A], sunitinib
KRAS	Mutation	Non–small cell lung cancer	Sotorasib
MET	Mutation, fusion	Non–small cell lung cancer	Cabozantinib[A], capmatinib, crizotinib[A], tepotinib
NTRK	Fusion	Many solid tumors at low frequency	Larotrectinib, entrectinib
PDGFRA/B	Mutation, fusion	Gastrointestinal stromal tumor, mastocytosis, hypereosinophilic syndrome	Avapritinib, imatinib[A], sorafenib[A], sunitinib[A], lenvatinib[A], pazopanib[A], ripretinib[A]
PIK3CA	Mutation	Breast	Umbralisib[A], duvelisib[A], idelalisib[A], copanlisib[A], alpelisib, temsirolimus[A], everolimus[A]
PML-RARA	Fusion	Myeloid leukemia	Arsenic trioxide, retinoic acid
RET	Mutation, fusion	Renal, thyroid, non–small cell lung cancer	Pralsetinib, selpercatinib, cabozantinib[A]
ROS1	Fusion	Non–small cell lung cancer	Entrectinib, crizotinib
SMO/PTCH1	Mutation	Medulloblastoma, basal cell carcinoma	Vismodegib

[A]Mutation-specific treatment supported by National Comprehensive Cancer Network guidelines that does not have full FDA approval. [B]Base antibody used alone or as antibody-drug conjugate.

Table 1.1: Genetic indications for targeted therapy in cancer

Targeting mutations in tyrosine kinases

Following the success of imatinib, there has been an enormous amount of interest in targeting other mutated kinases. As developments in sequencing have added to the number of candidate targets, parallel progress in chemical approaches has expanded the number of targets considered druggable. Kinases can be divided into two general types: tyrosine kinases, which act primarily as growth factor receptors or in direct interaction with growth factor receptors, and serine/threonine kinases, which respond to a range of cellular cues, including signaling downstream of tyrosine kinases. Kinase inhibitors may act through any of multiple mechanisms, including by competition for ATP in the ATP-binding pocket of the kinase in either active (type I) or inactive (type II) conformation, allosteric inhibition of kinase activity (types III and IV) through binding of other regions of the kinase, and/or other mechanisms (**Figure 1.2**)[17,18]. For tyrosine kinases, in addition to chemical inhibitors, monoclonal antibodies (mAbs) targeting the extracellular domains have emerged as a promising therapeutic approach[19,20].

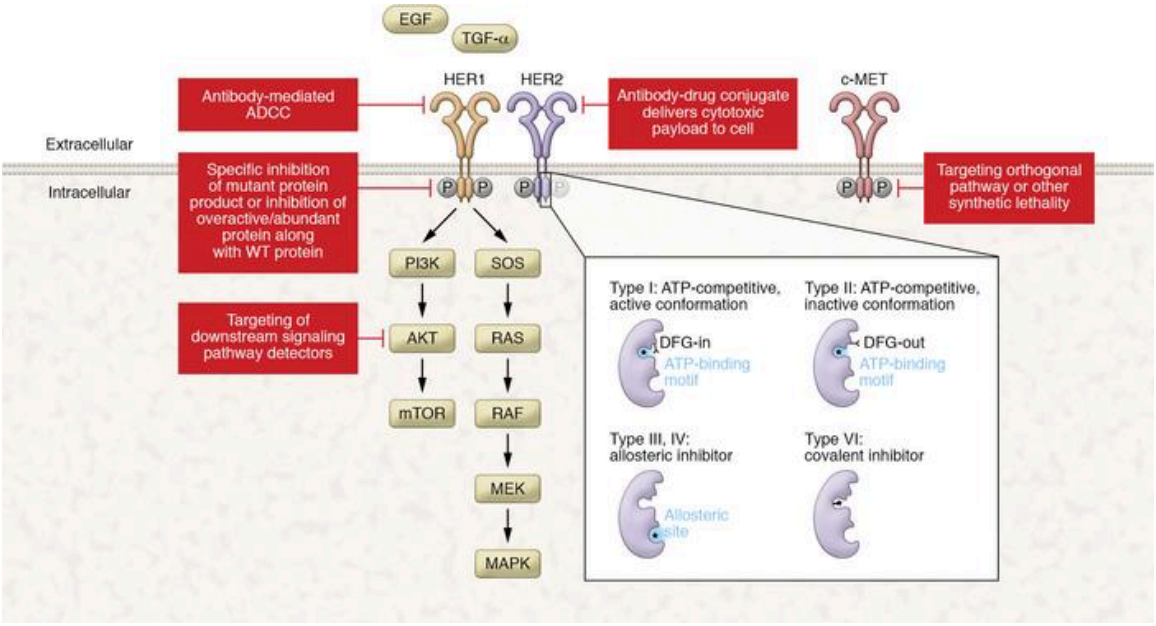

Figure 1.2: Targeting modalities for targeted therapies in cancer. Common modes of druggability associated with clinically approved molecules are depicted using the HER1/HER2 RTKs as examples. FDA-approved targeted therapies include small-molecule inhibitors and mAbs. Small-molecule inhibitors are commonly classified on the basis of the mechanism by which they bind their targets (inset). Small-molecule inhibitors in cancer can directly inhibit a mutant protein product, inhibit an overactive/overabundant protein product along with WT protein, or inhibit a signaling effector downstream of a mutated protein. In addition to inhibitors, mAbs are approved either with or without the addition of a drug conjugate, which, besides activating antibody-dependent cellular cytotoxicity (ADCC), also delivers cytotoxic payloads to targeted cells. DFG, aspartate-phenylalanine-glycine motif.

In 2001, the tyrosine kinase inhibitor (TKI) imatinib became the first FDA-approved targeted therapy for a known genetic alteration. Imatinib's initial approval was for CML, characterized by the presence of the Philadelphia chromosome, a molecular juxtaposition of the tyrosine kinase *ABL1* on chromosome 9 to *BCR* on chromosome 22[21]. The resultant fusion gene encodes an oncoprotein that is capable of autophosphorylation and constitutive activation of downstream signaling pathways including PI3K/AKT/mTOR, MAPK, and JAK/STAT, leading to unrestrained cell proliferation[22,23]. Before the development of imatinib, the 10-year survival rate of the approximately 90% of patients presenting with chronic-phase CML was less than 50%. Extraordinarily, treatment with imatinib increased the 10-year survival rate to approximately 80%[24,25]. Despite its success, two challenges with imatinib are resistance and side effects. Resistance occurs through several mechanisms, most commonly due to mutations in the kinase domain of BCR-ABL[26-28]. These mutations may develop while patients are on imatinib but may also be present in the CML prior to the start of treatment and may be selected for by insufficient drug levels[29]. To overcome resistance, next-generation kinase inhibitors with increased inhibitory activity toward BCR-ABL have been developed. Nilotinib, dasatinib, bosutinib, and ponatinib compete in the same

ATP-binding pocket as imatinib but with higher affinity and are able to overcome many resistance mutations[30-33]. More recently, the allosteric inhibitor asciminib has also been approved[34]. Because asciminib does not bind in the ATP-binding pocket of BCR-ABL but instead binds in the myristylation pocket that is responsible for maintaining the kinase in the autoinhibited state, asciminib is expected to overcome nearly all known resistance mutations[35]. Additionally, because the binding site of asciminib is entirely distinct from that of other BCR-ABL–targeted TKIs, combination targeting of BCR-ABL activity is possible and may prevent the acquisition of resistance[36]. Despite excellent efficacy, TKI therapy is generally given lifelong, as it appears that CML stem cells can persist at low levels in the presence of therapy, possibly due to quiescence or activation of other signaling pathways[37]. Side effects of CML therapy are common and have particularly detrimental effects on quality of life given lifelong treatment.

Drugs targeting the EGF/human EGFR (HER) family of receptor tyrosine kinases (RTKs) were the second large group of targeted therapies to be approved by the FDA. Under normal physiologic conditions, ligand binding to the extracellular domains of HER RTKs causes dimerization of receptors leading to autophosphorylation within the intracellular tyrosine kinase domains and consequent activation of downstream effectors[38]. Mutations of HER family members result in constitutive downstream pathway signaling and are found across a spectrum of cancers; the most common mutations include *EGFR*/*HER1* activating mutations in non–small cell lung cancer (NSCLC) and *HER2* amplifications/activating mutations in breast cancer (BC)[14]. Both EGFR and HER2 TKIs have been developed; TKIs against the latter are less widely used but have clinical efficacy in specific settings and are reviewed elsewhere[39]. Early-generation

EGFR inhibitors block both mutant and WT EGFR signaling reversibly (gefitinib/erlotinib) or irreversibly (afatinib/dacomitinib)[40-43]. Patients treated with these drugs often have dramatic initial responses to therapy but develop resistance mutations including T790M and experience side effects due to inhibition of WT EGFR. The development of the covalent EGFR inhibitor osimertinib represented a major step forward due to increased relative affinity for mutant EGFR over WT and retention of efficacy against the T790M mutation[44,45]. Nevertheless, resistance eventually occurs in all patients with stage IV *EGFR*-mutant NSCLC. While a subset of resistance occurs through mutations at osimertinib's reactive cysteine target C797, it is also common for resistance to occur through mechanisms that do not depend on specific mutations, such as histologic small cell transformation (**Figure 1.3**)[46,47].

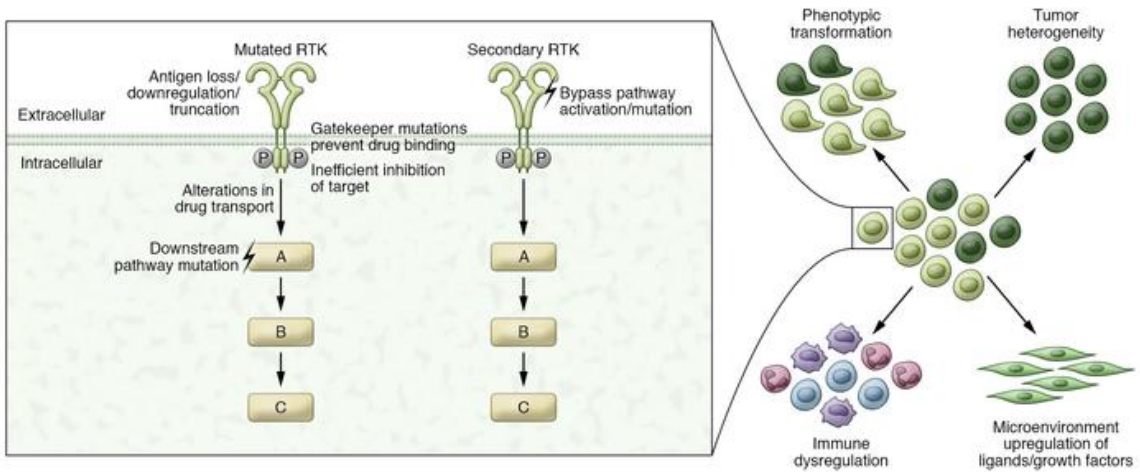

Figure 1.3: Mechanisms of resistance to targeted therapies against kinases in cancer. In response to kinase inhibitors, mutations in the kinase domain that prevent drug binding to the target are the most frequent resistant mechanisms. Other mechanisms of resistance to kinase inhibition include alterations in drug transport or metabolism and mutations in either downstream pathway effectors or alternative signaling pathway effectors. Resistance also occurs with mAbs targeting kinases, with loss/downregulation/truncation of the targeted antigen being the most common. Resistance mechanisms that affect both small-molecule inhibitors and mAbs are also common and include phenotypic transformation, tumor heterogeneity, immune dysregulation, and microenvironmental upregulation of ligands/growth factors.

Targeting HER family members with mAbs is another attractive therapeutic option. mAbs bind to the juxtamembrane portion of the extracellular domain of RTKs and act through multiple mechanisms, including antibody-dependent cellular cytotoxicity (ADCC), RTK internalization/degradation, and inhibition of RTK dimerization[19,20]. The first clinically approved HER2-targeting mAb, trastuzumab, has exceptional activity in HER2-positive BC[48]. Pertuzumab is another HER2 mAb that targets a different site on HER2 and is able to disrupt ligand-induced dimerization of HER2, thus also inhibiting its receptor partner HER3[49]. Since the binding sites of trastuzumab and pertuzumab are distinct, these agents are often combined to maximize efficacy[50]. A third HER2-targeting mAb, margetuximab, has improved ability to recruit effector immune cells and may retain efficacy after resistance to other mAbs has developed[51]. HER2-targeted antibody-drug conjugates that deliver cytotoxic payloads have also been developed, including trastuzumab-emtansine, trastuzumab-deruxtecan, and trastuzumab-duocarmazine[52]. EGFR mAbs, including cetuximab, panitumumab, and necitumumab, have shown limited activity in NSCLC but have specific indications in the treatment of colorectal cancer and squamous cell carcinoma of the head and neck[53]. Finally, bivalent mAbs targeting two oncogenic drivers are a further therapeutic strategy, and recently the bivalent mAb amivantamab targeting EGFR and MET has been approved for NSCLC[54]. While mAbs have proved clinically effective, many patients ultimately develop resistance to these agents due to immune-mediated escape from ADCC, intrinsic alterations in the RTK extracellular domain, and activation of alternative signaling pathways[55-58].

Targeting of mutations in *FGFR*/*PDGFR*/*VEGFR* family members is another area that has generated considerable clinical interest and has led to FDA approval of over a dozen drugs. Genetic aberrations in *FGFR1/2/3* occur in more than 10% of breast, bladder, and endometrial cancers as well as at lower frequencies in other tumors[14]. Mechanistically, activation of the FGFR/PDGFR/VEGFR pathways occurs through a process similar to that of activation of the HER RTKs, and mutations in these pathways likewise act to cause constitutive activation of the mutated RTK[59]. The primary and most well-studied downstream effect of FGFR/PDGFR/VEGFR signaling is increased angiogenesis. Most inhibitors against this class of RTKs to date have activity against all three RTK families and are more frequently used in a mutation-agnostic practice to limit angiogenesis rather than being employed for mutation-specific cancers[60]. While effective in certain contexts, these multikinase inhibitors have overall achieved modest clinical results, for multiple reasons including insufficient target inhibition and increased toxicity owing to multikinase inhibition. FGFR-specific inhibitors, including erdafitinib, infigratinib, and pemigatinib, have been developed more recently but have also generated limited responses[61-63]. The presence of an *FGFR* alteration alone is likely not sufficient for patient selection, since only a minority of patients with *FGFR* alterations respond to TKIs and a subset of *FGFR*-WT patients also respond. Preliminary data from clinical trials indicate that FGFR expression levels may be a superior predictor of response, and the development of further biomarkers will likely be necessary to guide patient selection[64]. *FGFR*-mutant tumors may also have other as-yet unidentified alterations that prevent addiction to FGFR, and it is also possible that even the existing specific

FGFR-targeting therapies may not be sufficiently potent and specific to elicit mutant-specific responses[65].

Overall, targeting mutations in tyrosine kinases has been a fruitful therapeutic strategy: BCR-ABL inhibitors have transformed treatment of CML, and both mAbs and TKIs are standard-of-care for *EGFR*-mutant NSCLC and HER2-positive BC. A variety of other TKIs (**Table 1.1**) also now play important roles in the treatment of cancers with *JAK2* and *FLT3* mutations in hematologic malignancies and *ALK*, *MET*, *NTRK*, *RET*, and *ROS1* mutations in multiple solid tumors. Both primary and acquired resistance remains a challenge in targeted therapy, with most patients experiencing disease progression. Common themes of resistance are generally at play with TKIs and include mutations within the tyrosine kinase domain of the targeted protein that prevent drug binding, mutations in downstream signaling effectors, activation of alternative signaling pathways, and histologic transformation (**Figure 1.3**). A further challenge has been to dissect the mechanisms of multi-targeted kinase inhibitors in particular tumors. Kinase inhibitors vary in their specificity and potency, with early inhibitors being mostly multi-targeted and more recent inhibitors having increased specificity and potency against single targets; however, no kinase inhibitor is completely specific, and the physiologic action is multikinase inhibition at least to some extent. Multikinase inhibitors have shown efficacy in certain contexts, and the lack of specificity has indeed facilitated their clinical use against multiple targets, but it has often been difficult to understand the specific target(s) responsible for therapeutic benefit, making the improvement of these inhibitors challenging. Considerable research is necessary to

understand the precise mechanisms of TKI response and resistance and to guide the development of the next generation of inhibitors.

Targeting mutations in downstream signaling effectors

Tyrosine kinases relay signaling from extracellular ligands to downstream signaling effectors. These effectors predominantly include serine/threonine kinases but also include other important proteins such as RAS. As highlighted in examples above, mutations in numerous tyrosine kinases are able to hijack downstream signaling pathways to drive oncogenesis. In addition, mutations in downstream signaling effectors themselves are also common in cancer. For mutations in serine/threonine kinases, similar therapeutic strategies to those used to target tyrosine kinases have been developed, with the exception that mAb approaches are only effective against kinases with extracellular domains. For mutations in non-kinase effectors, such as RAS, other targeting strategies have been explored. In addition to specifically targeting cancers defined by mutations in these effectors, inhibitors against these central pathways have also been used across a variety of genetically unselected tumors, with varying success.

Members of the MAPK signaling pathway are frequently mutated in cancer and include the *RAS* GTPases and the *RAF*/*MEK*/*ERK* serine/threonine kinases[66]. RAS is a plasma membrane–localized GTPase that cycles between its GDP-bound inactive state and its GTP-bound active state. In response to ligand binding, RTKs undergo autophosphorylation of sites that serve to recruit and activate RAS. RAS then initiates a signaling cascade whereby RAF, MEK1/2, and ERK1/2 are in turn phosphorylated and activated. ERK1/2 then translocates to the nucleus to phosphorylate a range of substrates,

leading to changes in gene expression and cellular functions. Gain-of-function mutations in *A/B/C-RAF*, *MEK1/2*, and *RAS* are all common in cancer[14]. Of the serine/threonine kinases, mutations in *BRAF* are the most common and in the majority of cases affect the V600 residue, producing a mutant BRAF protein that is able to constitutively signal as a monomer independently of RAS[67]. Sorafenib, a multikinase inhibitor, was the first RAF inhibitor investigated but had limited clinical activity, likely owing to a weak affinity for BRAF at clinically achievable concentrations[68,69]. The more recent RAF inhibitors vemurafenib, dabrafenib, and encorafenib have higher potency and are able to inhibit signaling by the monomeric V600E-mutant BRAF protein[70-72]. However, RAF inhibitors cause cutaneous lesions in many patients as a result of paradoxical increases in RAF activity and MAPK signaling in normal skin[73-75]. Addition of MEK inhibitors to RAF inhibitor therapy simultaneously abrogates this side effect while increasing MAPK suppression and prolonging responses in melanoma[76-78]. However, in some tumors, even with combined RAF/MEK inhibition, resistance occurs with sustained dependence on MAPK signaling, indicating that combination therapy may still be ineffective at achieving full inhibition[79]. In addition to mutations in *A/B/C-RAF*, mutations in *MEK1/2* also occur but are not sensitive to current MEK inhibitors, which are allosteric inhibitors that bind to a pocket adjacent to the catalytic site of MEK[80].

The *RAS* family genes *NRAS*, *KRAS*, and *HRAS* are among the most commonly mutated oncogenes in many different cancers[14]. Until recently, RAS itself has largely been viewed as “undruggable” since RAS lacks a hydrophobic druggable pocket and binds its ligand GTP at extremely high affinity[81,82]. Historically, efforts to target *RAS* mutations have focused on preventing RAS localization to the plasma

membrane. In order to be targeted to the plasma membrane, RAS must undergo several modifications, including prenylation by FTase or GGTase. FTase inhibitors have been tested extensively in clinical trials but have largely failed in *KRAS*/*NRAS*-mutant tumors because of compensatory modification by GGTases[83,84]. However, for *HRAS* mutations, the FTase inhibitor tipifarnib has shown promise and has been granted FDA breakthrough designation[85]. Recently, the attention has shifted toward directly targeting RAS-mutant proteins. Mutations in *RAS* largely occur at the positions G12, G13, and Q61, and the resultant mutant proteins vary in their rates of intrinsic GTP hydrolysis and nucleotide exchange. Of these mutants, the $KRAS^{G12C}$ mutation has proved amenable to targeting because of its relatively normal rate of GTP hydrolysis and the presence of a reactive cysteine residue[86,87]. Allosteric inhibitors, including sotorasib and adagrasib, have been developed that bind in a pocket specific to the GDP-inactive state, stabilizing it and preventing activation of RAS[88-90]. While effective, the durability of KRAS G12C inhibitors is generally short-lived. Resistance occurs through activation of RTKs and mutations in other *RAS* isoforms[91]. Targeting of other *RAS* mutations, including those in *HRAS* and *NRAS*, has thus far remained elusive owing to their high rates of GTP hydrolysis and lack of cysteine residues, although several recent studies have suggested novel targeting strategies[92].

The PI3K/AKT/mTOR pathway is another central signaling pathway in cancer whose effectors are frequently mutated. Under normal physiology, ligand binding to RTKs leads to PI3K targeting to the cytoplasmic domains of RTKs and consequent activation of the catalytic subunit of PI3K[93]. PI3K then phosphorylates the plasma membrane lipid substrate PIP2 to form PIP3, which recruits AKT, facilitating its

activation. AKT then phosphorylates and activates a host of downstream regulators, including the metabolic receptor mTOR. The PI3K/AKT/mTOR pathway is negatively regulated by PTEN, a phosphatase that dephosphorylates PIP3. Activating mutations and amplifications in *PI3K*, *AKT*, and *mTOR* are common, along with inactivating mutations in *PTEN*[14]. Inhibitors of PI3K have been most widely used, and FDA-approved drugs include idelalisib, copanlisib, duvelisib, umbralisib, and alpelisib[94-99]. Of these, only alpelisib is used for mutation-specific targeting (*PI3KCA*-mutant BC). Alpelisib was tested in a phase III clinical trial for advanced BC in patient populations with and without *PI3KCA* mutations and was found to be effective only in patients with a *PI3KCA* mutation[98]. However, other PI3K inhibitors have mutation-agnostic anticancer activity[94,95]. AKT inhibitors have not yet been approved by the FDA, but capivasertib has shown promise in phase II clinical trials, a benefit dependent on the presence of a mutation in *PI3K*/*AKT*/*mTOR*[100]. mTOR inhibitors, including everolimus and temsirolimus, have been FDA approved for a variety of indications, but none selective for a genetically defined patient population[101]. Despite several clinical trials, response to mTOR inhibition has not been shown to correlate with the presence of any specific pathway mutations[102,103].

Many serine/threonine kinase inhibitors have shown limited clinical efficacy, and the stratification of patients based on tumor genetics has proved complicated. Why subsets of patients with or without specific pathway mutations either respond or do not respond to the indicated targeted therapies remains unclear, and more research will be necessary to elucidate this. Nevertheless, success stories exist, such as with RAF and MEK inhibitors for BRAF V600–mutant tumors and the recent development of KRAS

G12C inhibitors. Moreover, the range of mutant effector proteins that have been drugged is expanding, and in addition to inhibitors of BRAF V600E and KRAS G12C, advances in chemistry have spurred the development of small molecules targeting other *RAF* and *RAS* mutations. As with TKIs, resistance similarly occurs through multiple mechanisms, many of which are poorly understood. Combination therapy, as successfully illustrated by dual BRAF/MEK inhibition, by targeting of two or more effectors in either the same or an orthogonal signaling pathway will likely be an important strategy in treating and preventing resistance. The combination of targeted therapies with standard chemotherapy has also been explored (e.g., trastuzumab and chemotherapy) and may be beneficial in certain contexts, although careful therapy selection will be required to avoid toxicities.

Targeting mutations in tumor suppressors

Tumor suppressors are among the most common genes mutated in cancer, but targeting them is particularly challenging, because functional restoration of a mutant protein product is generally more difficult than its inhibition. Nevertheless, some clinical success has been achieved. To date, FDA-approved targeted therapies for mutations in tumor suppressors have been designed to exploit synthetic lethality conferred by these mutations. Other therapeutic strategies are also being explored, although most remain in early-stage clinical trials.

Mutations in *BRCA1/2* are common, predominantly in breast and ovarian cancers, and provide an example of success in developing a molecularly targeted therapy for a mutation in a tumor suppressor. BRCA1 and BRCA2 are involved in maintaining genome

integrity by the repair of double-strand breaks (DSBs) through homologous recombination (HR)[104]. Mutations in *BRCA1/2* have been shown to confer sensitivity to PARP inhibitors[105]. PARP1 is a DNA damage sensor that binds to single-stranded DNA breaks and synthesizes poly(ADP-ribose) (PAR) chains on itself and target proteins in the vicinity of the DNA breaks, resulting in the recruitment of additional DNA repair effectors. PARP inhibitors compete with the PARP1 cofactor NAD^+, inhibiting PARP catalytic activity, "trapping" PARP on damaged DNA, and resulting in replication fork stalling and DSBs. In an HR-competent cell, HR proteins including BRCA1/2 are then recruited for DNA repair. However, *BRCA1/2*-mutant cells turn to error-prone, nonhomologous end joining, resulting in genome fragmentation and cell death. Numerous PARP inhibitors show substantial clinical efficacy, including olaparib, niraparib, rucaparib, talazoparib, and veliparib[106-110]. Interestingly, clinical benefit from PARP inhibition appears to be derived from PARP "trapping" on DNA rather than inhibition of catalytic activity[111,112]. Additionally, certain patients without *BRCA1/2* mutations respond to PARP inhibition, including at least some patients with mutations in other HR-related genes (e.g., *RAD51*, *PALB2*)[113-115]. Further biomarkers that predict response are necessary; in this regard, HR signature panels, which identify aberrations resulting from genomic instability, have shown promise[116,117]. Finally, although PARP inhibitors are clinically effective, resistance invariably occurs through multiple mechanisms, including mutations that decrease PARP trapping, restoration of HR pathway activity, and replication fork protection preventing fork collapse[118-121].

The tumor suppressor *TP53* is the most commonly mutated gene in cancer. Around 90% of *TP53* mutations are missense mutations occurring preferentially in the

DNA binding domain of the protein and result in loss of function and/or gain of function depending on the specific mutation and context[122]. The majority of *TP53* missense mutations alter the conformation of the p53 protein and result in its unfolding. Thus, efforts have been made to identify small molecules that can stabilize the native p53 conformation and thus restore p53 functionality[123,124]. APR-246, which has made it furthest in clinical trials, is a prodrug that is converted to electrophilic decomposition products that form covalent bonds with two cysteine residues in p53, resulting in thermostabilization of the mutant protein that favors the WT p53 conformation[125]. In preclinical models and early clinical trials, APR-246 was able to restore proper p53 DNA binding and activation of apoptosis[126-128]. However, although initially showing promising clinical efficacy, APR-246 failed to meet its primary endpoint in a recent phase III trial. This may have been due at least partially to patient selection, as this trial included patients with any of the multitude of *TP53* mutations rather than a more selected subset of patients with mutations for which a benefit may have been more likely. Other strategies are also being explored to target *TP53* mutations, including using oncolytic viruses able to replicate only in cells without p53 activity, reversing p53 gain-of-function signaling, exploiting synthetic dependencies, and developing vaccines for *TP53* mutant–specific neoantigens[129]. Unfortunately, no clinically approved drug targeting *TP53* mutations yet exists.

Targeting tumor suppressors remains challenging. Although synthetic dependencies conferred by mutations in tumor suppressors have been identified and targeted, this strategy has proved difficult for the majority of tumor suppressors. Further

research will be necessary to fully elucidate possible targetable synthetic dependencies and to develop alternative approaches for targeting mutations in tumor suppressors.

Targeting mutations in chromatin modifiers

Finally, targeting mutations in chromatin modifiers has in recent years emerged as a viable therapeutic strategy. Mutations in chromatin modifiers themselves are common in several cancers, and other signatures of epigenetic dysregulation, such as changes in DNA methylation and histone modifications, are pervasive across a variety of cancers. The first FDA-approved drugs indicated for mutations that as a direct consequence cause chromatin alterations were for mutations in the core metabolic enzymes *IDH1* and *IDH2*. The IDH1/2 isoforms are responsible for catalyzing the reversible oxidative decarboxylation of isocitrate to α-ketoglutarate (αKG), producing NADPH as a by-product. Mutations in *IDH1/2* occur frequently in acute myeloid leukemia (AML) and gliomas and are neomorphic mutations that lead to the aberrant production of 2-hydroxyglutarate (2-HG) while consuming NADPH[130]. Since 2-HG shares structural similarities to αKG, 2-HG is able to inhibit up to about 70 αKG-dependent enzymes, including the TET family of dioxygenases responsible for DNA demethylation[131]. *IDH1/2* mutations are mutually exclusive with *TET* mutations, and both are associated with DNA hypermethylation, indicating possible convergence upon a common oncogenic pathway[132,133]. *IDH1/2* mutations also likely simultaneously act through other oncogenic mechanisms including through inhibition of other αKG-dependent chromatin modifiers, reprogramming of cellular metabolism, and accumulation of ROS[134]. Inhibitors of both IDH1 and IDH2 have been developed. The

IDH1 inhibitor ivosidenib competes with the cofactor Mg^{++} to prevent active site formation, and the IDH2 inhibitor enasidenib binds and stabilizes the inactive form of the enzyme to prevent catalysis[135,136]. Both inhibitors are able to reduce 2-HG concentrations in the plasma by more than 90%, leading to decreased methylation, terminal differentiation, and cell death of *IDH*-mutant cancer cells[137]. Despite considerable activity in AML, the clinical setting in which they are most commonly used, long-term responses are rare[138,139]. Resistance invariably occurs involving IDH isoform switching or mutations in the IDH dimer interface, preventing drug binding[140,141]. In gliomas, frequent *IDH1/2* mutations are also observed but progress is even more limited, possibly owing to insufficient CNS penetration, an irreversible epigenetic landscape, or lack of tumor addiction to *IDH1/2* mutations[142]. To overcome some of these challenges, development of CNS-penetrant dual IDH inhibitors, including vorasidenib, which is currently in phase III trials, is an important objective[143].

Mutations in the histone methyltransferase *EZH2* have also been successfully targeted. EZH2 is the catalytic subunit of polycomb repressive complex 2 (PRC2), which is responsible for trimethylation of H3K27, a mediator of transcriptional silencing. Gain-of-function mutations in *EZH2* are common in B cell lymphomas, and loss-of-function mutations are frequent in other hematologic malignancies, indicating context-dependent roles for EZH2[144]. In B cell lymphomas, EZH2 is highly expressed and is required to maintain germinal center formation and prevent plasma cell differentiation[145]. *EZH2* gain-of-function mutations cause increased H3K27me3 at target genes, which leads to repression of cell cycle checkpoint genes and genes required for plasma cell differentiation, resulting in a transcriptional profile favoring proliferation and

self-renewal[146]. The EZH2 inhibitor tazemetostat inhibits EZH2 through competition with its cofactor *S*-adenosyl-L-methionine and is able to restore proper differentiation and induce apoptosis[147,148]. Interestingly, while tazemetostat shows the highest clinical efficacy in *EZH2*-mutant disease, it also provides some benefit in a subset of *EZH2*-WT lymphomas[149]. It is likely that these *EZH2*-WT tumors harbor other genetic or epigenetic alterations that sensitize to EZH2 inhibition and/or that EZH2 dependency is "inherited" by lymphoma cells derived from the germinal center, as has been suggested[150].

Targeted therapies against specific mutations in chromatin modifiers are beginning to see clinical success, and it is likely that this class of agents will expand over the next few years. A range of mutations in chromatin modifiers exist in cancer, particularly in hematologic malignancies, and many of these may have potential as drug targets. While mutations in chromatin modifiers are believed to be closely linked to tumor onset and progression, their exact roles in these processes will require future research to dissect. For example, while *IDH1/2* mutations are common early alterations in gliomas, some research suggests that these mutations switch from driver to passenger mutations as disease progresses, potentially explaining observed resistance to IDH inhibitors[142]. Likewise in AML, mutations in chromatin modifiers, including in *DNMT3A*, *TET2*, and *ASXL1*, are frequent early mutations, but their roles in disease maintenance, and thus whether they would represent therapeutic targets, remain unclear[4]. Moreover, the difficulty in assessing the unknown role of targeting early versus late mutations is exemplified by mutations in chromatin modifiers but is not restricted to this class alone and will require future research to address.

In sum, mutation-specific targeted therapies have demonstrated enormous success over the past two decades and remain an exciting area of research. The next decade will likely see an increase in the number of mutated genes in cancer considered druggable. The development of KRAS G12C inhibitors represents an example whereby a mutation previously considered "undruggable" can be targeted with novel chemistry. Developments in targeted therapies for *TP53* mutations, though they have not yet resulted in an FDA-approved drug, represent another area where creative strategies may be employed. Other strategies and chemical approaches are under investigation for a range of other targets. For example, proteolysis-targeting chimeras (PROTACs) allow targeting of a protein via conjugation of the protein's ligand to an E3 ubiquitin ligase, resulting in proteasome-mediated degradation of the target protein[151,152]. This approach greatly expands the types of proteins that can be targeted as, unlike with traditional small-molecule inhibitors, there is no need to block a specific catalytic or otherwise critical site. Other mutation-specific targeted therapy strategies, including cancer vaccines, are also in early-stage clinical trials[153].

Clonal hematopoiesis as an opportunity for targeted therapies

While the application of targeted therapies has thus far been confined to the treatment of overt malignancies, their use in cancer prevention to intercept premalignant conditions or other precursor states presents a significant opportunity. A variety of precancerous states have now been identified in a number of tissues, including the blood, skin, colon, and esophagus[154-159]. The frequency and penetrance of these precursor states vary based on the tissue type and cell of origin. In the blood, this state is the most readily accessible and as such one of the most well studied, and is known as clonal

hematopoiesis (CH), defined by the outgrowth of a genetically distinct subpopulation(s) of hematopoietic cells[154,155,160]. CH is highly associated with age and occurs frequently in elderly individuals, affecting more than 20% of individuals over the age of 60. CH is now well established to confer an increased risk of blood cancers including AML, believed to be due to the malignant transformation of CH-mutant clones. Additionally, large population-based studies have now demonstrated a clear link between the presence of CH and an increase in all-cause mortality[161]. This link has been shown to be at least partially attributable to a causative increase in cardiovascular disease (CVD), but also likely reflects an increase in the frequency of many other aging-associated diseases[162]. As such, CH presents a potential opportunity for the introduction of targeted therapies to prevent the malignant transformation and mitigate the comorbidities associated with CH.

The genomic landscape of CH is now well-defined and CH-associated mutations are known to be largely restricted to a small set of genes encoding chromatin modifiers, with ~80% of all CH-associated mutations occurring in *DNMT3A*, *TET2*, *ASXL1*, and *IDH1/2*. A smaller percentage of CH is accounted for by mutations in DNA damage associated genes (e.g. TP53, PPM1D), splicing factors (e.g. SF3B1, SRSF2, U2AF1, ZRSR2), and other rarer alterations[154]. Mutations in CH-associated genes are also typically found at high variant allele frequencies (VAF) in AML, consistent with their presumed roles as initiating mutations in this disease[4]. CH-associated mutations also occur in other myeloid malignancies including myelodysplastic syndrome (MDS) and myeloproliferative neoplasm (MPN) and CH may be an antecedent state to these malignancies as well[14].

Significant research has attempted to identify the mechanisms whereby these mutations in CH-associated genes enable clonal expansion. For mutations in DNA damage associated genes, mechanisms have been well defined, and it is understood that these mutations allow clonal outgrowth under the selection pressure of cytotoxic drugs owing to the ability of cells with these mutations to enter the cell cycle in the presence of DNA damage[163-165]. However, the mechanisms by which mutations in the more frequent CH-associated genes lead to CH have been poorly defined. For chromatin modifiers, prior human and murine studies have demonstrated that mutations in the encoding genes result in alterations in hematopoietic stem and progenitor cells (HSPCs) including an increase in self-renewal activity and a resultant expansion in this population[5,8,9,132,166]. Given the biological role of these enzymes, it is presumed that epigenetic changes secondary to these mutations result in transcriptional effects that mediate this increase in self-renewal and clonal expansion. However, the responsible epigenetic changes and consequent transcriptional effects have largely not been identified and why mutations in these chromatin modifiers lead to CH has yet to be defined.

The development of targeted therapies for CH-associated mutations is a significant endeavor that remains nascent. Genotype-specific therapies for mutations in the top three recurrently mutated genes *DNMT3A*, *TET2*, and *ASXL1* are lacking and have yet to show success in clinical trials. As exemplified above, while IDH1/2 inhibitors are clinically approved in AML, they are unable to induce durable responses in the vast majority of AML patients and have not been credentialed for use in CH[135,138,139,167]. IDH1/2 inhibitors are now being tested in a phase I/II clinical trial enrolling patients with *IDH1/2*-mutant clonal cytopenia of unknown significance (CCUS), a subset of CH that is

characterized by unexplained alterations in hematologic parameters (NCT05102370 and NCT05030441). Results on the first patients in this trial demonstrated resolution of aberrant blood cell counts, suggesting that targeting this precursor state may indeed present a potential intervention opportunity (unpublished data). Additionally, a phase I trial is currently underway accruing patients with *TET2*-mutant CH to receive treatment with ascorbic acid (vitamin C), based on preclinical studies establishing the ability of ascorbic acid supplementation in enhancing the residual function of TET proteins in TET2-mutant cells (NCT03418038). Preliminary results have not demonstrated any effect of this treatment on clonal expansion or transformation, suggesting additional targeted therapies may be necessary within this patient population[168]. Other potential targets for CH-associated genes have been suggested from preclinical studies but have yet to be clinically explored.

Progress on the identification of genotype-specific targets in CH has been limited by the lack of high-fidelity experimental systems capable of enabling unbiased screens for target identification. As discussed below, *in vivo* models of CH are not conducive to high-throughput screening and *ex vivo* systems to study CH are limited and have not yet been applied in unbiased screening. Additionally, since *DNMT3A*, *TET2*, and *ASXL1* are believed to function as tumor suppressor genes in CH and AML, there are substantial challenges in the development of targeted therapies for patients with mutations in these genes, as described above. As such, the identification of genes encoding synthetic lethal proteins for this class of mutations is a priority. The recent successes in developing targeted therapies against chromatin modifiers as highlighted above also suggest the opportunity to target synthetic lethal chromatin modifiers in this prevalent class of CH.

Introduction to the thesis

CH has now been well documented to be a clinically significant entity, with implications in hematological malignancy, cardiovascular disease, and other aging-associated diseases. The past decade has seen a wave of genomic research that has identified the most commonly recurring mutations in CH and there is also compelling data demonstrating that these mutations are early initiating mutations in AML. Preclinical studies, largely using murine models, have provided insights into the underlying mechanisms mediating pathogenesis in this precursor state. However, there are no targeted therapies available for patients with CH and the identification of such therapies in this indication remains challenging.

In my thesis, I have established an *ex vivo* co-culture system to study CH and adopted this system to systematically apply scalable unbiased functional genomic screens to facilitate target identification in CH. Chapter Two provides an overview of the development and key uses of this platform for perturbation and unbiased screening in primary, genetically defined HSPCs with and without CH-associated mutations. Chapter Three expands on the function and mechanism of a novel target identified in a common subset of CH and AML. Altogether, these findings identify an epigenetic target and epigenetically regulated signaling pathway as tractable vulnerabilities in a subset of CH and provide a platform for continued target identification in CH.

CHAPTER TWO *

DEVELOPMENT OF FUNCTIONAL GENOMIC SCREENING APPROACHES IN CONJUNCTION WITH A NOVEL EX VIVO CO-CULTURE SYSTEM FOR PRIMARY HEMATOPOIESIS STEM CELLS

Introduction

The identification of potential therapeutic targets in CH remains a significant challenge in large part due to the lack of available systems for unbiased screening in primary HSPCs. *In vivo* models of CH have been developed and have led to key

mechanistic insights but are not conducive to high-throughput unbiased screening. *Ex vivo* culture of primary HSPCs has historically been challenging but has benefited from recent developments. The application of an *ex vivo* system for unbiased high-throughput screening to identify targets in primary HSPCs harboring mutations in common CH-associated genes is of significant interest.

* **Waarts, M.R.**, Mowla, S., Boileau M., Benitez, A.R.M., Sango, J., Bagish, M., Maestre, I.F., Shan, Y., Eisman, S., Park, Y., Wereski, M., Csete, I., O'Connor, K., Romera-Vega, A., Miles, L.A., Xiao, W., Wu, X., Koche, R., Armstrong, S.A., Shih, A.H., Papapetrou, P., Butler, J.M., Cai, S.F., Bowman, R.L., Levine. (2024). CRISPR dependency screens in primary hematopoietic stem cells identify KDM3B as a genotype specific vulnerability in IDH2- and TET2-mutant cells. *Cancer Discovery (Accepted)*

Functional genomic screening of mutant versus wild-type HSPCs is an important approach to identify novel mechanisms of transformation and mutant-specific dependencies. In some cases, AML cell lines possess CH mutations and are amenable to systematic dependency screens; however, not all CH mutant genotypes are well represented in cell lines. Furthermore, the mechanisms that promote fitness in primary mutant HSPCs may not be shared with immortalized cell lines. Most importantly, these approaches do not allow for screening of mutant versus wild-type HSPCs, such that they may uncover dependencies in leukemia cell lines which reflect a common requirement in

both normal and mutant hematopoiesis. *Ex vivo* culture of primary murine HSPCs has benefited from recent developments that have established conditions for long-term maintenance of functional HSPCs[12,169,170]. Among these, co-culture of HSPCs with AKT1-activated bone marrow endothelial cells (BMECs) has been shown to maintain HSPCs with transplantation capacity *ex vivo* and results in expansion of HSPCs and hematopoietic output along the full spectrum of myelopoiesis[12,170].

Here, we adopted this system to establish a platform that allows for the rapid *ex vivo* interrogation and perturbation of primary murine HSPCs with mutations in the genes most frequently mutated in CH. We then used this system to perform epigenetic-focused CRISPR/Cas9 screens at scale and identify a catalog of functional dependencies in HSPCs with different CH-associated mutations.

Results

BMEC/HSPC co-cultures of CH-mutant HSPCs yield rapid ex vivo phenotypes

To establish an *ex vivo* platform for functional interrogation and perturbation of HSPCs with CH mutations, we first sought to evaluate the *ex vivo* phenotypes of mutant HSPCs co-cultured with BMECs. In line with previously published results, 7-day co-culture of wild-type HSPCs with BMECs resulted in dramatic expansion of hematopoietic cells ranging from long-term hematopoietic stem cells (LT-HSCs: Lineage$^-$Sca-1$^+$Kit$^+$CD150$^+$CD48$^-$) to granulocytic-macrophage progenitors (GMPs: Lineage$^-$Kit$^+$Sca-1$^-$CD34$^+$CD16/32$^+$) and megakaryocytic-erythroid progenitors (MEPs: Lineage$^-$Kit$^+$Sca-1$^-$CD34$^-$CD16/32$^-$) to mature myeloid cells (CD11b$^+$) (**Figure 2.1A-B**)[12]. We performed *in vivo* bone marrow transplantation studies to assess whether HSPCs

co-cultured with BMECs maintained functional self-renewal capacity. Expanded cells showed robust trilineage engraftment in the peripheral blood and within bone marrow stem and progenitor compartments of recipient mice (**Figure 2.1C-D**). Secondary transplantation studies similarly demonstrated engraftment, confirming that BMEC/HSPC co-cultures maintain functional HSCs (**Figure 2.1E**).

We crossed previously reported *Dnmt3a*$^{flox/flox}$, *Asxl1*$^{flox/flox}$, *Tet2*$^{flox/flox}$, and *Idh2*$^{R140Qflox/+}$ mice to the hematopoietic stem cell specific *Scl:CreERT* and the Cre-inducible tdTomato (tdT+) reporter allele to generate mouse genetic models of the common CH mutations[5,8,9,166]. We competitively cultured wild-type and mutant LSK (Lineage$^-$Sca-1$^+$Kit$^+$) cells in BMEC/HSPC co-cultures and assessed mutant chimerism within different hematopoietic compartments after a 7-day culture (**Figure 2.2A**). Within the lineage positive output containing mature myeloid cells, *Dnmt3a*$^{-/-}$, *Asxl1*$^{-/-}$, *Tet2*$^{-/-}$, and *Idh2*^{R140Q} cells all outcompeted their wild-type counterparts (**Figure 2.2B**). In the LT-HSC compartment, *Dnmt3a*$^{-/-}$ and *Idh2*^{R140Q} cells demonstrated a competitive advantage while *Asxl1*$^{-/-}$ cells were outcompeted by wild-type cells (**Figure 2.2C**) consistent with prior studies demonstrating the relative fitness conferred by these mutations[8,9,166]. Similar results were observed in lineage$^-$ and LSK cells, except as expected *Dnmt3a*$^{-/-}$ cells failed to outcompete wild-type cells at any progenitor level besides LT-HSCs (**Figure 2.1F-G**).

Next, we assessed if CH-mutant HSPCs would retain their phenotypes *in vivo* after co-culture with BMECs. Since *Idh2*^{R140Q} and *Asxl1*$^{-/-}$ HSPCs demonstrated the greatest *ex vivo* increases and decreases in competitive fitness, respectively, we performed transplantation studies using these models. Consistent with our *ex vivo* results, *Idh2*^{R140Q} cells outcompeted wild-type cells at the initial assessment of engraftment and

demonstrated a serial increase in chimerism in the peripheral blood (**Figure 2.2D**). In contrast, *Asxl1*$^{-/-}$ cells were outcompeted by wild-type cells at the first timepoint and showed a decline in chimerism in the peripheral blood (**Figure 2.2E**). In the bone marrow, *Idh2*^{R140Q} cells similarly outcompeted wild-type cells while *Asxl1*$^{-/-}$ cells lost to wild-type cells (**Figure 2.1H-I**). These studies are consistent with the phenotypes observed *in vivo* without antecedent BMEC cultures[8,9]. Collectively, these data demonstrate that CH-mutant HSPCs co-cultured with BMECs retain functional self-renewal activity while yielding rapid *ex vivo* phenotypes largely in line with *in vivo* CH phenotypes.

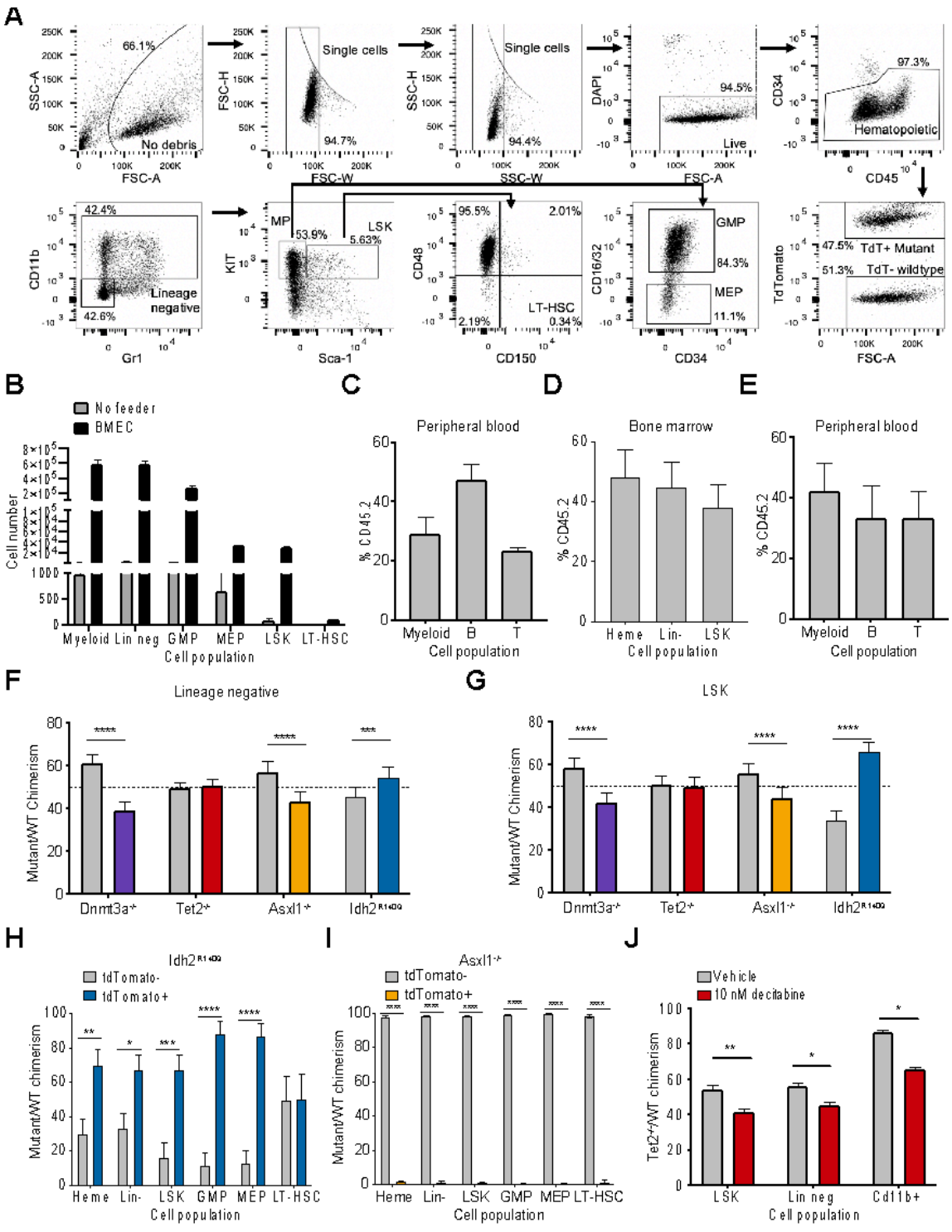

Figure 2.1: ***Ex vivo*** **characterization of BMEC/HSPC co-cultures. A,** Schematic representation of BMEC co-culture with HSPCs. LSK cells are isolated from wild-type or tdT^{+} CH-mutant mice and competitively cultured in a 1:1 ratio over a feeder layer of BMECs. Expanded cells are transplanted into recipient mice or analyzed by flow cytometry after 7 days. **B** and **C**, Flow cytometric analysis of tdT^{+} mutant and wild-type

chimerism measured after 7 days of culture within lineage$^+$ cells (**B**) or long-term hematopoietic stem cells (LT-HSCs) (**C**). Grey bars represent wild-type chimerism and colored bars represent mutant chimerism. (n = 9-12) **D** and **E**, Peripheral blood chimerism of recipient mice (% CD45.1) transplanted with cells from BMEC/HSPC co-cultures of wild-type (% CD45.2 tdT$^-$) versus *Idh2*^{R140Q} (% CD45.2 tdT$^+$) (**D**) or *Asxl1*$^{-/-}$ (% CD45.2 tdT$^+$) (**E**) cells. (n = 10) **F**, Representative flow cytometry plots and quantification of editing efficiency in HSPCs maintained in BMEC/HSPC co-cultures 7 days after lentiviral infection of sgRNAs. Editing was assessed by flow cytometric analysis of cell surface expression of CD45 or CD11b. Empty control represents Cas9 delivery only and measurement of CD45 negative cells. (n = 3-4). All data are mean ± SEM. *p < 0.05, **p < 0.01, ***p < 0.001, ****p < 0.0001

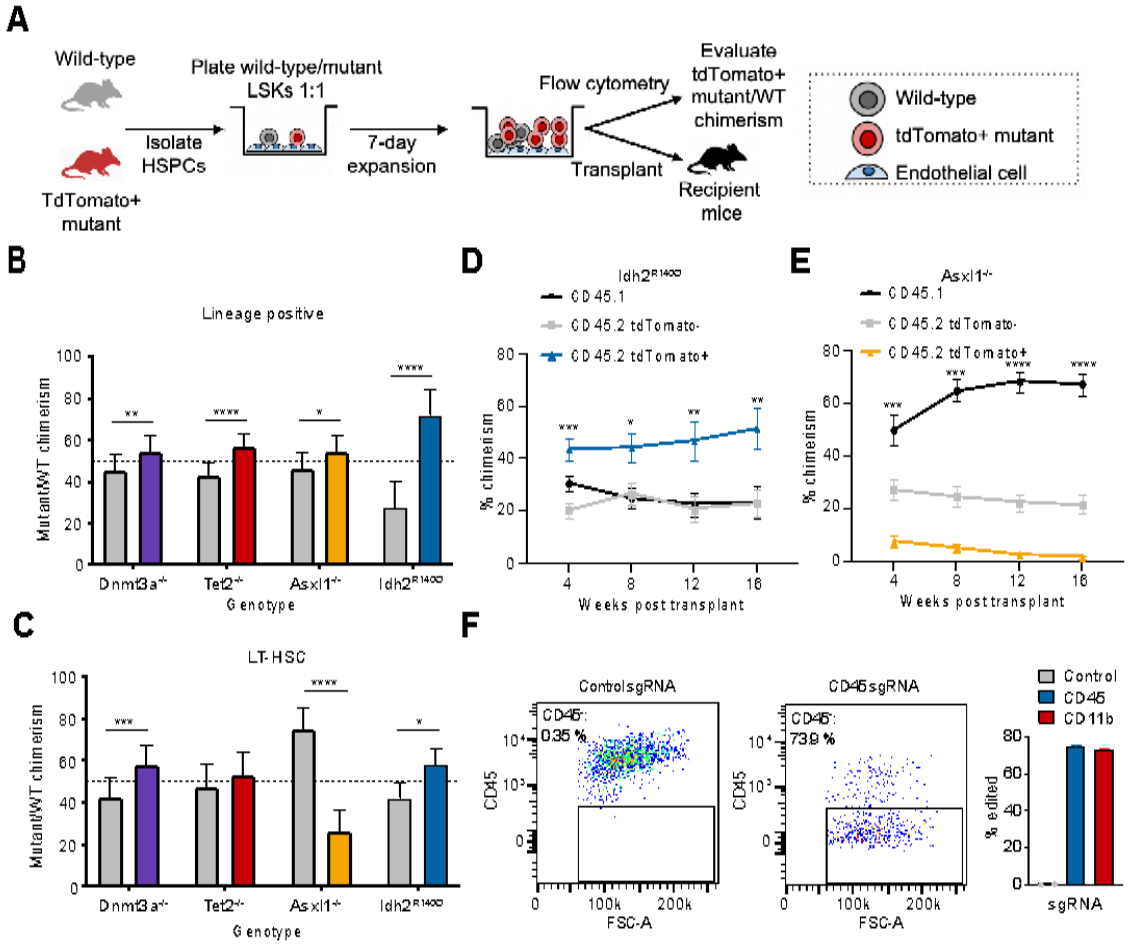

Figure 2.2: BMEC/HSPC co-cultures of CH-mutant HSPCs yield rapid *ex vivo* phenotypes. A, Schematic representation of BMEC co-culture with HSPCs. LSK cells are isolated from wild-type or tdT$^+$ CH-mutant mice and competitively cultured in a 1:1 ratio over a feeder layer of BMECs. Expanded cells are transplanted into recipient mice or analyzed by flow cytometry after 7 days. **B** and **C**, Flow cytometric analysis of tdT$^+$ mutant and wild-type chimerism measured after 7 days of culture within lineage$^+$ cells

(**B**) or long-term hematopoietic stem cells (LT-HSCs) (**C**). Grey bars represent wild-type chimerism and colored bars represent mutant chimerism. (n = 9-12) **D** and **E**, Peripheral blood chimerism of recipient mice (% CD45.1) transplanted with cells from BMEC/HSPC co-cultures of wild-type (% CD45.2 tdT^-) versus *Idh2*^{R140Q} (% CD45.2 tdT^+) (**D**) or *Asxl1*$^{-/-}$ (% CD45.2 tdT^+) (**E**) cells. (n = 10) **F**, Representative flow cytometry plots and quantification of editing efficiency in HSPCs maintained in BMEC/HSPC co-cultures 7 days after lentiviral infection of sgRNAs. Editing was assessed by flow cytometric analysis of cell surface expression of CD45 or CD11b. Empty control represents Cas9 delivery only and measurement of CD45 negative cells. (n = 3-4). All data are mean ± SEM. *p < 0.05, **p < 0.01, ***p < 0.001, ****p < 0.0001

Ex vivo small molecule and genetic perturbation in BMEC/HSPC co-cultures

We then asked whether this platform would allow for small molecule and/or genetic perturbation of primary mutant and wild-type HSPCs. To demonstrate the feasibility of small molecule perturbation, we competitively cultured *Tet2*$^{-/-}$ and wild-type HSPCs in the presence of the hypomethylating agent decitabine, which has previously been shown to mitigate the *in vivo* expansion of *Tet2*$^{-/-}$ cells in the blood[171]. As expected, decitabine treatment decreased *Tet2*$^{-/-}$ chimerism in BMEC/HSPC co-cultures with differential anti-mutant efficacy across the hematopoietic hierarchy (**Figure 2.1J**). To evaluate the potential for CRISPR/Cas9 gene editing of primary cells *ex vivo*, we infected HSPCs from Cas9-expressing mice with a lentivirus encoding a single guide RNA (sgRNA) targeting *Ptprc* (encoding CD45) or *Itgam* (encoding CD11b). Following BMEC/HSPC co-culture, we confirmed that edited cells were maintained at >70% editing efficiency at both loci (**Figure 2.2F**). These results demonstrate that the BMEC/HSPC co-culture system can serve as a platform for small molecule and genetic perturbations.

CRISPR screens in BMEC/HSPC co-cultures identify critical epigenetic-related genes in HSPCs

We next asked whether the BMEC/HSPC co-culture system could facilitate CRISPR/Cas9 screening of primary murine HSPCs. Given the critical role of epigenetic modifiers in CH, we used an epigenetic-focused lentiviral library with 997 sgRNAs targeting 191 genes[172]. We optimized multiple conditions for infection of HSPCs to achieve a multiplicity of infection (MOI) of 0.3-0.5 while maximizing cell viability and expansion (**Figure 2.3A-B**). Under optimized conditions, GFP^+ infected HSPCs maintained functional self-renewal capacity as assessed by long-term engraftment of GFP^+ cells in the peripheral blood and bone marrow of recipient mice (**Figure 2.3C-D**).

To determine whether we could maintain sufficient representation of sgRNA libraries *ex vivo*, HSPCs were infected with lentivirus encoding our CRISPR library and co-cultured with BMECs (**Figure 2.4A**). Genomic DNA was isolated from cells pre- and post-culture and amplified sgRNA libraries were subject to next-generation sequencing (NGS) to assess sgRNA representation at each time point. We observed robust representation of sgRNAs at both time points, with fewer than <1% of sgRNAs exhibiting stochastic dropout or enrichment following infection and culture (**Figure 2.3E**).

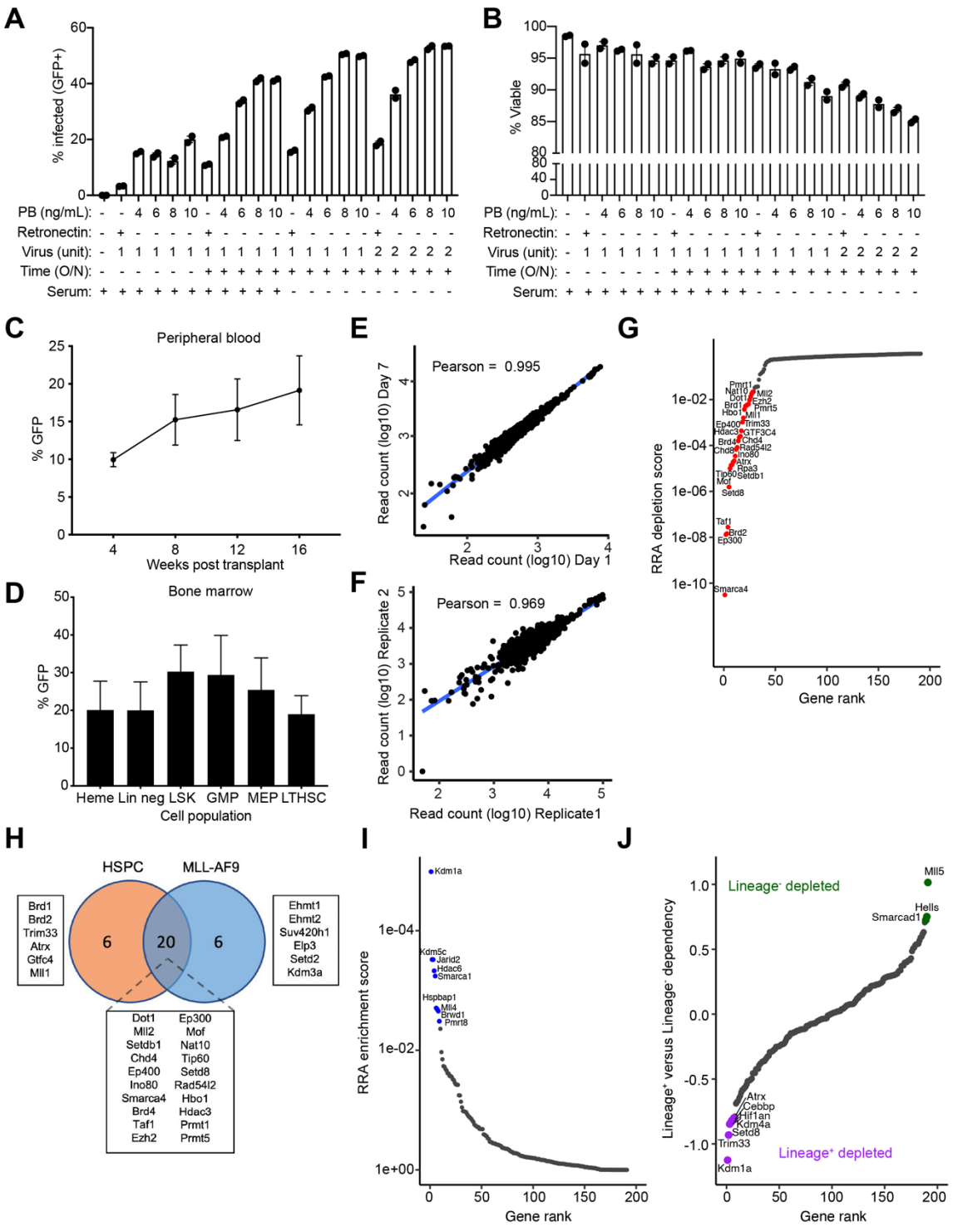

Figure 2.3: Development of CRISPR screens with BMEC/HSPC co-cultures. A, Percentage of GFP$^+$ infected cells as measured by flow cytometry 7 days after lentiviral infection. HSPCs were infected with a GFP$^+$ lentivirus encoding an epigenome library under the indicated conditions. PB, polybrene. O/N, overnight. (n = 2) **B**, Cell viability as measured by trypan blue exclusion 7 days after infection. HSPCs were infected with a

GFP^+ lentivirus encoding an epigenome library under the indicated conditions. PB, polybrene. O/N, overnight. (n = 2) **C**, GFP^+ peripheral blood chimerism within recipient mice transplanted with infected GFP^+ HSPCs from BMEC/HSPC co-cultures. (n = 10) **D**, GFP^+ chimerism within bone marrow cell compartments of recipient mice transplanted with infected GFP^+ HSPCs from BMEC/HSPC co-cultures. (n = 10) **E**, Correlation of normalized read counts from sgRNA libraries pre- and post-BMEC/HSPC co-culture of wild-type HSPCs without Cas9. **F**, Correlation of normalized read counts from sgRNA libraries prepared from the endpoint of independent screen replicates on Cas9-expressing HSPCs **G,** Genes with depleted sgRNAs in Cas9-expressing HSPCs as assessed by sgRNA abundance post-culture normalized to pre-culture. **H,** Venn diagram of genes with depleted sgRNAs in Cas9-expressing HSPCs and MLL-AF9; Nras leukemia cells. **I,** Genes with enriched sgRNAs in Cas9-expressing HSPCs as assessed by sgRNA abundance post-culture normalized to pre-culture. **J,** Genes with depleted or enriched sgRNAs in $lineage^+$ cells as compared to $lineage^-$ cells. All data are mean ± SEM.

We then performed a screen on wild-type HSPCs isolated from Cas9-expressing mice. Correlation of sgRNA abundance between replicates was high, demonstrating the robustness of this screening platform (**Figure 2.3F**). Assessment of sgRNA representation pre- and post-culture revealed 28 genes targeted by sgRNAs that were statistically significantly depleted in HSPCs (**Figure 2.3G**). These genes include known dependencies across multiple cellular contexts (e.g. *Rpa3*, *Smarca4*, *Ep300*, *Ep400*), HSPC-specific dependencies (e.g. *Mof*, *Prmt5*, *Hbo1*), and genes whose function in hematopoiesis has not yet been characterized (e.g. *Setd8*, *Nat10*, *Chd4*)[173-175]. A comparison of depleted genes in our screen to a previously published gene set of depleted genes in a screen of an MLL-AF9 leukemia cell line using the same sgRNA library revealed that >75% (20/26) of genes identified as dependencies in leukemia cells were also dependencies in our screen on wild-type HSPCs, suggesting these are not leukemia or MLL-fusion specific dependencies (**Figure 2.3H**)[172]. We also identified sgRNAs for 9 genes that were enriched after culture, consistent with positive selection (**Figure 2.3I**). These genes include those that encode established tumor suppressors in HSPCs (e.g.

Kdm1a and *Jarid2*) and genes whose role in hematopoiesis remains unclear (e.g. *Kdm5c*, *Hdac6*, *Smarca1*)[176,177]. Finally, we carried out an additional expansion step to ask whether we could identify genes responsible for maintaining the balance between progenitors and mature cells. Assessment of sgRNA representation in lineage$^-$ HSPCs and lineage$^+$ mature cells identified genes whose loss either preferentially targets HSPCs versus mature cells or alters differentiation (**Figure 2.3J**). Among these, *Kdm1a* and *Mll5* scored most highly for epigenetic regulators whose loss depleted lineage$^+$ or lineage$^-$ cells, respectively, consistent with published literature[176,178]. Together, these data demonstrate that CRISPR/Cas9 screens in the BMEC/HSPC co-culture system can elucidate critical epigenetic regulators which dictate the fitness and/or differentiation capacity of HSPCs.

CRISPR screens identify dependencies in CH-mutant HSPCs

We next performed CRISPR screens using *Dnmt3a*$^{-/-}$, *Asxl1*$^{-/-}$, *Tet2*$^{-/-}$, and *Idh2*^{R140Q} primary HSPCs to delineate if there were genotype-specific dependencies in mutant HSPCs. We calculated a dependency score for each target in each genotype and then evaluated the difference between dependency scores in mutant versus wild-type HSPCs. Notably, the vast majority of dependencies in wild-type HSPCs scored as dependencies across the spectrum of mutant HSPCs, consistent with a requirement for these genes in normal and mutant hematopoiesis (**Figure 2.4A**). Most importantly, these screens identified a set of genotype-specific dependencies with statistically significant increases in dependency scores in one or more mutant genotypes when compared to wild-type HSPCs (**Figure 2.4B-F**).

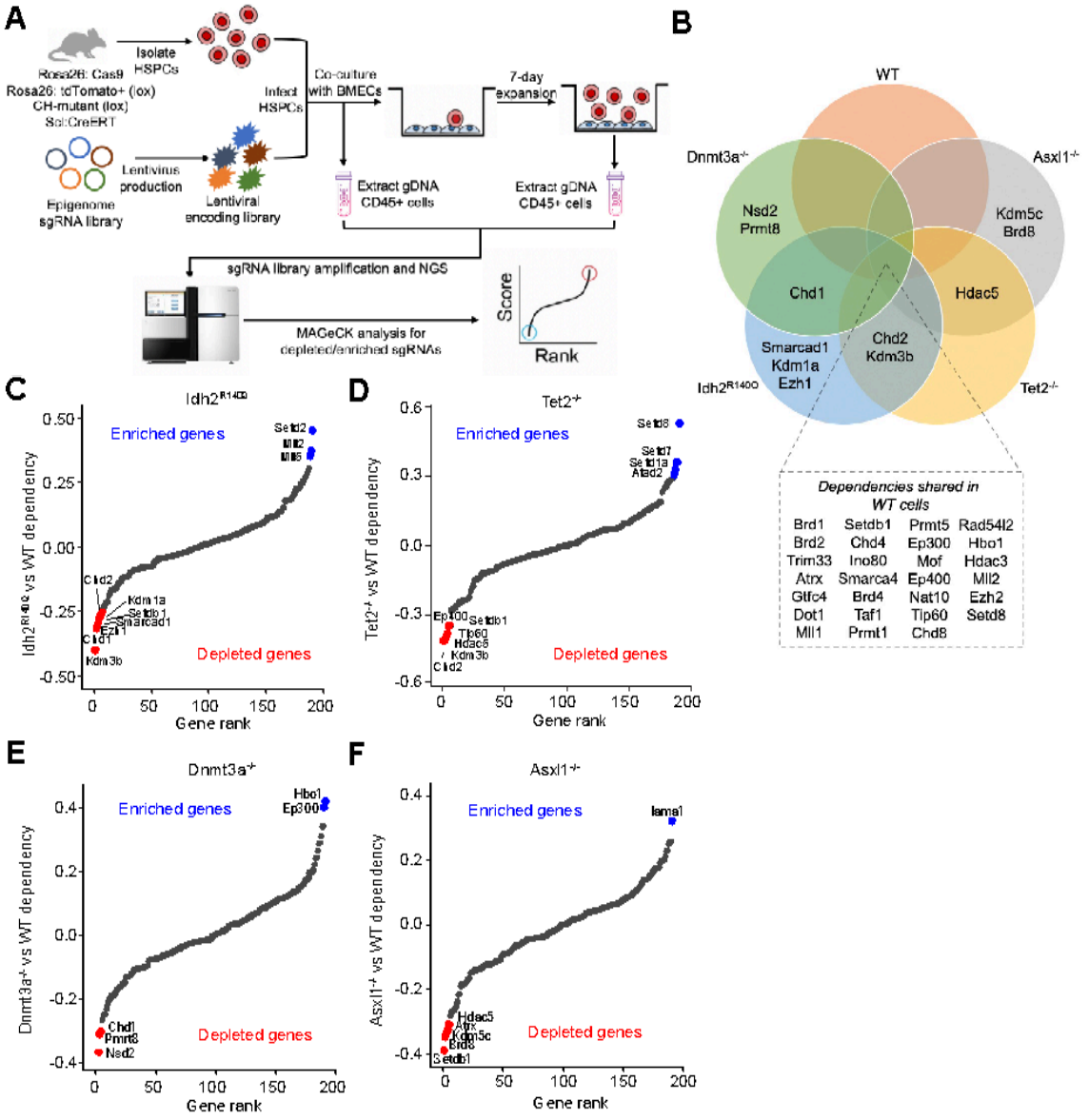

Figure 2.4: CRISPR screens identify vulnerabilities in HSPCs with different CH mutations. A, Schematic representation of CRISPR screens with BMEC/HSPC platform. HSPCs are isolated from Cas9-expressing mice, infected with a lentivirus encoding an epigenome sgRNA library, and co-cultured with BMECs. DNA is extracted pre- and post-culture for sgRNA library amplification and sequencing. MAGeCK is used to assess depleted and enriched sgRNAs. **B**, Venn diagram of genes targeted by sgRNAs relatively depleted in mutant HSPCs compared to wild-type HSPCs. Genes that are also depleted in wild-type HSPCs are marked as shared dependencies. **C-F**, Genes with depleted or enriched sgRNAs in *Idh2*^{R140Q} (**C**), *Tet2*$^{-/-}$ (**D**), Dnmt3a$^{-/-}$ (**E**), or Asxl1$^{-/-}$ (**F**) HSPCs as compared to wild-type HSPCs.

Discussion

CH is highly prevalent in elderly individuals and confers an increased risk of all-cause mortality, which is primarily attributable to an increased risk of both hematologic malignancy and cardiovascular disease[154,155,161]. However, there are currently no specific therapies for molecularly defined CH subtypes or for the mutations in epigenetic regulators observed in CH and which initiate the transformation trajectory to myeloid malignancies. Dependency identification in genetically defined CH subtypes has been hindered by the lack of *in vitro* systems that enable functional perturbation and that faithfully recapitulate mutant/wild-type hematopoietic fitness. We demonstrate that *ex vivo* co-culture of CH-mutant HSPCs with BMECs reads out the fitness advantage of CH mutant versus wild-type HSPCs. These co-cultures yield rapid *ex vivo* phenotypes that are consistent with mouse and human data for key CH mutant alleles, including the aberrant stem cell function of *Dnmt3a*- and *Asxl1*-mutant LT-HSCs[8,166]. Most importantly, CH-mutant HSPCs co-cultured with BMECs retain engraftment capacity and show concordant *in vivo* phenotypes when transplanted back into mice.

CRISPR screens are a powerful tool to identify vulnerabilities but have yet to be systematically applied to primary HSPCs, including in CH-mutant contexts. *In vivo* screens of CH-mutant HSPCs have not been reported, likely due to the challenge in maintaining large numbers of sgRNAs *in vivo*, which we confirm in our study. *Ex vivo* screens of HSPCs have also not been described, likely due to the difficulty in infecting and culturing primary HSPCs, the requirement for polyclonal expansion, and the need for sufficient cell divisions *ex vivo* to identify significantly depleted sgRNAs. In wild-type HSPCs, we reliably identify previously reported dependencies, including genes important in multiple cellular contexts and specifically in hematopoiesis (e.g., *Mof*, *Prmt5*,

Hbo1)[173-175]. More importantly, most of the dependencies found in our screen on wild-type HSPCs were also found in a previously published epigenetic CRISPR screen in MLL-AF9 leukemia cells and in the different CH genotypes we screened[172]. This includes previous targets which have been nominated and evaluated as leukemia-specific dependencies (e.g., *BRD4*, *PRMT5*, *DOT1L*) where efficacy has been limited by a lack of leukemia-specific therapeutic index[179-184]. By contrast, our approach of screening mutant and wild-type HSPCs in a defined co-culture system allowed us to identify a set of mutant-specific dependencies in CH-mutant HSPCs.

Materials and Methods

Experimental animals

All animal studies were performed in accordance with institutional guidelines established by Memorial Sloan Kettering Cancer Center (MSKCC) under the Institutional Animal Care and Use Committee-approved animal protocol (#07-10-016) and the Guide for the Care and Use of Laboratory Animals (National Academy of Sciences 1996). All experimental animals were maintained on a 12-hour light-dark cycle with access to water and standard chow ad libitum. Veterinary staff provided regular monitoring and husbandry care. All mice had intact immune systems, were drug and test naïve, and had not been involved in previous procedures. Animals were monitored daily for signs of disease or morbidity, bleeding, failure to thrive, infection, or fatigue and sacrificed immediately if they exhibited any signs of the above. All mice used in this study including *Tet2*$^{flox/flox}$, *Dnmt3a*$^{flox/flox}$, *Idh2*$^{R140Q/flox}$, *Asxl1*$^{flox/flox}$, *Scl:CreERT*, *Npm1*$^{flox\text{-}cA/+,}$ *Flt3*^{ITD}, *Vav:Cre*, *Rosa26:Cas9*, and *Rosa:TdT*$^{flox/flox}$ have been previously

described[5,8,166,185-191]. Mice with *Scl:CreERT* were administered 100 mg/kg tamoxifen two times (one day drug holiday in between dosing) via oral gavage to induce Cre recombinase activity. Age-and sex- matched 6–16-week-old mice were used in all experiments and only female mice were used as transplant recipients.

BMEC co-culture with HSPCs

AKT1-activated bone marrow endothelial cells (BMECs) were cultured as previously described[12]. BMECs were seeded 1-3 days prior to HSPC plating at a density of 70,000-150,000 BMECs/well in a fibronectin-coated 12-well plate. To obtain HSPCs, bone marrow cells were isolated from limb bones into FACS buffer (phosphate buffered saline [PBS] + 2% fetal bovine serum) via centrifugation and RBCs were lysed using RBC lysis buffer (Thermo). Lineage$^-$ HSPCs were isolated using the Lineage Cell Depletion Kit according to manufacturer's protocol (EasySep™, StemCell Technologies, Inc.). Cells were then resuspended in Fc (CD16/32) block for 15 minutes and then subsequently stained for lineage$^-$Sca1$^+$cKIT$^+$ (LSK) markers with antibodies targeting Sca-1 (D7) and KIT (2B8) for 30 minutes. All FACS antibodies were purchased from BD, BioLegend, or eBioscience. Following antibody incubation, cells were washed with FACS buffer and resuspended in a live/dead cell stain solution, either DAPI (Thermo, 1:1000 in FACS) or Helix NP NIR (Biolegend, 1:20,000 in FACS). LSK cells were then sorted on a FACSAria III. Subsequently, 2,000 LSKs were plated on a confluent monolayer of BMECs in a single well of a 12-well plate. Each well had 1 mL StemSpan SFEM with 10 ng/mL recombinant murine SCF (PeproTech) and/or additional cytokines as indicated. Co-cultures were maintained for a total of 7 days at 37°C and 5% CO2. A

complete media change was performed on day 4 of culture. On day 7, cells were harvested with Accutase (Biolegend) and used in downstream applications. For assays with day 14 readouts, CD45 cells were isolated with CD45 microbeads (Miltenyi Biotech) following manufacturers' protocol and replated onto fresh BMEC plates. For decitabine treatment, cells were treated with 10 nM decitabine (MedChem Express) with the corresponding vehicles.

Transplantation assays and in vivo experiments

For transplantation of cells from BMEC cultures, CD45 cells were isolated with CD45 microbeads (Miltenyi Biotech) following manufacturer's protocol. 500,000 to 1.0 x 10^6 $CD45^+$ cells were combined with 200,000 CD45.1 (Jackson Laboratories, Bar Harbor, ME) whole bone marrow cells. Cells were washed, resuspended in PBS, and transplanted via lateral tail vein injection into recipient mice. Recipient mice were lethally irradiated (900 cGy) 6–8-week-old female CD45.1 mice 16-24 hours before tail vein injection. For all transplants, peripheral blood was isolated at the indicated timepoints by submandibular bleeds and complete blood counts determined using a ProCyte Dx (IDEXX Laboratories, Westbrook, ME) according to manufacturer's protocol. For terminal tissue isolation, mice were euthanized with CO_2 asphyxiation and tissues were dissected and fixed with 4% paraformaldehyde for histopathological analysis. For whole bone marrow isolation, limb bones were dissected and whole bone marrow isolated using centrifugation followed by RBC lysis (BioLegend) for 10 minutes.

Ex vivo CRISPR screen

For *ex vivo* CRISPR screens, whole bone marrow was isolated from donor mice as described above and HSPCs were isolated using the Lineage Cell Depletion Kit according to manufacturer's protocol (EasySep™, StemCell Technologies, Inc.). Lentivirus and 12 ug/mL polybrene (AmericanBio) were incubated in 1 mL StemSpan SFEM (StemCell Technologies) containing 6 ng/mL IL-3 (Peprotech), 10 ng/mL IL-6 (Peprotech), and 20 ng/mL SCF (Peprotech) for 10 minutes at room temperature. For titration experiments involving retronectin, virus was added to retronectin (Takara) coated plates without addition of polybrene. For titration experiments involving serum, IMDM + 10% FBS was used instead of StemSpan. 1.0 x 10^6 HSPCs were added to each infection along with 30 μM L of 1 M HEPES (Thermo). Each infection was transferred to a single well of a 6-well plate and cells were centrifuged at 800 rcf for 1 hour at 32°C, following which an additional 2 mL of StemSpan SFEM containing 6 ng/mL IL-3, 10 ng/mL IL-6, and 20 ng/mL SCF was added to each well. Cells were infected at an efficiency of 20-40% so that most cells received only one sgRNA. Cells were incubated overnight at 37°C with 5% CO_2. 16 hours after infection, cells were harvested, and cell numbers were determined using an automated cell counter (ViCell Blue, Beckman Coulter). A minimum of 3.3 x 10^6 cells were collected for baseline sequencing, sufficient for a representation of 1,000 cells per sgRNA. A minimum of 3.3 x 10^6 cells additional cells were plated over BMEC monolayers in 12-well plates at a cell density of 50,000 HSPCs/well in StemSpan SFEM with 10 ng/mL SCF (Peprotech) and 50 ng/mL TPO (Peprotech). A complete media change was performed on day 4 post HSPC plating. On day 7, co-cultures were harvested with Accutase (Biolegend) and cells were collected for sequencing. For identifying cell-type specific dependencies, co-cultures were harvested

and lineage$^-$ cells were isolated with the Lineage Cell Depletion Kit (StemCell Technologies) with spike-in of 5 µl biotinylated CD31 antibody (Biolegend) to remove BMECs. HSPCs were then replated onto fresh BMEC plates. On day 14, co-cultures were harvested and cells were separated into lineage$^-$ and lineage$^+$ fractions with Lineage Cell Depletion Kit. Samples of lineage$^-$ and lineage$^+$ cells were collected for sequencing. Cell pellets for sequencing were lysed, genomic DNA was extracted using the Purogene kit (Qiagen), and DNA quantified using Qubit (Thermo). Genomic DNA was PCR amplified to add Illumina adapters and multiplexing barcodes. Amplicons were quantified by Qubit and Bioanalyzer (Agilent) and sequenced on an Illumina HiSeq 2500.

Lentivirus production

For lentivirus production, plasmids were co-transfected into 293Ts with the packaging vector psPAX2 and the envelope vector pMD2.G using the jetPRIME transfection reagent (Polyplus) following manufacturer's protocol. Media was changed 24 hours post transfection. Viral-containing supernatant was collected 72 hours after transfection and passed through a 0.45-micron filter. For lentivirus used to infect HSPCs, virus was ultracentrifuged at 24,000 rpm for 2 hours at 4°C using a Sorvall Ultracentrifuge (Thermo). Viral pellets were resuspended in Stemspan SFEM (StemCell Technologies) and resuspended on a rotator overnight at 4°C, following which virus was aliquoted and stored at -80 C for long-term storage.

Flow cytometry and sorting

Freshly isolated cells were washed with FACS buffer (phosphate buffered saline (PBS) + 2% fetal bovine serum). For cell surface staining, cells were then resuspended in Fc (CD16/32) block for 15 minutes at 4°C and then subsequently incubated with antibody cocktails for an additional 15 minutes at 4°C. For peripheral blood analysis, antibodies targeted CD3 (17A2), CD45R/B220 (RA3-6B2), Gr-1 (RB6-8C5), CD11b 450 (M1/70), CD45.2 (104), Kit (2B8), and CD45.1 (A20). For bone marrow analysis, additional antibodies targeted Sca-1 (D7), FcγRII/III (2.4G2), CD34 (RAM34), CD150 (9D1), and CD48 (HM48-1). For analysis of BMEC co-cultures, antibodies targeted Gr-1 (RB6-8C5), CD11b 450 (M1/70), CD45.2 (104), Kit (2B8), and Sca-1 (D7). If LT-HSC analysis was necessary, antibodies targeting CD150 (9D1) and CD48 (HM48-1) were included. All antibodies were purchased from BD, BioLegend or eBioscience. Following antibody incubation, cells were washed with FACS buffer and resuspended in FACS buffer containing a live/dead cell stain, either DAPI (1:1000 in FACS buffer, Thermo) or Helix NP NIR (1:20,000 in FACS buffer, Biolegend). Flow cytometry was performed on a BD LSRFortessa (BD Biosciences) using FACSDiva and FlowJo (v10.9). Cell isolation with FACS was performed on an FACSAriaIII (BD Biosciences).

Data analysis for CRISPR screens

Sequencing reads were aligned to the screened library and counts were obtained for each sgRNA. Enrichment and depletion of genes in wild-type cells were analyzed using the MAGeCK package by comparing read counts at the final timepoint with counts from the initial timepoint[192]. The MAGeCK-MLE package was used to compute

normalized dependency scores for each gene across each genotype. An FDR cutoff of 0.25 was used for all analyses.

Statistical analyses

Statistical analyses were performed using Student's t-test using GraphPad Prism (GraphPad Software, San Diego, CA) unless otherwise noted. $P < 0.05$ was considered statistically significant. The number of animals and experimental replications can be found in the respective figure legends.

CHAPTER THREE *
IDENTIFICATION OF KDM3B AS A TARGET IN A SUBSET OF CLONAL HEMATOPOIESIS

Introduction

Despite the clear association of CH with an increased risk of both AML and all-cause mortality, there is a paucity of targets identified to restrain CH. Our results in Chapter Two provide a catalogue of novel potential therapeutic targets for the subset of CH marked the most commonly recurring mutations. After consideration of all candidate hits, *Kdm3b* was prioritized for further study because: 1) *Kdm3b* was the top hit in both $Tet2^{KO}$ and $Idh2^{R140Q}$ cells, 2) the *Kdm3* family members, *Kdm3a* and *Jmjd1c,* were also depleted selectively in these genotypes, suggesting a possible family effect, 2) $Tet2^{KO}$ and $Idh2^{R140Q}$ are believed to enable CH through a shared molecular pathway, thus indicating the mechanisms of the uncovered dependencies may be shared between these genotypes, 3) *Kdm3b* loss is tolerated in mouse models, suggesting a potential therapeutic index, 4) KDM3 enzymes are believed to be amenable to small molecule inhibition, and 5) the role of *Kdm3* family members in hematopoiesis is largely unknown.

* **Waarts, M.R.**, Mowla, S., Boileau M., Benitez, A.R.M., Sango, J., Bagish, M., Maestre, I.F., Shan, Y., Eisman, S., Park, Y., Wereski, M., Csete, I., O'Connor, K., Romera-Vega, A., Miles, L.A., Xiao, W., Wu, X., Koche, R., Armstrong, S.A., Shih,

A.H., Papapetrou, P., Butler, J.M., Cai, S.F., Bowman, R.L., Levine. (2024). CRISPR dependency screens in primary hematopoietic stem cells identify KDM3B as a genotype specific vulnerability in IDH2- and TET2-mutant cells. *Cancer Discovery (Accepted)*

Kdm3b and *Jmjd1c* are both members of the family of Jumanji-domain containing histone lysine demethylases and are both well-established for their role in demethylation of H3K9me1/2, amongst other histone targets[193,194]. These enzymes have also both been described as having context-dependent roles in hematological malignancies. Multiple studies have demonstrated the dependency of *Jmjd1c* in an MLL-AF9;Nras-driven leukemia model, but *Jmjd1c* was found to be dispensable in $Jak2^{V617F}$-driven MPN and native hematopoiesis[195-198]. Similarly, *Kdm3b* has been proposed to play a role in leukemogenesis through induction of the leukemia oncogene *Lmo2* but is not essential in native hematopoiesis[199]. The specific dependencies of *JMJD1C* and *KDM3B* in *TET2*- or *IDH2*-mutant CH or AML have not been reported. The similar biological activity of JMJD1C and KDM3B suggests these dependencies may operate via similar mechanisms.

The shared dependency of *Kdm3b* and *Jmjd1c* in both $Tet2^{KO}$ and $Idh2^{R140Q}$ HSPCs also suggests that both genotypes may be dependent on these enzymes through common mechanisms. TET2 is an alpha-ketoglutarate dependent enzyme responsible for the hydroxylation of 5-methylcytosines (5-mC) to 5-hydroxymethylcytosine (5-hmC), leading to DNA demethylation[200]. Loss of function mutations in *TET2* are found frequently in CH and AML and functionally contribute to an increase in self-renewal activity of mutant HSPCs, believed to be due to hypermethylation at key loci[5,185]. Meanwhile, mutations in *IDH2*, the enzyme that catalyzes the conversion of isocitrate to α-KG, are also common in CH and AML. These gain of function mutations, primarily

observed as R140Q, are believed to contribute to disease primarily through neomorphic production of 2-HG leading to inhibition of TET2[132,201]. Consistent with this, mutations in *IDH2* and *TET2* are mutually exclusive in patients with CH and AML, further supporting that these two mutations may act through a shared pathway[4]. This suggests that the observed *Jmjd1c* and *Kdm3b* dependencies in $Idh2^{R140Q}$ and $Tet2^{KO}$ cells may be dependent on reduced TET2 activity. Here, we investigate the function and mechanism of the *KDM3* family member dependency in CH and AML.

Results

Kdm3b is a dependency in Idh2- and Tet2-mutant HSPCs ex vivo

In our original screens in Chapter Two, we observed that *Kdm3b* was a top dependency in both $Idh2^{R140Q}$ and $Tet2^{-/-}$ cells (**Figure 2.4**)[194,199]. Additionally, while not scoring below the threshold of statistical significance, we observed a trend towards depletion of *Jmjd1c*, a paralog of *Kdm3b*, in $Idh2^{R140Q}$ and $Tet2^{-/-}$ cells but not wild-type cells or other mutant genotypes (**Figure 2.4**)[202]. To determine whether *Kdm3b* was a mutant-specific dependency in *Idh2*- and *Tet2*-mutant HSPCs, we competitively co-cultured $Tet2^{-/-}$ or $Idh2^{R140Q}$ HSPCs with wild-type HSPCs and infected them with a BFP^+ lentivirus encoding a single sgRNA against *Kdm3b* or the control *Rosa26* (*Rosa*) locus. Following co-culture with BMECs, we assessed mutant chimerism within the fraction of BFP^+ sgRNA-containing cells. As expected, within cells carrying a *Rosa*-targeted sgRNA, both $Idh2^{R140Q}$ and $Tet2^{-/-}$ cells outcompeted wild-type cells (**Figure 3.1 and Figure 3.2A-E**). However, loss of *Kdm3b* led to a mutant-specific significant reduction in $Idh2^{R140Q}$ and $Tet2^{-/-}$ chimerism in $lineage^-$, LSK, and mature

myeloid cells (**Figure 3.1 and Figure 3.2A-E**). Loss of *Jmjd1c* also reduced the relative fitness of *Idh2*^{R140Q} and *Tet2*$^{-/-}$ lineage^{-}, LSK, and mature myeloid cells (**Figure 3.2F-L**). Consistent with the data from our CRISPR screens, *Kdm3b* loss led to a more profound depletion of mutant cells as compared to *Jmjd1c* loss. Loss of *Kdm3b* or *Jmjd1c* had no effect on the fitness of wild-type LSK, lineage^{-}, and mature myeloid cells as demonstrated by the stable frequency of *Kdm3b* and *Jmjd1c* sgRNA-carrying cells during *ex vivo* culture, indicating that the relative dependence of mutant cells on *Kdm3b* and *Jmjd1c* is not due to differential effects on wild-type cells (**Figure 3.2M-O**). These findings demonstrate that *Kdm3b* and *Jmjd1c* are mutant-specific dependencies in *Idh2*- and *Tet2*-mutant HSPCs *ex vivo*.

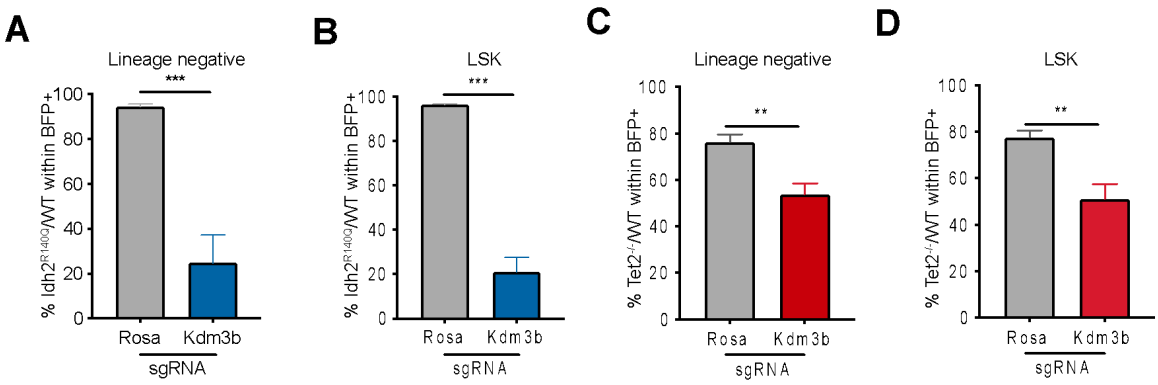

Figure 3.1: *Kdm3b* is an *ex vivo* dependency in *Idh2*- and *Tet2*-mutant HSPCs. A and **B**, *Idh2*^{R140Q} tdT^{+} chimerism as assessed by flow cytometry in lineage^{-} (**A**) or LSK (**B**) infected cells measured after 14 days of BMEC/HSPC co-culture. Wild-type and *Idh2*^{R140Q} tdT^{+} HSPCs were mixed 1:1 and infected with a BFP^{+} lentivirus encoding an sgRNA targeting *Rosa* or *Kdm3b*. (n = 3) **C** and **D**, *Tet2*$^{-/-}$ tdT^{+} chimerism as assessed by flow cytometry in lineage^{-} (**C**) or LSK (**D**) infected cells measured after 14 days of BMEC/HSPC co-culture. Wild-type and *Tet2*$^{-/-}$ tdT^{+} HSPCs were mixed 1:1 and infected with a BFP^{+} lentivirus encoding an sgRNA targeting *Rosa* or *Kdm3b*. (n = 3). All data are mean ± SEM. **p < 0.01, ***p < 0.001

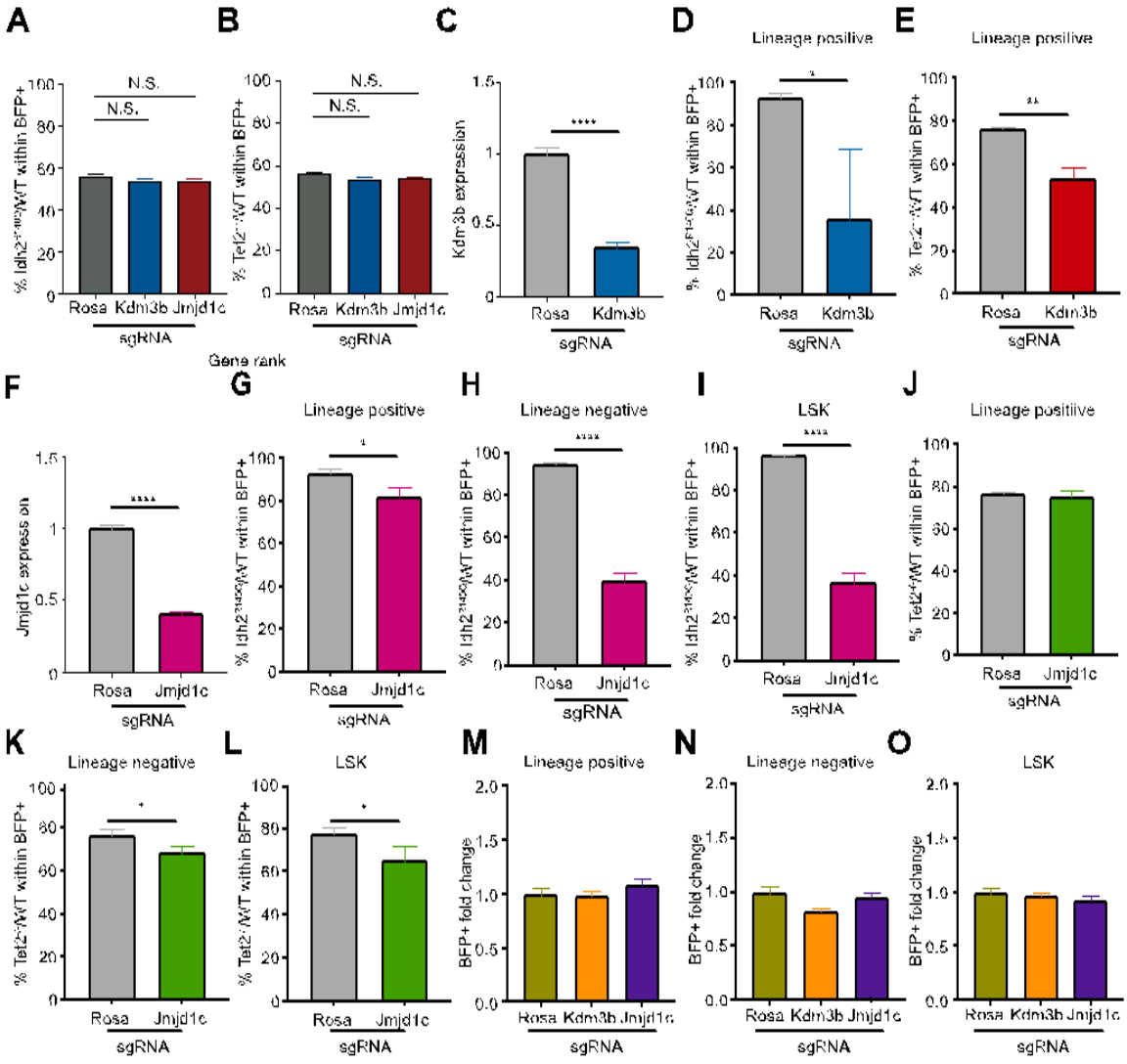

Figure 3.2: *Jmjd1c* is a dependency in *Idh2*- and *Tet2*-mutant HSPCs. A and **B,** *Idh2*^{R140Q} (**A**) or *Tet2*$^{-/-}$ (**B**) tdT^{+} chimerism in infected cells measured by flow cytometry at the initial timepoint 48 hours post-infection. Wild-type and mutant tdT^{+} HSPCs were mixed 1:1 and infected with a BFP^{+} lentivirus encoding an sgRNA targeting *Rosa*, *Kdm3b,* or *Jmjd1c*. (n = 3) **C,** *Kdm3b* expression levels as measured by quantitative polymerase-chain reaction on HSPCs infected with a lentivirus encoding a single sgRNA targeting *Rosa* or *Kdm3b*. (n = 4) **D**, *Idh2*^{R140Q} tdT^{+} chimerism in lineage^{+} infected cells measured by flow cytometry after 14 days of BMEC/HSPC co-culture. Wild-type and *Idh2*^{R140Q} tdT^{+} HSPCs were mixed 1:1 and infected with a BFP^{+} lentivirus encoding an sgRNA targeting *Rosa* or *Kdm3b*. (n = 3) **E**, *Tet2*$^{-/-}$ tdT^{+} chimerism in lineage^{+} infected cells measured by flow cytometry after 14 days of BMEC/HSPC co-culture. Wild-type and *Tet2*$^{-/-}$ tdT^{+} HSPCs were mixed 1:1 and infected with a BFP^{+} lentivirus encoding an sgRNA targeting *Rosa* or *Kdm3b*. (n = 3) **F,** *Jmjd1c* expression levels as measured by quantitative polymerase-chain reaction on HSPCs infected with a lentivirus encoding a single sgRNA targeting *Rosa* or *Jmjd1c*. (n = 4) **G-I**, *Idh2*^{R140Q} tdT^{+} chimerism in lineage^{+}

(**G**), lineage$^-$ (**H**) or LSK (**I**) infected cells measured by flow cytometry after 14 days of BMEC/HSPC co-culture. Wild-type and *Idh2*^{R140Q} tdT$^+$ HSPCs were mixed 1:1 and infected with a BFP$^+$ lentivirus encoding an sgRNA targeting *Rosa* or *Jmjd1c*. (n = 3) **J-L**, *Tet2*$^{-/-}$ tdT$^+$ chimerism in lineage$^+$ (**J**), lineage$^-$ (**K**) or LSK (**L**) infected cells measured by flow cytometry after 14 days of BMEC/HSPC co-culture. Wild-type and *Tet2*$^{-/-}$ tdT$^+$ HSPCs were mixed 1:1 and infected with a BFP$^+$ lentivirus encoding an sgRNA targeting *Rosa* or *Jmjd1c*. (n = 3) **M-O,** BFP$^+$ fold change in lineage$^+$ (**M**), lineage$^-$ (**N**) or LSK (**O**) cells as measured by flow cytometry after 14 days of BMEC/HSPC co-culture and normalized to % BFP$^+$ 2 days post-infection. Wild-type HSPCs were infected with a BFP$^+$ lentivirus encoding a single sgRNA. (n = 3) All data are mean ± SEM. *p < 0.05, **p < 0.01, ***p < 0.001, ****p < 0.0001

Kdm3b is a dependency in Idh2- and Tet2-mutant HSPCs in vivo

We next investigated if *Kdm3b* was a mutant-specific dependency in *Idh2*^{R140Q} and *Tet2*$^{-/-}$ HSPCs *in vivo*. Given that BMEC/HSPC co-cultures infected with sgRNA libraries retain engraftment capacity, we first obtained *in vivo* readouts of our *ex vivo* CRISPR screens. We performed transplantation studies of BMEC/HSPC co-cultures and sequenced sgRNA libraries constructed from the peripheral blood and bone marrow of recipient mice. However, only 10-20% of sgRNAs were sufficiently represented in the peripheral blood and bone marrow, suggesting that the limited number of HSPCs which survive the transplantation bottleneck *in vivo* are insufficient to maintain representation of large CRISPR libraries (**Figure 3.3A**)[203]. Thus, we constructed a focused sgRNA validation library consisting of 47 sgRNAs targeting the top hits from our screen, the *Kdm3* family members, and positive and negative control sgRNAs. Sixteen weeks after transplant, sgRNA libraries were prepared from peripheral blood and bone marrow lineage$^-$ HSPCs from recipient mice transplanted with either *Idh2*^{R140Q} or wild-type infected HSPCs (**Figure 3.4A**). Using this smaller library, we identified sufficient representation of >95% of sgRNAs in both the peripheral blood and bone marrow (**Figure 3.3B**). For mice engrafted with wild-type HSPCs, the only depleted gene was the

positive control *Rpa3* (**Figure 3.3C-D**). We calculated normalized dependency scores for each target gene in *Idh2*^{R140Q} versus wild-type cells and confirmed *Kdm3b* as a top dependency in *Idh2*^{R140Q} cells, both in the peripheral blood and bone marrow (**Figure 3.3E and Figure 3.4B**). *Kdm3a* also scored strongly *in vivo* as a mutant-specific dependency while *Jmjd1c* showed a trend for mutant-specific depletion that did not reach statistical significance.

We next performed *in vivo* studies investigating the requirement for *Kdm3b* in *Tet2*$^{-/-}$ or *Idh2*^{R140Q} HSPCs compared to wild-type HSPCs. We infected mutant and wild-type HSPCs with a BFP^{+} lentivirus encoding a single sgRNA against *Kdm3b* or *Rosa* and competitively transplanted these HSPCs into recipient mice. We observed outgrowth of *Idh2*^{R140Q} and *Tet2*$^{-/-}$ cells in the peripheral blood of the *Rosa* control group; however, the competitive advantage of *Idh2*^{R140Q} and *Tet2*$^{-/-}$ HSPCs was fully abrogated with loss of *Kdm3b* (**Figure 3.3F-G and Figure 3.4C-D**). Analysis of the bone marrow at 20 weeks revealed that loss of *Kdm3b* selectively reduced *Idh2*^{R140Q} and *Tet2*$^{-/-}$ chimerism in HSPC subsets including within the LT-HSC compartment (**Figure 3.3H-K and Figure 3.4 E-F**). To functionally verify that *Kdm3b* loss abrogates the self-renewal of *Idh2*^{R140Q} and *Tet2*$^{-/-}$ HSPCs, we performed secondary transplantation studies. We found that *Idh2*^{R140Q} and *Tet2*$^{-/-}$ cells carrying the *Kdm3b*-targeted sgRNA were nearly absent from the peripheral blood and bone marrow of secondary recipients, while *Idh2*^{R140Q} and *Tet2*$^{-/-}$ cells carrying the *Rosa*-targeted sgRNA robustly outcompeted wild-type cells (**Figure 3.3L-O and Figure 3.4G-H**). We observed similar results in primary and secondary transplants with loss of *Jmjd1c* (**Figure 3.5A-L**). Consistent with our *ex vivo* studies, *Kdm3b* or *Jmjd1c* loss had no effect on the fitness of wild-type cells *in vivo* as

assessed by the stable frequency of *Kdm3b* and *Jmjd1c* sgRNA-carrying cells in the peripheral blood and bone marrow of recipient mice (**Figure 3.3P-Q and Figure 3.5.M-N**).

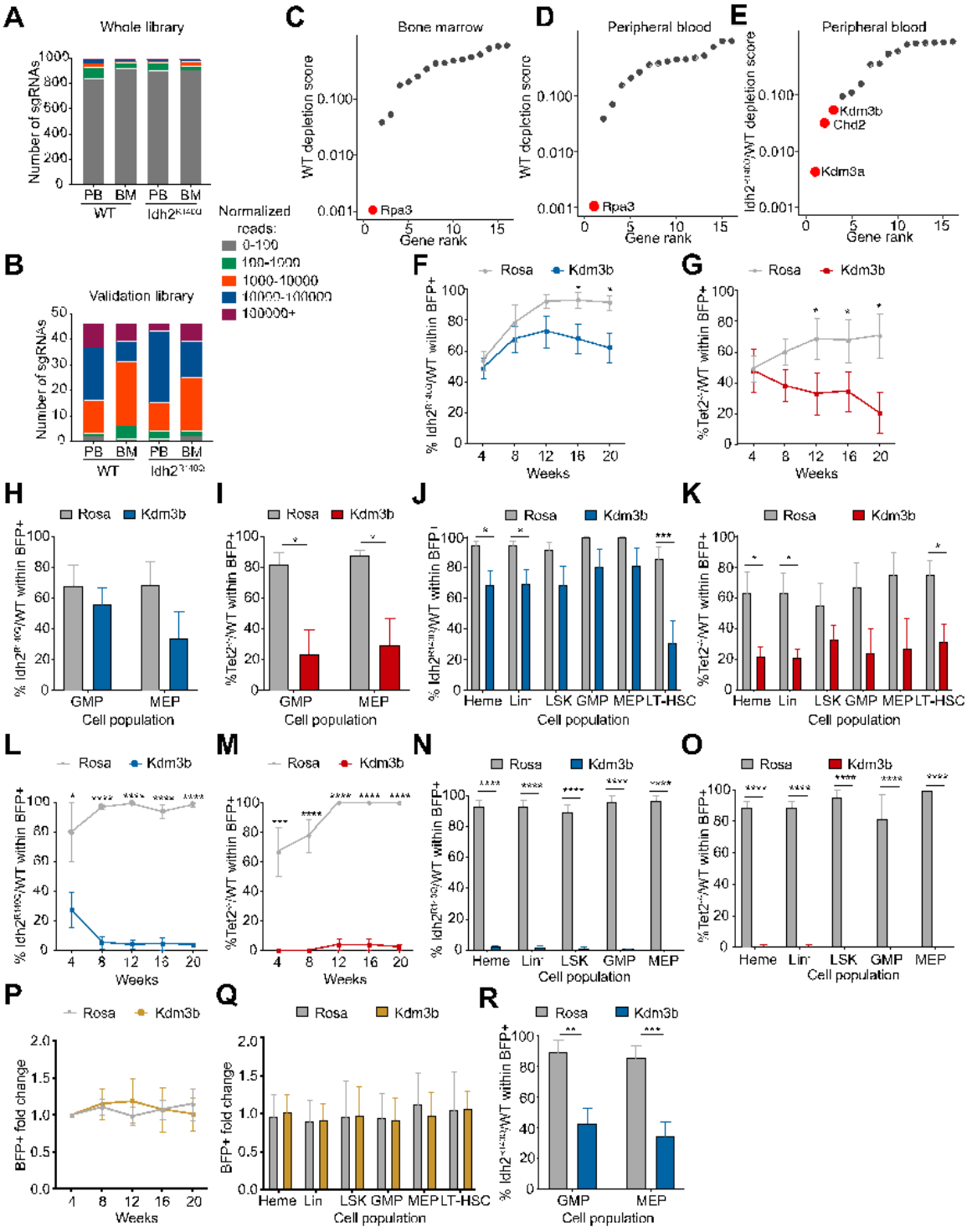

Figure 3.3: *In vivo* validation of *Kdm3b* dependency. A and **B**, Number of sgRNAs detected with the indicated normalized read counts. sgRNA libraries were prepared from the peripheral blood (PB) or bone marrow (BM) of recipient mice engrafted with wild-type or $Idh2^{R140Q}$ cells. Engrafted cells were infected with lentivirus encoding the epigenome library (**A**) or validation library (**B**) (DNA pooled from n = 10 mice). **C** and **D**, Genes with sgRNAs depleted in the bone marrow (**C**) or peripheral blood (**D**) of recipient mice engrafted with wild-type cells infected with lentivirus encoding the validation sgRNA library. (DNA pooled from n = 10 mice). **E**, Genes with depleted sgRNAs in the peripheral blood of recipient mice engrafted with $Idh2^{R140Q}$ cells as compared to wild-type cells. (DNA pooled from n = 10 mice). **F** and **G,** Peripheral blood chimerism of $Idh2^{R140Q}$ (**F**) or $Tet2^{-/-}$ (**G**) within infected cells engrafted in recipient mice. Wild-type and mutant tdT^+ HSPCs were mixed 1:1, infected with a BFP^+ lentivirus encoding a validation sgRNA targeting *Rosa* or *Kdm3b*, and transplanted into recipient mice. (n = 5-8) **H** and **I**, $Idh2^{R140Q}$ (**H**) or $Tet2^{-/-}$ (**I**) chimerism within infected cells in bone marrow compartments of recipient mice. Wild-type and mutant tdT^+ HSPCs were mixed 1:1, infected with a BFP^+ lentivirus encoding an sgRNA targeting *Rosa* or *Kdm3b*, and transplanted into recipient mice. (n = 5-8). **J** and **K,** $Idh2^{R140Q}$ (**J**) or $Tet2^{-/-}$ (**K**) chimerism within infected cells in bone marrow compartments of recipient mice. Wild-type and mutant tdT^+ HSPCs were mixed 1:1, infected with a BFP^+ lentivirus encoding a validation sgRNA targeting *Rosa* or *Kdm3b*, and transplanted into recipient mice. (n = 5-8). **L** and **M**, Peripheral blood chimerism within infected cells of secondary transplant recipient mice engrafted with cells from $Idh2^{R140Q}$ (**L**) or $Tet2^{-/-}$ (**M**) primary transplants from Fig. 3C-F. (n = 5-8). **N** and **O**, $Idh2^{R140Q}$ (**N**) or $Tet2^{-/-}$ (**O**) chimerism within infected cells in bone marrow compartments of recipient mice engrafted with cells from primary transplants from Fig. 3C-F. (n = 5-8). **P,** BFP^+ fold change in the peripheral blood in cells engrafted in recipient mice as normalized to % BFP^+ at the first timepoint. Wild-type HSPCs were infected with a BFP^+ lentivirus encoding an sgRNA targeting *Rosa* or *Kdm3b* and transplanted into recipient mice. (n = 4-8). **Q,** BFP^+ fold change in bone marrow compartments of recipient mice as normalized to % BFP^+ at the first timepoint. Wild-type HSPCs were infected with a BFP^+ lentivirus encoding an sgRNA targeting *Rosa* or *Kdm3b* and transplanted into recipient mice. (n = 4-8). **R,** $Idh2^{R140Q}$ chimerism within infected cells in bone marrow compartments of recipient mice. HSPCs were isolated from wild-type or tdT^+ $Idh2^{R140Q}$-mutant mice, mixed in a 1:1 ratio, infected with a BFP^+ lentivirus encoding a doxycycline-inducible sgRNA, and transplanted into recipient mice. Mice were treated with doxycycline 8 weeks post-transplant. (n = 10-14). All data are mean ± SEM. *p < 0.05, **p < 0.01, ***p < 0.001, ****p < 0.0001

Finally, to assess the effects of *Kdm3b* loss on established clonal dominance, we infected $Idh2^{R140Q}$ and wild-type HSPCs with a BFP^+ lentivirus encoding a doxycycline-inducible sgRNA targeting *Kdm3b* or *Rosa*. After $Idh2^{R140Q}$ cells established clonal dominance at 8 weeks, knock-out of *Kdm3b* or *Rosa* was induced (**Figure 3.4I**).

Loss of *Kdm3b* restrained further outgrowth of *Idh2*^{R140Q} cells in both the peripheral blood and bone marrow of recipient mice, suggesting that *Kdm3b* may be a target in established clonal hematopoiesis (**Figure 3.3R and Figure 3.4J-K**). These data show that *Kdm3b* and *Jmjd1c* represent critical epigenetic dependencies required for the self-renewal of *Idh2*^{R140Q} and *Tet2*$^{-/-}$ mutant HSPCs but not wild-type stem/progenitor cells.

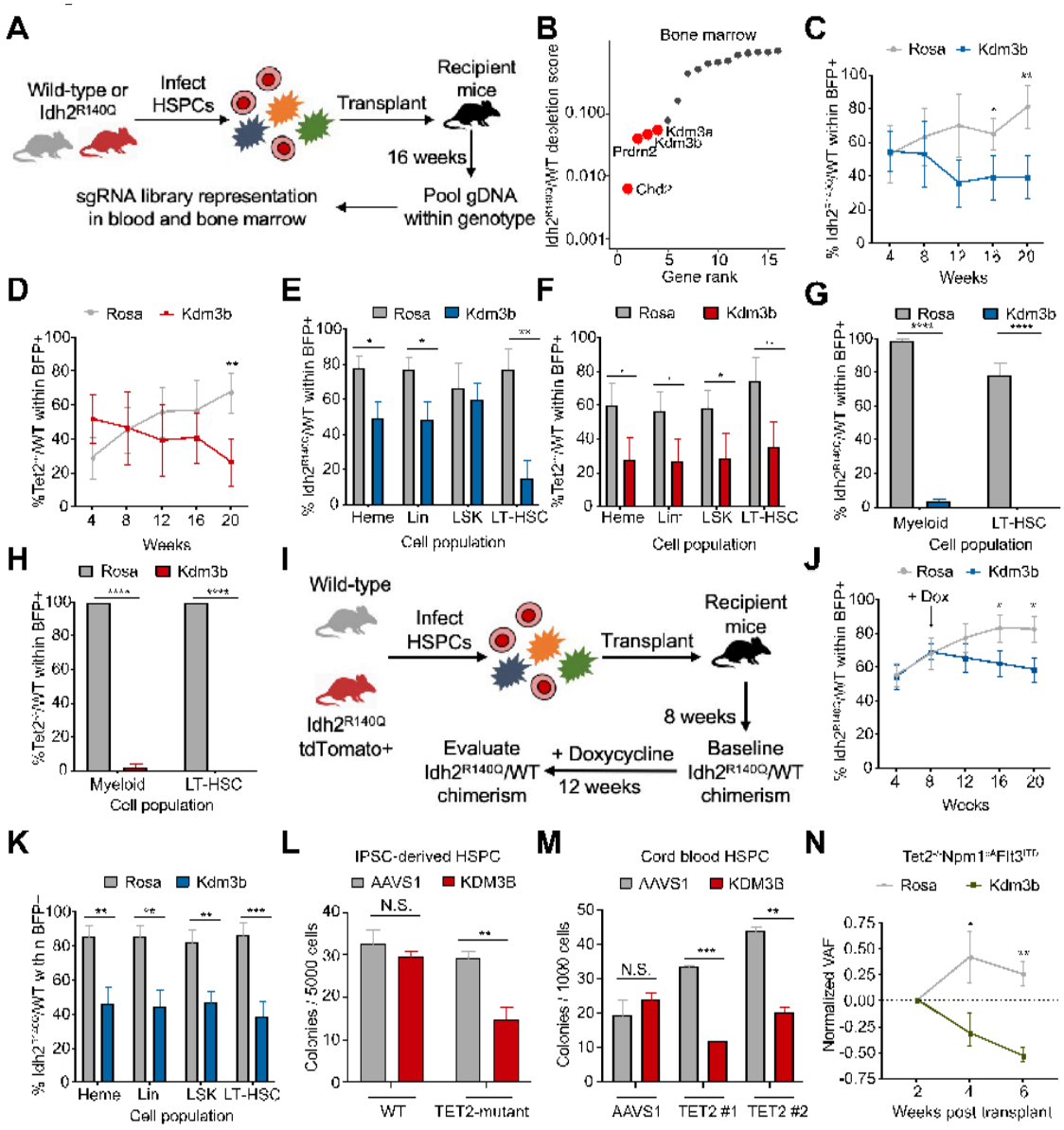

Figure 3.4: *Kdm3b* is a dependency in *Idh2*- and *Tet2*-mutant HSPCs. A, Schematic representation of *in vivo* CRISPR screens. HSPCs from *Idh2*^{R140Q} or WT mice were

infected with a lentivirus encoding a library of sgRNAs targeting dependencies identified in *ex vivo* screens. HSPCs were transplanted and sgRNA abundance was assessed in recipient mice 16 weeks after transplant. **B**, Genes with depleted sgRNAs in the bone marrow of recipient mice engrafted with $Idh2^{R140Q}$ cells as compared to wild-type cells. (DNA pooled from n = 10 mice) **C** and **D**, Peripheral blood chimerism of $Idh2^{R140Q}$ (**C**) or $Tet2^{-/-}$ (**D**) within infected cells engrafted in recipient mice. Wild-type and mutant tdT^+ HSPCs were mixed 1:1, infected with a BFP^+ lentivirus encoding an sgRNA targeting *Rosa* or *Kdm3b*, and transplanted into recipient mice. (n = 5-8) **E** and **F**, $Idh2^{R140Q}$ (**E**) or $Tet2^{-/-}$ (**F**) chimerism within infected cells in bone marrow compartments of recipient mice. Wild-type and mutant tdT^+ HSPCs were mixed 1:1, infected with a BFP^+ lentivirus encoding an sgRNA targeting *Rosa* or *Kdm3b*, and transplanted into recipient mice. (n = 5-8) **G** and **H**, Chimerism within infected myeloid cells in the peripheral blood and LT-HSCs in the bone marrow of recipient mice engrafted with cells from $Idh2^{R140Q}$ (**G**) or $Tet2^{-/-}$ (**H**) primary transplants from Fig. 3C-F. (n = 3-5) **I,** Schematic representation of inducible sgRNA experiments. HSPCs were isolated from wild-type or tdT^+ $Idh2^{R140Q}$-mutant mice, mixed in a 1:1 ratio, infected with a BFP^+ lentivirus encoding a doxycycline-inducible sgRNA, and transplanted into recipient mice. Mice were treated with doxycycline (Dox) 8 weeks post-transplant to induce expression of sgRNAs. Chimerism within infected cells in the peripheral blood and bone marrow of recipient mice was assessed 20 weeks post-transplant. **J,** Peripheral blood chimerism of $Idh2^{R140Q}$ within infected cells engrafted in recipient mice. HSPCs were isolated from wild-type or tdT^+ $Idh2^{R140Q}$-mutant mice, mixed in a 1:1 ratio, infected with a BFP^+ lentivirus encoding a doxycycline-inducible sgRNA, and transplanted into recipient mice. Mice were treated with doxycycline 8 weeks post-transplant as indicated. (n = 10-14) **K,** $Idh2^{R140Q}$ chimerism within infected cells in bone marrow compartments of recipient mice. HSPCs were isolated from wild-type or tdT^+ $Idh2^{R140Q}$-mutant mice, mixed in a 1:1 ratio, infected with a BFP^+ lentivirus encoding a doxycycline-inducible sgRNA, and transplanted into recipient mice. Mice were treated with doxycycline 8 weeks post-transplant. (n = 10-14) **L**, Colony forming assay of wild-type or *TET2*-mutant iPSC-derived HSPCs electroporated with RNPs targeting *AAVS1* or *KDM3B*. Colonies were scored 10 days after plating. (n = 3) **M**, Colony forming assay of cord blood HSPCs sequentially electroporated with sgRNAs against *AAVS1* or *TET2* followed by additional sgRNAs against *AAVS1* or *KDM3B*. Colonies were scored 12 days after plating. (n = 2) **N**, *Rosa* or *Kdm3b* variant allele frequency (VAF) in the peripheral blood of recipient mice engrafted with $Tet2^{-/-}/Npm1^{c}/Flt3^{ITD}$ leukemic cells electroporated with RNPs targeting *Rosa* or *Kdm3b*. (n = 3). VAFs were assessed by NGS and normalized to week 2. All data are mean ± SEM. *p < 0.05, **p < 0.01, ***p < 0.001, ****p < 0.0001

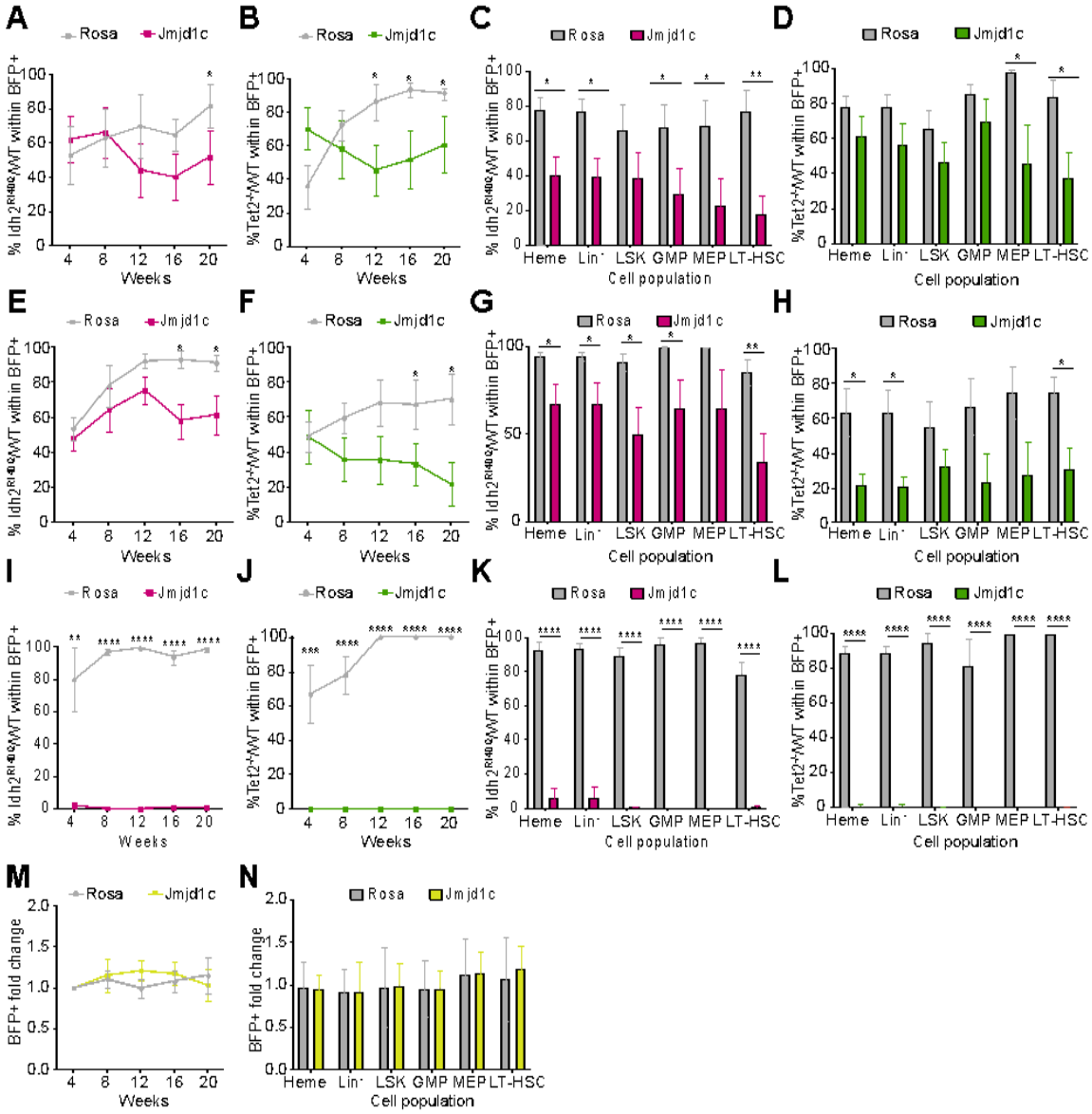

Figure 3.5: *In vivo* validation of *Jmjd1c* dependency. A and **B**, Peripheral blood chimerism of *Idh2*^{R140Q} (**A**) or *Tet2*$^{-/-}$ (**B**) within infected cells engrafted in recipient mice. Wild-type and mutant tdT^{+} HSPCs were mixed 1:1, infected with a BFP^{+} lentivirus encoding an sgRNA targeting *Rosa* or *Jmjd1c*, and transplanted into recipient mice. (n = 5-8) **C** and **D**, *Idh2*^{R140Q} (**C**) or *Tet2*$^{-/-}$ (**D**) chimerism within infected cells in bone marrow compartments of recipient mice. Wild-type and mutant tdT^{+} HSPCs were mixed 1:1, infected with a BFP^{+} lentivirus encoding an sgRNA targeting *Rosa* or *Jmjd1c*, and transplanted into recipient mice. (n = 5-8) **E** and **F,** Peripheral blood chimerism of *Idh2*^{R140Q} (**E**) or *Tet2*$^{-/-}$ (**F**) within infected cells engrafted in recipient mice. Wild-type and mutant tdT^{+} HSPCs were mixed 1:1, infected with a BFP^{+} lentivirus encoding a validation sgRNA targeting *Rosa* or *Jmjd1c*, and transplanted into recipient mice. (n = 5-8) **G** and **H,** *Idh2*^{R140Q} (**G**) or *Tet2*$^{-/-}$ (**H**) chimerism within infected cells in bone marrow compartments of recipient mice. Wild-type and mutant tdT^{+} HSPCs were mixed 1:1,

infected with a BFP$^+$ lentivirus encoding a validation sgRNA targeting *Rosa* or *Jmjd1c*, and transplanted into recipient mice. (n = 5-8) **I** and **J**, Peripheral blood chimerism of *Idh2*^{R140Q} (**I**) or *Tet2*$^{-/-}$ (**J**) within infected cells of secondary transplant recipients engrafted with cells from primary transplants from Supplementary Fig. 5A-D. (n = 5-8) **K** and **L**, *Idh2*^{R140Q} (**K**) or *Tet2*$^{-/-}$ (**L**) chimerism within infected cells in bone marrow compartments of recipient mice engrafted with cells from primary transplants from Supplementary Fig. 5A-D. (n = 5-8). **M,** BFP$^+$ fold change in the peripheral blood in cells engrafted in recipient mice as normalized to % BFP$^+$ at the first timepoint. Wild-type HSPCs were infected with a BFP$^+$ lentivirus encoding an sgRNA targeting *Rosa* or *Jmjd1c* and transplanted into recipient mice. (n = 4-8). **N,** BFP$^+$ fold change in bone marrow compartments of recipient mice as normalized to % BFP$^+$ at the first timepoint. Wild-type HSPCs were infected with a BFP$^+$ lentivirus encoding an sgRNA targeting *Rosa* or *Jmjd1c* and transplanted into recipient mice. (n = 4-8). All data are mean ± SEM. *p < 0.05, **p < 0.01, ***p < 0.001, ****p < 0.0001

Kdm3b is a dependency in CH-mutant human HSPCs and in Tet2-mutant AML

We next sought to delineate whether *KDM3B* and *JMJD1C* are mutant-specific dependencies in human CH-mutant cells. We first assessed the effects of *KDM3B* and *JMJD1C* loss in isogenic *TET2*-mutant and wild-type human iPSC-derived HSPCs. *KDM3B* and *JMJD1C* disruption attenuated the colony-forming potential of *TET2*-mutant HSPCs but not of isogenic *TET2* wild-type HSPCs (**Figure 3.4L and Figure 3.6A-B**). Competition of wild-type and *TET2*-mutant HSPCs in liquid culture demonstrated that *KDM3B* and *JMJD1C* loss both conferred a growth disadvantage to *TET2*-mutant cells, both within the CD34$^+$ HSPC compartment and total hematopoietic output (**Figure 3.6C-D**). *KDM3B* and *JMDJ1C* loss did not affect the growth of wild-type iPSC-derived HSPCs (**Figure 3.6E-F**). We next performed sequential CRISPR editing of *TET2* or the *AAVS1* control locus followed by *KDM3B* editing in human umbilical cord blood HSPCs. *KDM3B* loss led to a decrease in the colony-forming potential of *TET2*-edited HSPCs but not of control *AAVS1*-edited HSPCs in both primary and secondary colony plating assays

(**Figure 3.4M and Figure 3.6G-H**). These results demonstrate *KDM3B* and *JMJD1C* are mutant-specific dependencies in human HSPCs with *TET2* mutations.

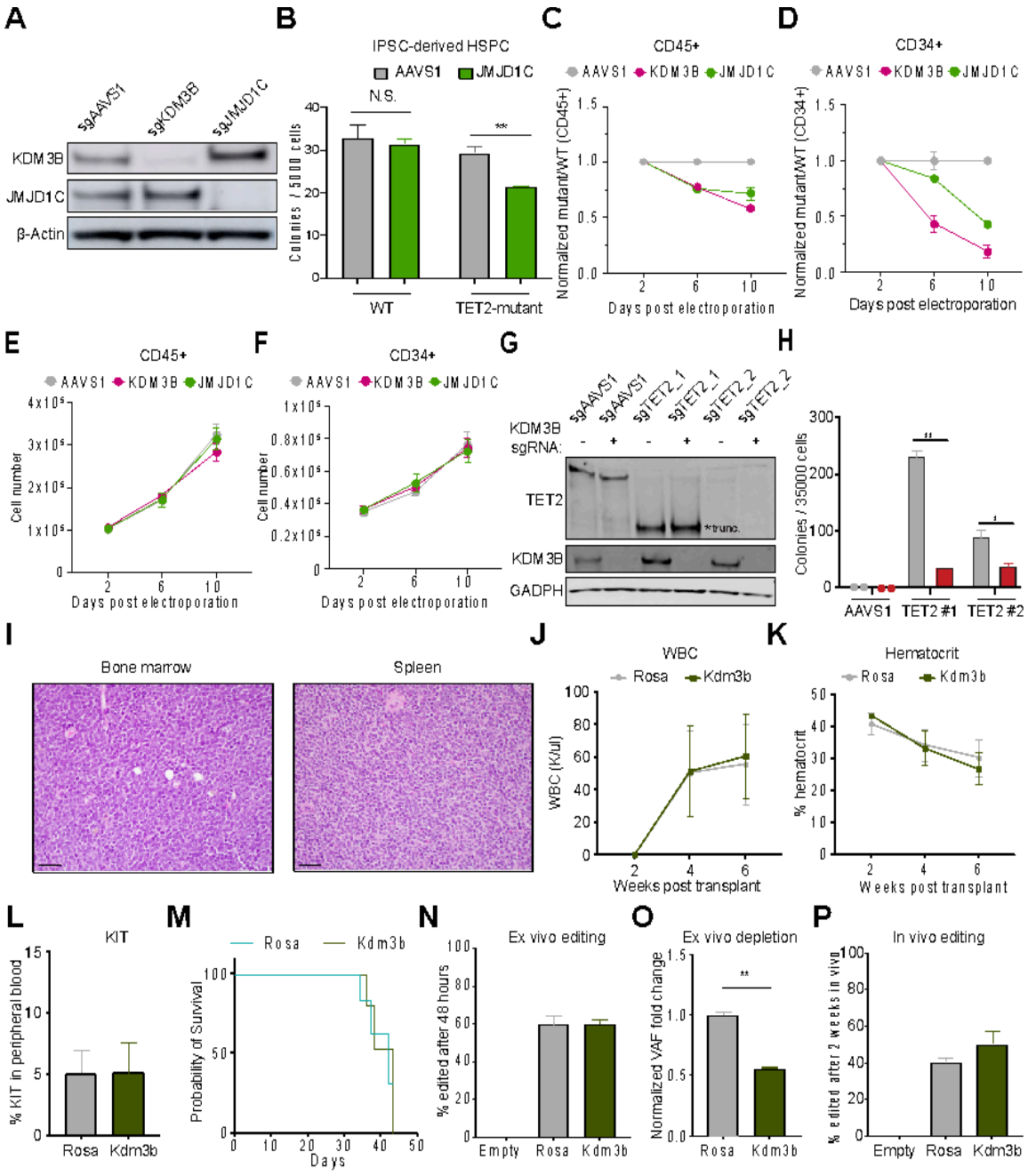

Figure 3.6: Validation of *KDM3B* and *JMJD1C* dependencies in human HSPCs and *Tet2*$^{-/-}$*Npm1*^{cA}*Flt3*^{ITD} leukemia model. A, Western blot showing protein abundance of KDM3B and JMJD1C in iPSC-derived HSPCs electroporated with RNPs targeting *AAVS1*, *KDM3B*, or *JMJD1C*. (Representative of n = 2) **B**, Colony forming assay of wild-type or *TET2*-mutant iPSC-derived HSPCs electroporated with RNPs targeting

AAVS1 or *JMJD1C*. Colonies were scored 10 days after plating. (n = 3) **C** and **D**, *TET2*-mutant to wild-type ratio in $CD45^+$ (**B**) or $CD45^+CD34^+$ (**C**) iPSC-derived hematopoietic cells measured following electroporation of RNPs targeting *AAVS1*, *KDM3B*, or *JMJD1C*. Mutant/wild-type ratio was normalized to the first timepoint and assessed by flow cytometry for GFP^+ (wild-type cells). (n = 3) **E** and **F,** Total cell numbers of wild-type $CD45^+$ or $CD45^+CD34^+$ iPSC-derived hematopoietic cells measured following electroporation of RNPS targeting *AAVS1*, *KDM3B*, or *JMJD1C*. **G,** Western blot showing protein abundance of TET2 and KDM3B in cord blood HSPCs electroporated with RNPs targeting *AAVS1* or *TET2* and *AAVS1* or *KDM3B*. *denotes truncated TET2 protein without its catalytic domain (Representative of n = 2) **H,** Colony forming secondary replating assay of cord blood HSPCs sequentially electroporated with sgRNAs against *AAVS1* or *TET2* followed by additional sgRNAs against *AAVS1* or *KDM3B*. Colonies were scored 12 days after plating. (n = 2) **I,** H&E staining of bone marrow and spleen of $Tet2^{-/-}/Npm1^{cA}/Flt3^{ITD}$ leukemic mice. (Representative of n = 6). All images represented at 400X magnification. Scale bar. 20μm. **J** and **K**, Peripheral blood count trends of white blood cells (WBC) (**J**) or % hematocrit (**K**) in $Tet2^{-/-}/Npm1^{cA}/Flt3^{ITD}$ leukemic mice. (n = 6) **L**, Percentage of KIT^+ cells in the peripheral blood of $Tet2^{-/-}/Npm1^{cA}/Flt3^{ITD}$ leukemic mice as assessed by flow cytometry. (n = 6) **M,** Kaplan-Meier survival analysis of $Tet2^{-/-}/Npm1^{cA}/Flt3^{ITD}$ leukemic mice engrafted with cells electroporated with *Rosa* or *Kdm3b* RNPs. (n = 8) **N**, Percentage of *Rosa*- or *Kdm3b*-edited $Tet2^{-/-}/Npm1^{cA}/Flt3^{ITD}$ leukemic cells 48 hours after electroporation of RNPs. Editing assessed by NGS of amplified sgRNA target sites. Empty control represents Cas9 delivery only and measurement of *Rosa*-edited cells. (n = 2) **O**, Normalized *Rosa* or *Kdm3b* variant allele frequency (VAF) in $Tet2^{-/-}/Npm1^{cA}/Flt3^{ITD}$ leukemic cells measured 10 days after electroporation of RNPs and BMEC co-culture. VAF was normalized to 48 hours after electroporation. (n = 3) **P**, Percentage of *Rosa*- or *Kdm3b*-edited $Tet2^{-/-}/Npm1^{cA}/Flt3^{ITD}$ leukemic cells in the peripheral blood of recipient mice measured 2 weeks after transplant of electroporated cells. Editing assessed by NGS of amplified sgRNA target sites. Empty control represents Cas9 delivery only and measurement of *Rosa*-edited cells. (n = 2). All data are mean ± SEM. *$p < 0.05$, **$p < 0.01$

Kdm3b is a dependency in CH-mutant human HSPCs in Tet2-mutant AML

We then asked if the dependency of *Kdm3b* in *Idh2*- and *Tet2*-mutant pre-malignant cells would extend to transformed leukemic cells with *Idh2* or *Tet2* mutations. Previously, we have demonstrated that mice harboring a combination of $Tet2^{-/-}$ and $Flt3^{ITD}$ mutations develop a long-latency AML[185]. We crossed an $Npm1^{cA}$ allele to this model to generate a rapid and lethal AML, which was characterized by leukocytosis, anemia, Kit^+ cells in the peripheral blood, and infiltration of the bone marrow and spleen

by immature blasts (**Figure 3.6I-M**). Since leukemic cells bearing this allelic combination did not express Cas9, we electroporated Cas9/sgRNA ribonucleoproteins (RNPs) targeting *Rosa* or *Kdm3b*. We confirmed that delivery of RNPs targeting *Rosa* and *Kdm3b* achieved ~50% editing frequency (**Figure 3.6N**). We observed that *Rosa*-edited cells were maintained at a steady frequency during *ex vivo* culture while *Kdm3b*-edited cells were depleted (**Figure 3.6O**). To assess the requirement for *Kdm3b* in *Tet2*-mutant leukemia *in vivo*, we transplanted *Rosa*- or *Kdm3b*-edited leukemic blasts and tracked the frequency of edited cells in the peripheral blood of recipient mice. Edited cells demonstrated engraftment capacity as assessed at the initial 2-week timepoint *in vivo* (**Figure 3.6P**). We found that *Kdm3b*-edited cells, but not *Rosa*-edited cells, were progressively depleted from the peripheral blood of leukemic mice (**Figure 3.4N**). We conclude that loss of *Kdm3b* reduces the fitness of *Tet2*-mutant AML cells *in vivo*.

2-HG production is necessary and sufficient to confer Kdm3b dependency in HSPCs

Mutations in *IDH2*, which catalyzes the conversion of isocitrate to α-KG, result in neomorphic production of 2-HG, leading to inhibition of TET2 and other α-KG dependent enzymes[132,134,204,205]. We therefore investigated whether the *Kdm3b* dependency in *Idh2*-mutant cells is 2-HG dependent. We treated wild-type HSPCs carrying sgRNAs targeting *Rosa* or *Kdm3b* with cell-permeable 2-HG to assess whether 2-HG could render wild-type cells dependent on *Kdm3b*. 2-HG treatment did not affect cell growth and did not alter the fitness of HSPCs transduced with a *Rosa* sgRNA (**Figure 3.7A**). By contrast, 2-HG treatment resulted in depletion of lineage$^-$, LSK, and mature myeloid cells carrying a *Kdm3b* sgRNA (**Figure 3.7B and Figure 3.8A-B**). Treatment of *Idh2*^{R140Q} HSPCs with

2-HG further enhanced the dependency of mutant cells on *Kdm3b* (**Figure 3.7C-E**). These findings suggest that 2-HG production is sufficient to render HSPCs dependent on *Kdm3b*.

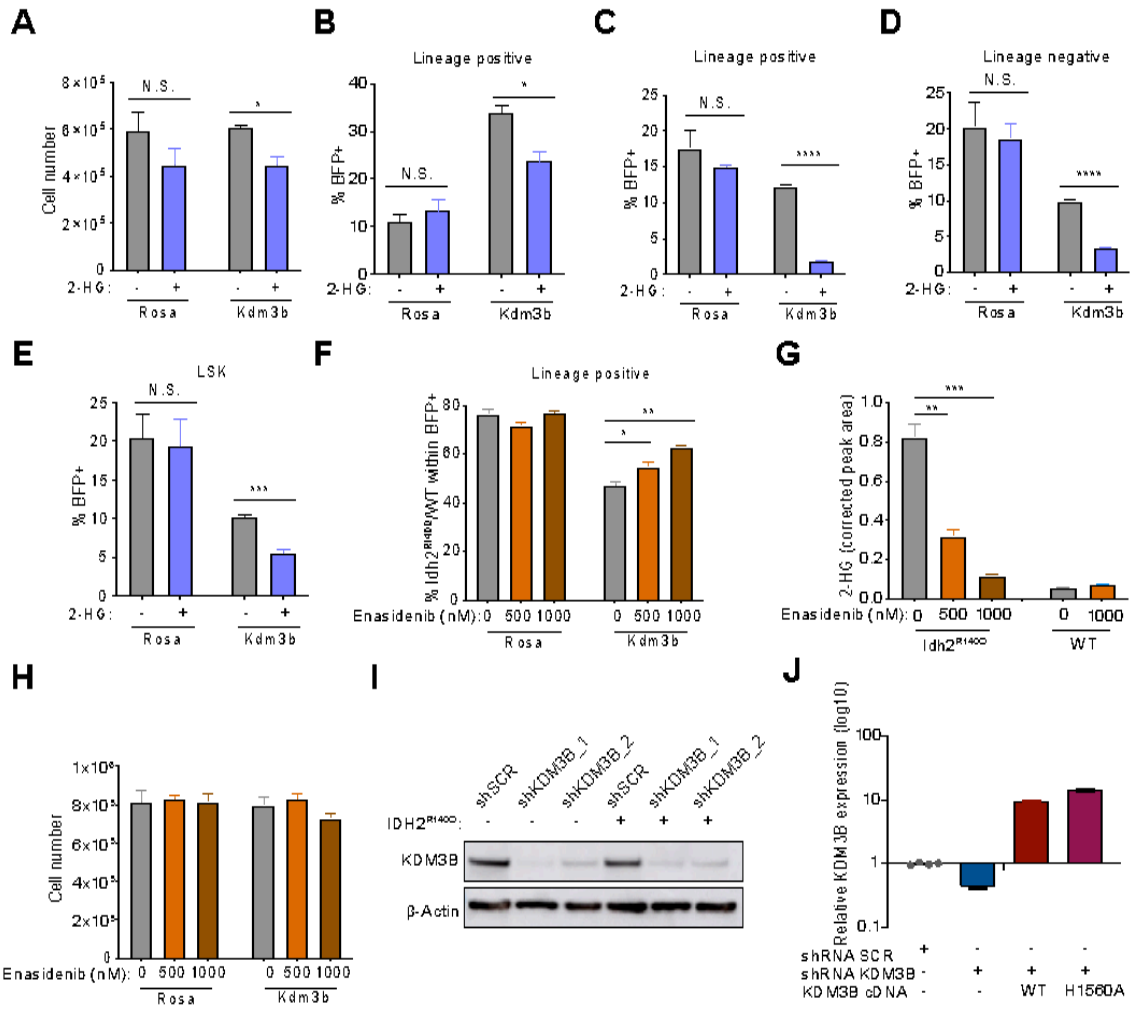

Figure 3.7: Role of 2-HG and KDM3B catalytic activity in *KDM3B* dependency. A, Cell growth measured 14 days after *Rosa* or *Kdm3b* sgRNA delivery in wild-type HSPCs. HSPCs were co-cultured with BMECs and treated with vehicle or 500 μM 2-HG. (n = 3) **B**, Flow cytometry measurement of BFP$^+$ wild-type lineage$^+$ cells measured after 14 days of BMEC/HSPC co-culture. Wild-type HSPCs were infected with a BFP$^+$ lentivirus encoding an sgRNA targeting *Rosa* or *Kdm3b* and treated with vehicle or 500 μM 2-HG. (n = 3) **C-E**, Flow cytometry measurement of BFP$^+$ *Idh2*^{R140Q} lineage$^+$ (**C**), lineage$^-$ (**D**) or LSK (**E**) cells measured after 14 days of BMEC/HSPC co-culture. *Idh2*^{R140Q} HSPCs were infected with a BFP$^+$ lentivirus encoding an sgRNA targeting *Rosa* or *Kdm3b* and treated with vehicle or 500 μM 2-HG. (n = 3) **F**, *Idh2*^{R140Q} tdT$^+$ chimerism in lineage$^+$ infected cells measured by flow cytometry after 14 days of BMEC/HSPC co-culture. Wild-type and *Idh2*^{R140Q} tdT$^+$ HSPCs were mixed 1:1, infected with a BFP$^+$ lentivirus encoding an

sgRNA targeting *Rosa* or *Kdm3b*, and treated with increasing doses of enasidenib. (n = 3) **G**, 2-HG levels as assessed by mass spectrometry in wild-type or *Idh2*^{R140Q} cells treated with increasing doses of enasidenib. Cells were co-cultured with BMECs for 14 days. (n = 3) **H**, Cell growth measured 14 days after *Rosa* or *Kdm3b* sgRNA delivery in HSPCs. HSPCs were co-cultured with BMECs and treated with increasing doses of enasidenib. (n = 3) **I**, Western blot showing protein abundance of KDM3B in TF-1 cells infected with lentivirus encoding single shRNAs targeting *SCR* or *KDM3B*. (Representative of n = 2) **J**, Relative *KDM3B* expression as assessed by quantitative polymerase-chain reaction in TF-1 cells infected with lentivirus encoding the indicated shRNA and/or cDNA. (n = 4). All data are mean ± SEM. *p < 0.05, **p < 0.01, ***p < 0.001, ****p < 0.0001

Conversely, treatment of wild-type and *Idh2*^{R140Q} HSPCs with the IDH2 inhibitor enasidenib reversed the mutant-specific effect of *Kdm3b* depletion on the fitness of *Idh2*^{R140Q} lineage^{-}, LSK, and mature myeloid cells (**Figure 3.7F and Figure 3.8C-D**). Treatment with enasidenib resulted in a dose-dependent reduction in 2-HG levels in *Idh2*^{R140Q} HSPCs co-cultured with BMECs, as has previously been shown in other contexts, but did not affect cell growth or alter *Idh2*^{R140Q} chimerism in the *Rosa* control (**Figure 3.7G-H**)[136,137]. These findings demonstrate that 2-HG production by mutant IDH2 confers *Kdm3b* dependency in *Idh2*-mutant HSPCs.

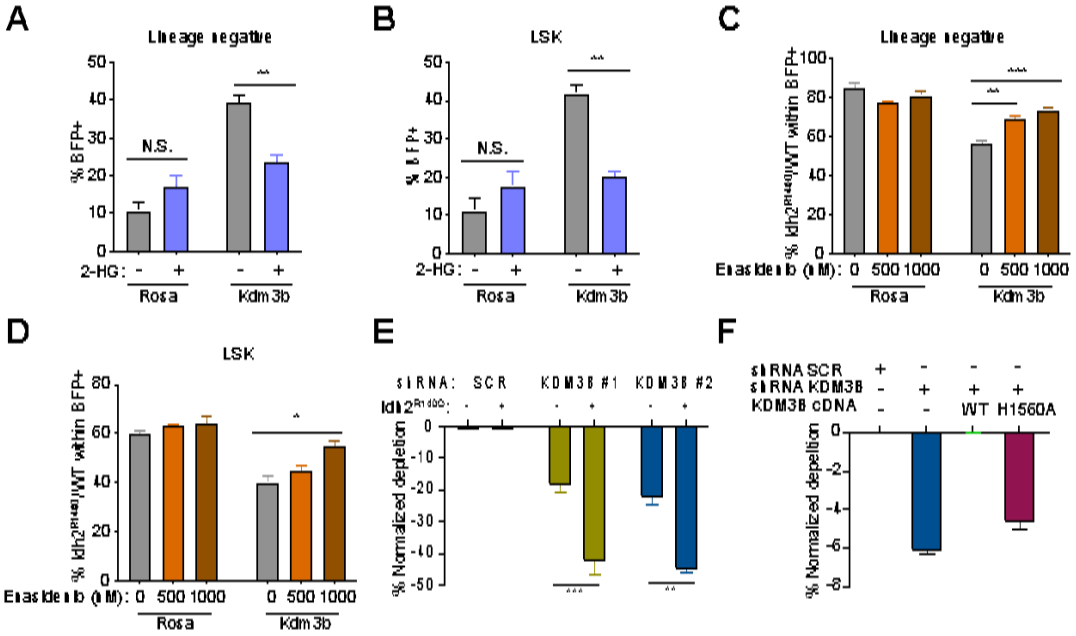

Figure 3.8: *Kdm3b* vulnerability in *Idh2*-mutant cells is dependent on 2-HG and loss of KDM3B enzymatic activity. A and **B**, Flow cytometry measurement of BFP^+ infected wild-type $lineage^-$ (**A**) or LSK (**B**) cells measured after 14 days of BMEC/HSPC co-culture. Wild-type HSPCs were infected with a BFP^+ lentivirus encoding an sgRNA targeting *Rosa* or *Kdm3b* and treated with vehicle or 500 μM 2-HG. (n = 3) **C** and **D**, $Idh2^{R140Q}$ tdT^+ chimerism as measured by flow cytometry in $lineage^-$ (**C**) or LSK (**D**) infected cells measured after 14 days of BMEC/HSPC co-culture. Wild-type and $Idh2^{R140Q}$ tdT^+ HSPCs were mixed 1:1, infected with a BFP^+ lentivirus encoding an sgRNA targeting *Rosa* or *Kdm3b*, and treated with increasing doses of enasidenib. (n = 3) (**E**) Depletion of BFP^+ shRNAs targeting *KDM3B* or scrambled (*SCR*) control in TF-1 cells isogenic for the *IDH2 R140Q* mutation. Measured as % BFP^+ by flow cytometry 14 days after infection and normalized to % BFP+ 2 days after infection. (n = 3) (**F**) Depletion of BFP^+ shRNAs targeting *KDM3B* or scrambled (*SCR*) control within TF-1 cells isogenic for the *IDH2 R140Q* mutation and carrying the indicated $NGFR^+$ cDNA. Measured as % BFP^+NGFR^+ by flow cytometry 14 days after infection and normalized to % BFP^+NGFR^+ by flow cytometry 14 days after infection. (n = 3). All data are mean ± SEM. *p < 0.05, **p < 0.01, ***p < 0.001

KDM3B enzymatic activity is required in IDH2-mutant cells

We next asked if the *Idh2*-mutant requirement for *Kdm3b* is dependent on the catalytic activity of KDM3B. To test this, we utilized TF-1 erythroleukemia cell lines isogenic for the $IDH2^{R140Q}$ mutation, a model which has been used extensively to assess the function of *IDH2* mutations[137,206]. To determine if *KDM3B* is a dependency in these cell lines, we performed genetic knockdown (KD) experiments using BFP^+ shRNAs targeting *KDM3B* or scrambled control (*SCR*). We confirmed that *KDM3B* shRNAs led to efficient knockdown of *KDM3B* in this hyperdiploid cell line (**Figure 3.7I**). We observed that shRNAs targeting *KDM3B*, but not *SCR*, were depleted in TF-1 cells following culture. TF-1 cells without an *IDH2* mutation ($TF\text{-}1^{WT}$) showed modest sensitivity to *KDM3B* KD, which was enhanced in TF-1 cells with the $IDH2^{R140Q}$ mutation ($TF\text{-}1^{IDH2\text{-}R140Q}$) (Fig. 4E). We then performed genetic rescue experiments by overexpressing wild-type KDM3B or KDM3B with a p.H1560A mutation

(KDM3B-H1560A) that has previously been shown to abrogate KDM3B catalytic demethylase activity[207]. We confirmed expression of wild-type KDM3B and KDM3B-H1560A (**Figure 3.7J**). Only wild-type KDM3B was able to rescue the loss of fitness conferred by *KDM3B*-targeted shRNAs in TF-1$^{IDH2\text{-}R140Q}$ cells, whereas expression of KDM3B-H1560A had no effect (**Figure 3.8F**). We conclude that KDM3B enzymatic activity is required in *IDH2*-mutant cells.

KDM3B **and mutant** ***IDH2*** **coordinately regulate the epigenetic and transcriptomic state of common loci including cytokine receptors**

We next performed RNA-sequencing (RNA-seq) on TF-1^{WT} cells and TF-1$^{IDH2\text{-}R140Q}$ cells expressing shRNAs targeting *KDM3B* or scrambled control (*SCR*). Gene set enrichment analysis revealed that TF-1$^{IDH2\text{-}R140Q}$ cells with *KDM3B* KD had increased expression of gene sets associated with apoptosis and decreased expression of gene sets associated with cell-cycle regulation as compared to TF-1$^{IDH2\text{-}R140Q}$ cells with *SCR* KD, consistent with our results demonstrating subsequent depletion of *KDM3B* KD cells (**Figure 3.9A-B**). We observed a significant overlap of transcriptional changes induced by *KDM3B* knockdown (*KDM3B* KD TF-1$^{IDH2\text{-}R140Q}$ vs *SCR* KD TF-1$^{IDH2\text{-}R140Q}$) as we did by introduction of the *IDH2*^{R140Q} mutation (TF-1$^{IDH2\text{-}R140Q}$ vs TF-1^{WT}; **Figure 3.9C-D**). To investigate whether the mutant *IDH2* allele and *KDM3B* KD were coordinately regulating a shared set of loci, we calculated single sample gene set enrichment analysis (ssGSEA) scores using the set of genes downregulated in *KDM3B* KD TF-1$^{IDH2\text{-}R140Q}$ cells compared to *SCR* KD TF-1$^{IDH2\text{-}R140Q}$ cells. ssGSEA is an extension of the GSEA method and is commonly used to calculate individual sample scores that

reflect the degree to which genes in a particular gene set are enriched[208]. This analysis revealed that *SCR* KD TF-1$^{IDH2\text{-}R140Q}$ cells had a significant reduction in shared gene set expression compared to *SCR* KD TF-1^{WT} cells, with increased attenuation in the expression of these genes in *KDM3B* KD TF-1$^{IDH2\text{-}R140Q}$ cells (**Figure 3.9E**). We observed a similar pattern for the gene set upregulated in *KDM3B* KD TF-1$^{IDH2\text{-}R140Q}$ cells (**Figure 3.9F**).

RNA-seq on HSPCs from wild-type or *Idh2*^{R140Q} mice carrying *Rosa*- or *Kdm3b*-targeting sgRNAs confirmed that a majority of the transcriptional changes in *Idh2*^{R140Q} cells with loss of *Kdm3b* were also found in HSPCs with either the *Idh2 R140Q* mutation or *Kdm3b* loss alone (**Figure 3.10A**). ssGSEA analysis of the gene set downregulated in *Idh2*^{R140Q} cells with loss of *Kdm3b* demonstrated that either the *Idh2*^{R140Q} mutation or *Kdm3b* loss alone resulted in downregulated expression of these genes, with the combination of mutations resulting in the strongest transcriptional suppression (**Figure 3.10B**). Our findings suggest that *KDM3B* and the *IDH2* mutation coordinately regulate the transcriptional output of a distinct set of genes, with the greatest changes in cells with concurrent *IDH2* neomorphic function and *KDM3B* disruption.

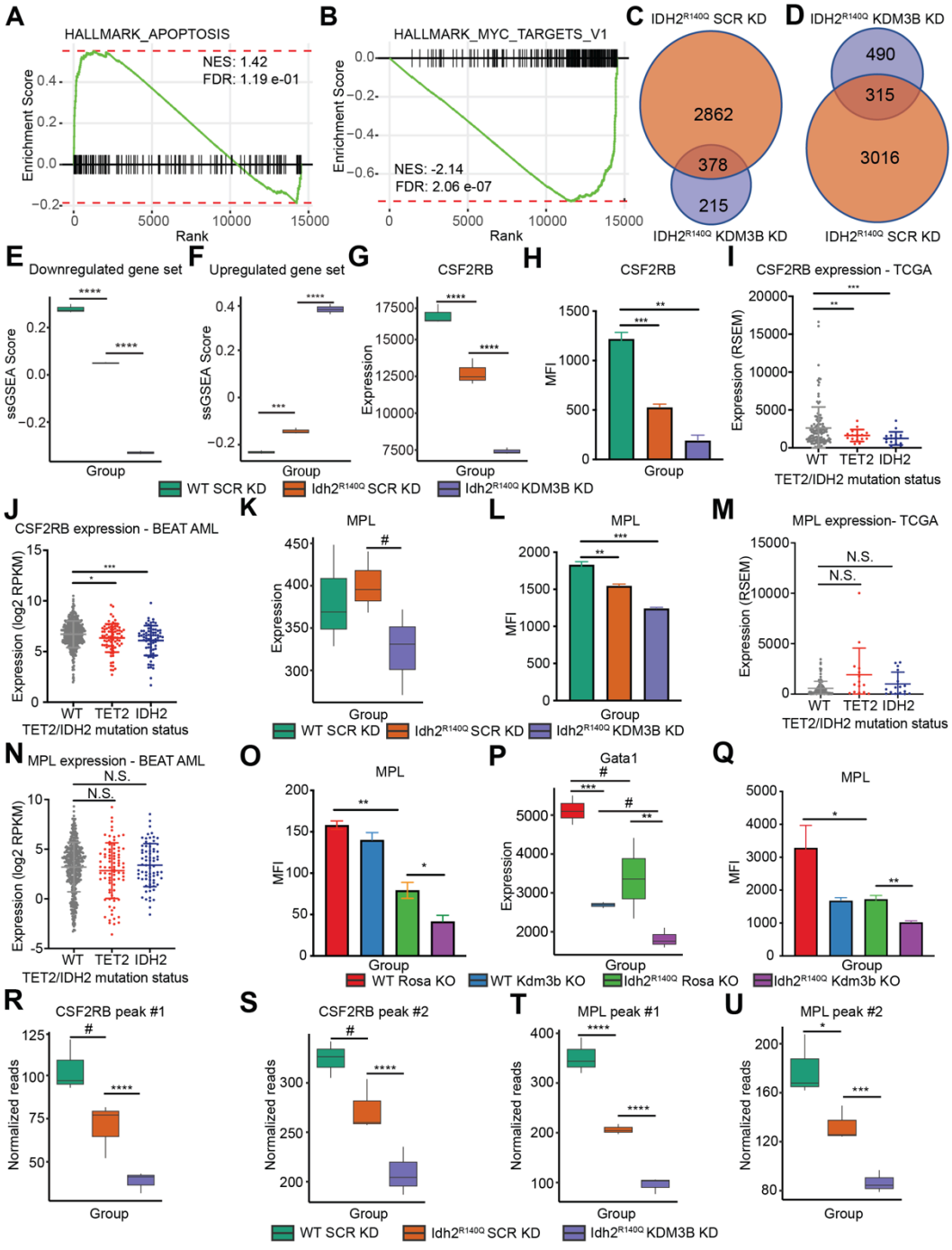

Figure 3.9: Chromatin and transcriptional changes mediated by *KDM3B*. **A** and **B**, GSEA plots depicting a positive enrichment in apoptotic targets (**A**) and a negative enrichment in MYC targets (**B**) in *KDM3B* KD *IDH2 R140Q* mutant TF-1 cells as compared to *SCR* KD *IDH2 R140Q* mutant TF-1 cells. **C** and **D**, Venn diagrams displaying the overlap of genes downregulated (**C**) or upregulated (**D**) between the indicated contrasts (*KDM3B* KD *IDH2 R140Q* TF-1 compared to *SCR* KD *IDH2 R140Q* TF-1 and *SCR* KD *IDH2 R140Q* TF-1 vs *SCR* KD WT TF-1). **E** and **F**, ssGSEA scores of

the gene set derived from downregulated (**E**) or upregulated (**F**) genes in *KDM3B* KD *IDH2 R140Q* TF-1 cells as compared to *SCR* KD *IDH2 R140Q* TF-1 cells. (n = 3) **G,** *CSF2RB* expression in TF-1 cells in the indicated groups by RNA-seq data. (n = 3) **H,** CSF2RB MFI as measured by flow cytometry in TF-1 cells in the indicated groups. TF-1 cells were infected with a lentivirus encoding a single shRNA targeting *SCR* or *KDM3B*. (n = 3) **I** and **J**, *CSF2RB* expression in primary AML samples from TCGA (**I**) or BEAT-AML (**J**) cohorts with the indicated *TET2* or *IDH2* mutations. **K,** *MPL* expression in TF-1 cells in the indicated groups by RNA-seq data. (n = 3) **L,** MPL MFI as measured by flow cytometry in TF-1 cells in the indicated groups. TF-1 cells were infected with a lentivirus encoding a single shRNA targeting *SCR* or *KDM3B*. (n = 3) **M** and **N,** *MPL* expression in primary AML samples from TCGA (**M**) or BEAT-AML (**N**) cohorts with the indicated *TET2* or *IDH2* mutations. **O,** MPL MFI as measured by flow cytometry in lineage$^-$Kit$^+$ infected cells measured after 7 days of BMEC/HSPC co-culture. Wild-type and *Idh2*^{R140Q} HSPCs were infected with a BFP$^+$ lentivirus encoding an sgRNA targeting *Rosa* or *Kdm3b*. (n = 3) **P,** Normalized expression of *Gata1* in primary HSPCs in the indicated groups as extracted from RNA-seq data. (n = 3). **Q,** MPL MFI as measured by flow cytometry in cord blood HSPCs 10 days following infection with lentivirus encoding *IDH2* wild-type or *IDH2 R140Q* cDNA and electroporation of *AAVS1* or *KDM3B* RNPs. (n = 3) **R**-**U**, Normalized ATAC-seq signal in TF-1 cells of peaks at *CSF2RB* (**R** and **S**) or *MPL* (**T** and **U**) in the indicated groups. All data are mean ± SEM. *p < 0.05, **p < 0.01, ***p < 0.001, ****p < 0.0001, #FDR < 0.1

We therefore hypothesized that *IDH2*-mutant cells might be deleteriously impacted by the additional effects of *KDM3B* loss of function on the expression of key genes critical for survival. In the TF-1 context, we noted that *CSF2RB*, which encodes the common beta chain subunit of the receptor for GM-CSF, IL-3, and IL-5 and is the essential receptor upstream of JAK/STAT signaling in TF-1 cells, was downregulated in cells expressing *IDH2*^{R140Q} and further downregulated with *KDM3B* knockdown (**Figure 3.9G-H**)[209]. In primary AML patient samples, expression of *CSF2RB* is significantly reduced in *TET2*- and *IDH2*-mutant samples in both the TCGA and BEAT-AML cohorts (**Figure 3.9I-J**). We also observed that the thrombopoietin receptor *MPL*, which has relatively low expression in transformed TF-1 cells, was downregulated with *KDM3B* knockdown (**Figure 3.9K-L**). *MPL* had low or no expression in the majority of samples in the TCGA and BEAT-AML cohorts and its expression was not further decreased in

TET2- or *IDH2*-mutant samples (**Figure 3.9M-N**). Within primary HSPCs, *Csf2rb* is highly expressed on myeloid progenitors but dispensable for hematopoietic stem cells, while *Mpl* is highly expressed and critical to the self-renewal activity of LT-HSCs[210-212]. We observed that *Mpl* expression was downregulated with the *Idh2* mutation or *Kdm3b* loss alone and more significantly downregulated in $Idh2^{R140Q}$ cells with concurrent *Kdm3b* loss (**Figure 3.9O and Figure 3.10C**). *Gata1*, which functions downstream of *Mpl*, also followed a similar expression pattern (**Figure 3.9P**). We observed a similar expression profile of MPL in human cord blood HSPCs to that seen in murine HSPCs (**Figure 3.9Q**). Consistent with prior studies, we did not detect *CSF2RB* expression in murine- or human-derived hematopoietic stem cells (data not shown)[213-215]. Taken together, our data suggests that the *IDH2* mutation and *KDM3B* regulate the expression of critical cytokine receptors that mediate downstream JAK/STAT signaling, with the specific receptors expressed and regulated dependent on cellular context.

To evaluate whether these loci are coordinately regulated by the mutant *IDH2* allele and *KDM3B* at the chromatin level, we performed assays for transposase-accessible chromatin with high throughput sequencing (ATAC-seq) on TF-1^{WT} cells and TF-$1^{IDH2\text{-}R140Q}$ cells expressing shRNAs targeting *KDM3B* or scrambled control (*SCR*). Loci linked to genes with decreased expression in *KDM3B* KD TF-$1^{IDH2\text{-}R140Q}$ cells had the lowest chromatin accessibility in *KDM3B* KD TF-$1^{IDH2\text{-}R140Q}$ cells and intermediate accessibility in *SCR* KD TF-$1^{IDH2\text{-}R140Q}$ cells (**Figure 3.10D**). Among these, the *CSF2RB* locus displayed decreased chromatin accessibility with expression of the *IDH2* mutation and a further reduction in chromatin accessibility with *KDM3B* knockdown (**Figure 3.9R-S and Figure 3.10E).** Interestingly, the *MPL* locus also demonstrated a similar

accessibility profile to the *CSF2RB* locus despite low expression of *MPL* in TF-1 cells, suggesting epigenetic regulation of the *MPL* locus is altered by the *IDH2* mutation and *KDM3B* even at lower levels of transcriptional output (**Figure 3.9T-U and Figure 3.10E**). Our findings suggest that *KDM3B* and the *IDH2* mutation cooperate at the chromatin level to modulate accessibility and resultant transcription of a shared set of target genes including critical cytokine receptors.

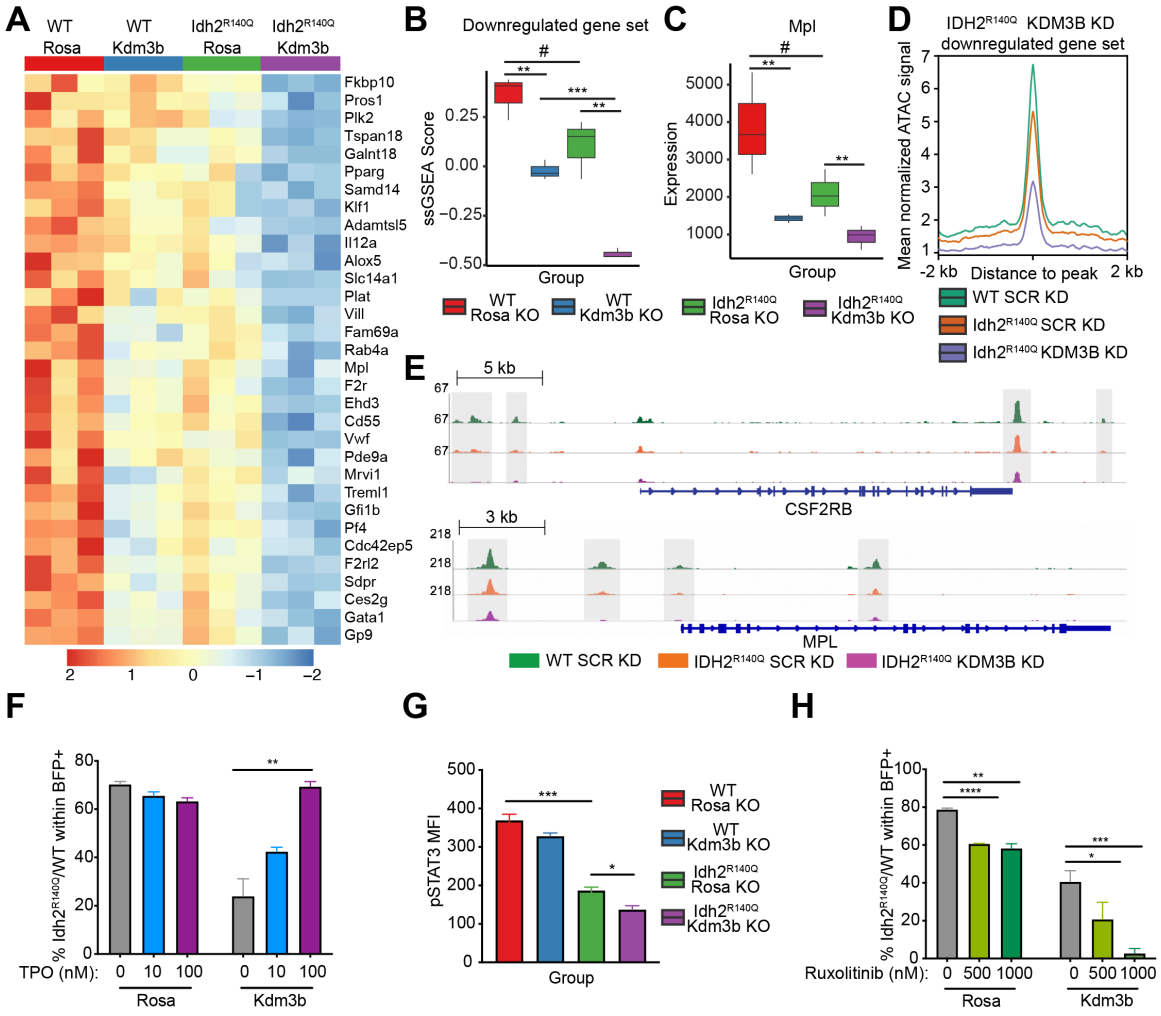

Figure 3.10: *KDM3B* regulates the expression of critical cytokine receptors in *IDH2*-mutant cells. A, Heatmap showing relative gene expression of differentially expressed genes in *Kdm3b* KO *Idh2*^{R140Q} HSPCs as compared to *Rosa* KO wild-type HSPCs. Denoted groups shown are wild-type or *Idh2*^{R140Q} HSPCs with *Rosa* or *Kdm3b* KO. **B**, ssGSEA scores of the gene set derived from downregulated genes in *Kdm3b* KO

Idh2^{R140Q} HSPCs. (n = 3) **C**, *Mpl* expression in primary HSPCs in the indicated groups by RNA-seq data. (n = 3) **D,** Mean normalized ATAC-seq signal at genes with decreased expression in *KDM3B* KD *IDH2 R140Q* TF-1 cells. **E**, Normalized ATAC-seq signal in TF-1 cells on surrounding loci at *CSF2RB* and *MPL*. **F**, *Idh2*^{R140Q} tdT^{+} chimerism as measured by flow cytometry in LSK infected cells measured after 14 days of BMEC/HSPC co-culture. Wild-type and *Idh2*^{R140Q} tdT^{+} HSPCs were mixed 1:1, infected with a BFP^{+} lentivirus encoding an sgRNA targeting *Rosa* or *Kdm3b*, and treated with increasing doses of TPO. (n = 3) **G**, Median fluorescent intensity (MFI) of phospho-STAT3 (pSTAT3) as measured by flow cytometry in lineage^{-}Kit^{+} infected cells measured after 7 days of BMEC/HSPC co-culture. Wild-type and *Idh2*^{R140Q} HSPCs were infected with a BFP^{+} lentivirus encoding an sgRNA targeting *Rosa* or *Kdm3b*. (n = 3) **H**, *Idh2*^{R140Q} tdT^{+} chimerism as measured by flow cytometry in LSK infected cells measured after 14 days of BMEC/HSPC co-culture. Wild-type and *Idh2*^{R140Q} tdT^{+} HSPCs were mixed 1:1, infected with a BFP^{+} lentivirus encoding an sgRNA targeting *Rosa* or *Kdm3b*, and treated with increasing doses of ruxolitinib. (n = 3). All data are mean ± SEM. *p < 0.05, **p < 0.01, ***p < 0.001, ****p < 0.0001, #FDR < 0.1

KDM3B disruption accentuates dependency on JAK-mediated cytokine receptor signaling in IDH2-mutant cells

We next hypothesized that reduced cytokine receptor signaling is a dependency in *IDH2*-mutant cells and that this dependency is further accentuated by reduced KDM3B activity. We first investigated whether increased ligand-mediated receptor activation could rescue the *KDM3B* dependency in TF-1$^{IDH2\text{-}R140Q}$ cells. We observed that treatment of TF-1$^{IDH2\text{-}R140Q}$ cells with the CSF2RB ligands GM-CSF and IL-3 reversed the deleterious effect of *KDM3B* disruption on mutant cell fitness (**Figure 3.11A**). To assess whether low levels of *Mpl* were responsible for the competitive disadvantage of primary *Idh2*^{R140Q} HSPCs with *Kdm3b* loss, we competitively cultured *Idh2*^{R140Q} and wild-type HSPCs carrying sgRNAs targeting *Rosa* or *Kdm3b* and treated them with increasing concentrations of TPO. As previously described, TPO treatment increased total cell numbers and the frequency of MEPs (**Figure 3.11B-C**)[216]. TPO treatment did not alter the competitive fitness of *Rosa*-carrying *Idh2*^{R140Q} cells but showed a dose-dependent reversal

of the effect of *Kdm3b* depletion on the relative fitness of *Idh2*^{R140Q} lineage^{-}, LSK and mature cells (**Figure 3.10F and Figure 3.11D-E**). GM-CSF was unable to rescue the *Kdm3b* depletion in *Idh2*^{R140Q} HSPCs, consistent with the lack of *Csf2rb* expression in hematopoietic stem cells and the stem-cell-specific essentiality of *Kdm3b* in *Idh2*^{R140Q} cells (**Figure 3.11F-I**).

JAK kinases, most notably JAK2, are the signaling kinases that activate cytokine-mediated transduction pathways[217]. JAK/STAT signaling was decreased in *Idh2*^{R140Q} HSPCs and further suppressed in *Idh2*^{R140Q} HSPCs with *Kdm3b* loss, paralleling the expression pattern of *Mpl* in these cells (**Figure 3.10G**). TPO treatment was sufficient to restore JAK/STAT signaling in *Idh2*^{R140Q} HSPCs with *Kdm3b* loss, consistent with its ability to functionally rescue *Kdm3b* depletion in *Idh2*^{R140Q} cells (**Figure 3.11J**). We next investigated whether *Idh2*^{R140Q} HSPCs would have increased sensitivity to JAK kinase inhibition. We used the chimerism assay to test the effect of increasing doses of the JAK1/2 inhibitor ruxolitinib on *Idh2*^{R140Q} versus wild-type HSPCs harboring either *Rosa* or *Kdm3b* sgRNAs. Treatment with ruxolitinib reduced *Idh2*^{R140Q} chimerism in *Rosa* control lineage^{-}, LSK, and mature myeloid cells, with an even greater reduction in *Idh2*^{R140Q} chimerism in the setting of concurrent *Kdm3b* loss (**Figure 3.10H and Figure 3.11K-M**). These results indicate that *Idh2*-mutant cells are preferentially sensitive to inhibition of the KDM3B-MPL-JAK signaling axis and suggest the potential benefit of targeting cytokine signaling in these mutant genotypes, alone or in combination with KDM3B inhibition.

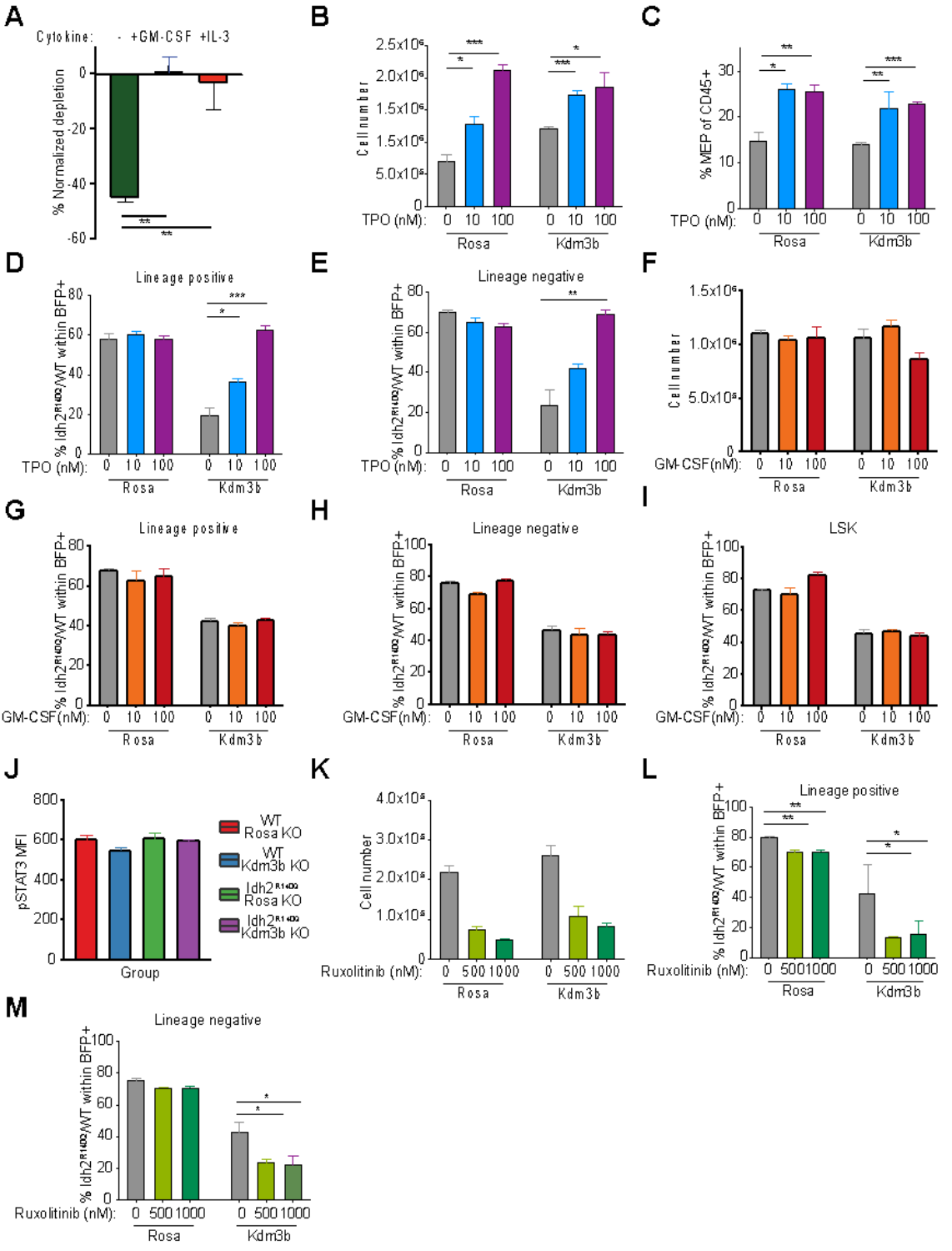

Figure 3.11: Effects on TPO, GM-CSF, and ruxolitinib on *Idh2*^{R140Q} HSPCs. A, Depletion of a BFP^{+} shRNA targeting *KDM3B* in *IDH2 R140Q* TF-1 cells in the presence of the indicated cytokine. Measured as % BFP^{+} by flow cytometry 14 days after infection and normalized to % BFP^{+} 2 days after infection. (n = 3) **B**, Cell growth measured 14

days after *Rosa* or *Kdm3b* sgRNA delivery in wild-type HSPCs. HSPCs were co-cultured with BMECs and treated with increasing doses of TPO. (n = 3) **C**, Percentage of MEPs in $CD45^+$ cells measured by flow cytometry after 14 days of BMEC/HSPC co-culture. Wild-type and $Idh2^{R140Q}$ tdT^+ HSPCs were mixed 1:1, infected with a BFP^+ lentivirus encoding an sgRNA targeting *Rosa* or *Kdm3b*, and treated with increasing doses of TPO. (n = 3) **D** and **E**, $Idh2^{R140Q}$ tdT^+ chimerism in $lineage^+$ (**D**) or $lineage^-$ (**E**) infected cells measured by flow cytometry after 14 days of BMEC/HSPC co-culture. Wild-type and $Idh2^{R140Q}$ tdT^+ HSPCs were mixed 1:1, infected with a BFP^+ lentivirus encoding an sgRNA targeting *Rosa* or *Kdm3b*, and treated with increasing doses of TPO. (n = 3) **F,** Cell growth measured 14 days after *Rosa* or *Kdm3b* sgRNA delivery in wild-type HSPCs. HSPCs were co-cultured with BMECs and treated with increasing doses of GM-CSF. (n = 3) **G-I,** $Idh2^{R140Q}$ tdT^+ chimerism in $lineage^+$ (**G**), $lineage^-$ (**H**), or LSK (**I**) infected cells measured by flow cytometry after 14 days of BMEC/HSPC co-culture. Wild-type and $Idh2^{R140Q}$ tdT^+ HSPCs were mixed 1:1, infected with a BFP^+ lentivirus encoding an sgRNA targeting *Rosa* or *Kdm3b*, and treated with increasing doses of GM-CSF. (n = 3) **J,** MFI of phospho-STAT3 (pSTAT3) as measured by flow cytometry in $lineage^-Kit^+$ infected cells measured after 7 days of BMEC/HSPC co-culture. Wild-type and $Idh2^{R140Q}$ HSPCs were infected with a BFP^+ lentivirus encoding an sgRNA targeting *Rosa* or *Kdm3b* and treated with 100 nM TPO. (n = 3) **K,** Cell growth measured 14 days after *Rosa* or *Kdm3b* sgRNA delivery in wild-type HSPCs. HSPCs were co-cultured with BMECs and treated with increasing doses of ruxolitinib. (n = 3) **L** and **M**, $Idh2^{R140Q}$ tdT^+ chimerism in $lineage^+$ (**L**) and $lineage^-$ (**M**) infected cells measured by flow cytometry after 14 days of BMEC/HSPC co-culture. Wild-type and $Idh2^{R140Q}$ tdT^+ HSPCs were mixed 1:1, infected with a BFP^+ lentivirus encoding an sgRNA targeting *Rosa* or *Kdm3b*, and treated with increasing doses of ruxolitnib. (n = 3). All data are mean ± SEM. *p < 0.05, **p < 0.01, ***p < 0.001

Discussion

The identification of *Kdm3b* as critical in both *Idh2*- and *Tet2*-mutant cells resonates with the established hypothesis that *IDH2*-mediated pathogenesis is due at least in part to TET2 inhibition by neomorphic production of 2-HG[132,134]. Here, we show using gain and loss of function approaches that 2-HG is necessary and sufficient to promote *Kdm3b* dependency, and that mutant IDH2 neomorphic function is required for *Kdm3b* dependency in *IDH2*-mutant cells. Of note, we also found that the *Kdm3b* family members *Jmjd1c* and *Kdm3a* were relative dependencies in *Idh2*- and *Tet2*-mutant cells,

suggesting that the H3K9me1/2 demethylase activity shared by these enzymes may have a shared role in mediating transformation by *TET2*/*IDH2* mutations.

We found that a majority of genes with transcriptional changes in *IDH2*-mutant cells with loss of *KDM3B* were coordinately regulated by both the *IDH2* mutation and loss of *KDM3B*. This synergy in transcriptional output is consistent with *KDM3B* being an α-KG dependent enzyme susceptible to 2-HG mediated inhibition and suggests that the remaining *KDM3B* activity in *IDH2*-mutant cells is essential for their continued fitness[134]. This led us to hypothesize that *IDH2*-mutant cells may not be able to tolerate the further disruption of the *IDH2*-mutant transcriptional program induced by *KDM3B* loss. Although accurate quantification of broadly distributed H3K9me1/2 challenges our ability to identify direct *KDM3B* targets, the coordinate changes in chromatin accessibility and transcriptional output observed with the *IDH2* mutation and loss of *KDM3B* suggest synergistic alterations in epigenetic state at key loci, including alterations in H3K9 methylation and/or DNA methylation[218]. Importantly, we showed that the expression and accessibility of hematopoietic cytokine receptors were coordinately regulated by *IDH2* mutant activity and loss of *KDM3B* and that ligand-induced receptor activation can rescue the effect of *KDM3B* attenuation in both TF-1 and primary cells. Of note, we observed that the specific cytokine receptors regulated by the *IDH2* mutation and *KDM3B* partially differed between hematopoietic stem cells and transformed leukemic cells, suggesting that cytokine-mediated signaling and its regulation may be dependent on the cellular context including the transformation state and potentially species differences[219,220]. The differential requirement for cytokine receptor signaling in *IDH2*-mutant cells is consistent with previous studies elucidating differential cytokine

receptor signaling in normal and malignant hematopoiesis and suggests that further dissection of the mechanisms governing receptor signaling and the functional impact of cytokine-mediated inflammatory signaling in CH and myeloid malignancies is warranted[221-224].

Most importantly, our data suggests new potential therapeutic approaches for the treatment of CH and myeloid malignancies with mutations in *TET2*/*IDH2*. First, we show that KDM3B enzymatic activity is necessary for the survival of *IDH2*-mutant cells, suggesting that either small molecule KDM3B enzymatic inhibitors or PROTAC degraders may have potential mutant-specific therapeutic efficacy. Second, we show that dysregulation of cytokine receptor signaling is a critical feature of *IDH2*-mutant cells, such that small molecule JAK kinase inhibitors and other anti-cytokine therapeutic modalities may have efficacy in this mutant context. Third, we show that the *Kdm3b* dependency is also observed in *Tet2*-mutant AML, such that these therapeutic approaches are of potential importance in the pre-leukemic and leukemic context. Notably, while we demonstrated that *Tet2*-mutant AML cells with *Kdm3b* loss were rapidly depleted *in vivo*, limitations in editing efficiencies in primary cells prevented us from directly assessing the effect of *Kdm3b* loss on disease outcomes and future work will be required to fully delineate the role of *KDM3B* in leukemia maintenance. We also acknowledge that another limitation of our work is that clonal outgrowth often occurs under selection pressures and as such further work is also necessary to assess whether our identified targets are dependencies in the context of different selection pressures[162]. Critically, our work provides a path for new target discovery in mutant hematopoietic stem cells which can inform the development of novel therapies to intercept or treat myeloid transformation,

and we expect similar approaches to delineate additional therapeutic targets in mutationally defined CH and myeloid malignancy subsets.

Materials and Methods

Experimental animals

All animal studies were performed in accordance with institutional guidelines established by Memorial Sloan Kettering Cancer Center (MSKCC) under the Institutional Animal Care and Use Committee-approved animal protocol (#07-10-016) and the Guide for the Care and Use of Laboratory Animals (National Academy of Sciences 1996). All experimental animals were maintained on a 12-hour light-dark cycle with access to water and standard chow ad libitum. Veterinary staff provided regular monitoring and husbandry care. All mice had intact immune systems, were drug and test naïve, and had not been involved in previous procedures. Animals were monitored daily for signs of disease or morbidity, bleeding, failure to thrive, infection, or fatigue and sacrificed immediately if they exhibited any signs of the above. All mice used in this study including *Tet2*$^{flox/flox}$, *Dnmt3a*$^{flox/flox}$, *Idh2*$^{R140Q/flox}$, *Asxl1*$^{flox/flox}$, *Scl:CreERT*, *Npm1*$^{flox\text{-}cA/+,}$ *Flt3*^{ITD}, *Vav:Cre*, *Rosa26:Cas9*, and *Rosa:TdT*$^{flox/flox}$ have been previously described[5,8,166,185-191]. Mice with *Scl:CreERT* were administered 100 mg/kg tamoxifen two times (one day drug holiday in between dosing) via oral gavage to induce Cre recombinase activity. Age-and sex- matched 6–16-week-old mice were used in all experiments and only female mice were used as transplant recipients.

BMEC co-culture with HSPCs

AKT1-activated bone marrow endothelial cells (BMECs) were cultured as previously described[12]. BMECs were seeded 1-3 days prior to HSPC plating at a density of 70,000-150,000 BMECs/well in a fibronectin-coated 12-well plate. To obtain HSPCs, bone marrow cells were isolated from limb bones into FACS buffer (phosphate buffered saline [PBS] + 2% fetal bovine serum) via centrifugation and RBCs were lysed using RBC lysis buffer (Thermo). Lineage$^-$ HSPCs were isolated using the Lineage Cell Depletion Kit according to manufacturer's protocol (EasySep™, StemCell Technologies, Inc.). Cells were then resuspended in Fc (CD16/32) block for 15 minutes and then subsequently stained for lineage$^-$Sca1$^+$cKIT$^+$ (LSK) markers with antibodies targeting Sca-1 (D7) and KIT (2B8) for 30 minutes. All FACS antibodies were purchased from BD, BioLegend, or eBioscience. Following antibody incubation, cells were washed with FACS buffer and resuspended in a live/dead cell stain solution, either DAPI (Thermo, 1:1000 in FACS) or Helix NP NIR (Biolegend, 1:20,000 in FACS). LSK cells were then sorted on a FACSAria III. Subsequently, 2,000 LSKs were plated on a confluent monolayer of BMECs in a single well of a 12-well plate. Each well had 1 mL StemSpan SFEM with 10 ng/mL recombinant murine SCF (PeproTech) and/or additional cytokines as indicated. Co-cultures were maintained for a total of 7 days at 37°C and 5% CO2. A complete media change was performed on day 4 of culture. On day 7, cells were harvested with Accutase (Biolegend) and used in downstream applications. For assays with day 14 readouts, CD45 cells were isolated with CD45 microbeads (Miltenyi Biotech) following manufacturers' protocol and replated onto fresh BMEC plates. For assays with infected cells, lentivirus and 12 ug/mL polybrene (AmericanBio) were combined in 1 mL StemSpan SFEM (StemCell Technologies) containing 6 ng/mL IL-3

(Peprotech), 10 ng/mL IL-6 (Peprotech), and 20 ng/mL SCF (Peprotech) for 10 minutes at room temperature. LSKs were added to each infection along with 30 uL of 1 M HEPES (Thermo). Each infection was transferred to a single well of a 6-well plate and cells were centrifuged at 800 rcf for 1 hour at 32°C, following which an additional 2 mL of StemSpan SFEM containing 6 ng/mL IL-3, 10 ng/mL IL-6, and 20 ng/mL SCF was added to each well. 16 hours after infection, cells were harvested and plated over BMECs. For drug treatments, cells were treated with 10 nM decitabine (MedChem Express), 500 μM Octyl-(R)-2-HG (Sigma), 100 nM or 500 nM enasidenib (MedChem Express), or 500 nM or 1000 nM ruxolitinib (MedChem Express) with their corresponding vehicles.

Transplantation assays and in vivo experiments

For *in vivo* single sgRNA validation studies, lineage$^-$ HSPCs were isolated from donor mice using the Lineage Cell Depletion Kit according to manufacturer's protocol (EasySep™, StemCell Technologies, Inc.) and infected with lentivirus as described above. Following overnight culture, cells were washed with PBS and 300,000-500,000 infected lineage$^-$ cells were transplanted with 200,000 CD45.1 whole bone marrow cells into lethally irradiated (900 cgy) recipient CD45.2 mice. For inducible single sgRNA studies, mice were treated with doxycycline chow approx. 625 mg/kg (Envigo) daily after 8 weeks. For all secondary transplants described, 1.0 x 10^6 whole bone marrow cells harvested from primary transplants were transplanted into lethally irradiated secondary recipient CD45.2 mice. For the *Tet2*$^{-/-}$*Npm1*^{cA}*Flt3*^{ITD} leukemic model, KIT$^+$ cells were isolated using CD117 microbeads (Miltenyi Biotech) following manufacturer's protocol,

electroporated as described below, and transplanted into lethally irradiated CD45.1 recipient mice. For all transplants, peripheral blood was isolated at the indicated timepoints by submandibular bleeds and complete blood counts determined using a ProCyte Dx (IDEXX Laboratories, Westbrook, ME) according to manufacturer's protocol. For terminal tissue isolation, mice were euthanized with CO_2 asphyxiation and tissues were dissected and fixed with 4% paraformaldehyde for histopathological analysis. For whole bone marrow isolation, limb bones were dissected and whole bone marrow isolated using centrifugation followed by RBC lysis (BioLegend) for 10 minutes.

In vivo CRISPR screen

For *in vivo* CRISPR screens, HSPCs were isolated from donor mice as described above. Lentivirus and 12 ug/mL polybrene (AmericanBio) were incubated in 1 mL StemSpan SFEM (StemCell Technologies) containing 6 ng/mL IL-3 (Peprotech), 10 ng/mL IL-6 (Peprotech), and 20 ng/mL SCF (Peprotech) for 10 minutes at room temperature. 1.0 x 10^6 HSPCs were added to each infection along with 30 µL of 1 M HEPES (Thermo). Each infection was transferred to a single well of a 6-well plate and cells were centrifuged at 800 rcf for 1 hour at 32°C, following which an additional 2 mL of StemSpan SFEM containing 6 ng/mL IL-3, 10 ng/mL IL-6, and 20 ng/mL SCF was added to each well. Cells were infected at an efficiency of 20-40% so that most cells received only one sgRNA. 16 hours after infection, cells were harvested, and cell numbers were determined using an automated cell counter (ViCell Blue, Beckman Coulter). Cells were washed with PBS and 300,000-500,000 infected lineage$^-$ cells were transplanted with 200,000 CD45.1 whole bone marrow cells into lethally irradiated (900

cGy) recipient CD45.2 mice. Each screen had 10 transplant recipients. 16 weeks after transplant, mice were euthanized with CO2 asphyxiation and peripheral blood and bone marrow were harvested. HSPCs were isolated using the Lineage Cell Depletion Kit according to manufacturer's protocol (StemCell Technologies). Cells were pooled at equal cell numbers between recipient mice and genomic DNA was extracted using the DNeasy blood and tissue kit (Qiagen). DNA was quantified using Qubit (Thermo). Genomic DNA was PCR amplified to add Illumina adapters and multiplexing barcodes. Amplicons were quantified by Qubit and Bioanalyzer (Agilent) and sequenced on Illumina HiSeq 2500.

Cell line culture

Human parental TF-1 cells wild-type or isogenic for the *IDH2*^{R140Q} mutation were obtained from Jian Xu (University of Texas Southwestern Medical Center)[206]. Cell lines were used in experiments before reaching 10 passages. Cell lines used in experiments were confirmed to be negative for *Mycoplasma*. Wild-type TF-1 cells were cultured in RPMI 1640 medium supplemented with 2 ng/mL recombinant human GM-CSF (Peprotech). TF-1 cells with the *IDH2*^{R140Q} mutation were cultured without GM-CSF. For rescue experiments with additional cytokines, 50 ng/mL IL-3 (Peprotech) was added. HEK293T cells were cultured in DMEM supplemented with sodium pyruvate (Thermo) and L-glutamine (Thermo). All cell lines were cultured in medium containing 10% FBS and 1% penicillin/streptomycin at 37°C with 5% CO_2.

Cloning

Validation libraries were cloned as previously described[225]. Briefly, protospacer sequences, unique from those used in the full CRISPR library, for each target gene were identified using the CRISPick algorithm (Broad Institute) and custom DNA oligonucleotide pools were ordered from IDT[226]. DNA oligonucleotide pools were PCR amplified to add Gibson homology arms and then gel purified using the Gel Extraction Kit (Qiagen) following the manufacturer's protocol. The sgRNA expression backbone LentiGuide-BFP was cloned with a single Gibson reaction (New England Biolabs) replacing the Puromycin in LentiGuide-Puro with BFP. LentiGuide-BFP was BsmBI digested, and the digested product was purified using the Gel Extraction Kit (Qiagen). Libraries were constructed by Gibson reaction of the digested LentiGuide-BFP backbone and the amplified oligonucleotides bearing Gibson homology arms. DNA was electroporated into Endura electrocompetent bacteria (Lucigen). Sufficient numbers of bacterial colonies were harvested to obtain 1000X representation of each sgRNA. DNA from bacteria was extracted using the Maxiprep kit (Qiagen), quantified using Qubit (Thermo), and PCR amplified to add Illumina adapters and multiplexing barcodes. Amplicons were quantified by Qubit and Bioanalyzer (Agilent) and sequenced on Illumina HiSeq 2500. For cloning individual sgRNAs, protospacer sequences for each target gene were identified using the CRISPick algorithm (Broad Institute) and complementary oligonucleotides containing BsmBI-overhang sequences were synthesized (IDT). For single sgRNA validation experiments, sgRNA sequences were designed to be unique from those used in the original screen. Complementary oligonucleotides were annealed and ligated into BsmBI-digested LentiGuide-BFP. The inducible sgRNA expression backbone Tet-pLKO-BFP was cloned with a single Gibson

reaction replacing the mCerulean with BFP in SiC-V2-Cas9G7 (Addgene). Single sgRNAs were cloned into this vector using Gibson reaction. For *IDH2* overexpression constructs, *IDH2* wild-type or *IDH2 R140Q* cDNA was obtained as a gift (Andrew Intlekofer) and Gibson cloning was used to insert the cDNA into pSMAL (Addgene). For *KDM3B* overexpression constructs, a single Gibson reaction was used to replace the GFP with the extracellular domain of NGFR in the lentiviral expression backbone pLenti-CMV-GFP-PKG-Puro (Addgene). The *KDM3B* full-length cDNA was obtained from Origene and Gibson cloning was used to replace the Puro with *KDM3B*. The Site Directed Mutagenesis XL II Kit (Agilent) was used to create a point mutation encoding for a catalytic dead version of KDM3B. For individual sgRNAs and cDNA constructs, DNA was transformed into Stabl3 chemically competent bacteria (Thermo), bacterial DNA was extracted from colonies using Miniprep or Midiprep Kits (Qiagen), and plasmids were sequence confirmed using Sanger sequencing (Genewiz).

Lentivirus production

For lentivirus production, plasmids were co-transfected into 293Ts with the packaging vector psPAX2 and the envelope vector pMD2.G using the jetPRIME transfection reagent (Polyplus) following manufacturer's protocol. Media was changed 24 hours post transfection. Viral-containing supernatant was collected 72 hours after transfection and passed through a 0.45-micron filter. For lentivirus used to infect HSPCs, virus was ultracentrifuged at 24,000 rpm for 2 hours at 4°C using a Sorvall Ultracentrifuge (Thermo). Viral pellets were resuspended in Stemspan SFEM (StemCell

Technologies) and resuspended on a rotator overnight at 4°C, following which virus was aliquoted and stored at -80 C for long-term storage.

AAV production

Fluorescent protein cassette and homology arms were cloned into the pAAV-MCS vector (CellBio Labs) using Gibson Assembly (New England Biolabs). Virus was produced and purified using the AAVpro Purification Kit Maxi (Takara). Briefly, 293T were transfected with AAV vector and pDGM6 (AddGene). Cells were collected 48h post-transfection and purified as per manufacture's protocol. Viruses were titered by qPCR using the AAVpro Titration Kit (Takara).

Flow cytometry and sorting

Freshly isolated cells were washed with FACS buffer (phosphate buffered saline (PBS) + 2% fetal bovine serum). For cell surface staining, cells were then resuspended in Fc (CD16/32) block for 15 minutes at 4°C and then subsequently incubated with antibody cocktails for an additional 15 minutes at 4°C. For biotin-conjugated primary antibodies, cells were washed three times with FACS and incubated with anti-streptavidin secondary antibodies for an additional 15 minutes at 4°C. For intracellular staining, cells were washed and stained with Zombie Viability Dye (Biolegend). Cell surface staining was performed as described above. Cells were then fixed with IC fixation buffer (Thermo) for 20 min and permeabilized with methanol for 30 min. Cells were then washed, incubated with antibody cocktails for intracellular markers for 30 min, washed again, and resuspended in FACS. For peripheral blood analysis, antibodies targeted CD3 (17A2),

CD45R/B220 (RA3-6B2), Gr-1 (RB6-8C5), CD11b 450 (M1/70), CD45.2 (104), Kit (2B8), and CD45.1 (A20). For bone marrow analysis, additional antibodies targeted Sca-1 (D7), FcγRII/III (2.4G2), CD34 (RAM34), CD150 (9D1), and CD48 (HM48-1). For analysis of BMEC co-cultures, antibodies targeted Gr-1 (RB6-8C5), CD11b 450 (M1/70), CD45.2 (104), Kit (2B8), Sca-1 (D7), and CD110 (AMM2). For intracellular staining, an antibody targeting phospho-STAT3 (Tyr705) (13A3-1) was used. If LT-HSC analysis was necessary, antibodies targeting CD150 (9D1) and CD48 (HM48-1) were included. For experiments with TF-1 cells, antibodies targeting CD271 (ME20.4), CD110 (S16017A), and CD131 (1C1) were used. For cord blood experiments, an antibody targeting CD110 (S16017A) was used. For biotin-conjugated primary antibodies, an anti-streptavidin secondary antibody was used. All antibodies were purchased from BD, BioLegend or eBioscience. Following antibody incubation, cells were washed with FACS buffer and resuspended in FACS buffer containing a live/dead cell stain, either DAPI (1:1000 in FACS buffer, Thermo) or Helix NP NIR (1:20,000 in FACS buffer, Biolegend). Flow cytometry was performed on a BD LSRFortessa (BD Biosciences) using FACSDiva and FlowJo (v10.9). Cell isolation with FACS was performed on an FACSAriaIII (BD Biosciences).

Western blot

Whole-cell protein lysates were prepared from equal cell numbers using RIPA buffer (Thermo) containing protease inhibitor cocktail (Thermo). Lysates were sonicated for 1 min (10 sec ON, 10 sec OFF) at 30% amplitude using Branson Digital Sonifier (Branson). Proteins were separated by NuPAGE 3-8% Tris-Acetate Gels and transferred

to nitrocellulose membranes overnight at 30 V. Membranes were blocked for 1 hour in 5% milk-TBST (Sigma) and incubated with primary antibodies overnight. Membranes were incubated with HRP-conjugated secondary antibodies for 1 hour and imaged using SuperSignal West Femto maximum sensitivity substrate (Thermo). The following antibodies were used: β-Actin (Cell Signaling 4970S), KDM3B (Abcam ab217046), JMJD1C (Santa Cruz BA-09), and TET2 (Proteintech 21207-1-AP).

Electroporation of HSPCs

For simultaneous delivery of Cas9 and sgRNAs into HSPCs, ribonucleoproteins (RNPs) were electroporated as previously described[227]. Briefly, protospacer sequences for each target gene were identified using the CRISPick algorithm (Broad institute) and sgRNAs encoding these sequences were ordered from IDT. 10 ug sgRNA was incubated with 10 μg Cas9 protein (IDT) for 15 minutes at room temperature to generate RNPs. RNPs were then added to 1.0 x 10^6 - 3.0 x 10^6 HSPCs and electroporated using Neon transfection system (Thermo) following manufacturer's protocol. For murine HSPCs, conditions were 1700 V, 20 ms, 1 pulse. For human iPSC-derived HSPCs, conditions were 1600 V, 10 ms, 3 pulses. Electroporated cells were plated in fresh media without antibiotics for 1-2 hours, following which cells were used for BMEC co-culture or transplanted into recipient mice.

IPSC-derived HSPC culture

$TET2^{+/-}$ human iPSCs were generated through CRISPR/Cas9-mediated gene editing to remove the genomic region spanning exons 3-11 of one allele of *TET2* in the

previously described normal iPSC line N-2.12[228]. Culture of human iPSCs and hematopoietic differentiation was performed using a spin-EB protocol as previously described[229]. In the end of the differentiation culture, the cells were collected and dissociated with accutase into single cells and used for liquid culture growth assays and methocult CFU assays. For liquid culture growth assays, *TET2*$^{+/-}$ iPSC-HSPCs and isogenic *TET2*-WT iPSC-HSPCs stably expressing GFP, either individually or mixed in a 1:1 ratio, were electroporated with RNPs targeting *AAVS1*, *KDM3B* or *JMJD1C*, and cultured for 10 days. Flow cytometry was used to assess the GFP$^+$ and GFP$^-$ fractions within CD45$^+$ and CD34$^+$ cells. For methocult CFU assays, cells were electroporated and 5,000 cells were plated into Methocult H4434 (StemCell Technologies). Colonies were counted after 10 days.

Cord blood editing

Human cord blood was obtained from full-term deliveries from healthy donors (Pasquerello tissue bank at Dana Farber Cancer Institute or Cleveland Cord Blood Center). Mononuclear cells were obtained by Ficoll centrifugation (GE Healthcare) and were enriched for CD34$^+$ cells using the CD34 MicroBead UltraPure kit (Miltenyi). CD34$^+$ cord blood cells were pre-stimulated for 72h in StemSpan SFEM II (StemCell Technologies) supplemented with 300 ng/ml SCF and FLT3L, 100 ng/ml TPO and IL-6, 1 μM UM729, 1 μM SR1 (all StemCell Technlogies). For introduction of *TET2* loss, CD34$^+$ cord blood cells were nucleoporated using P3 Primary Cell 4D-Nucleofector™ X Kit S (Lonza) and the CA-137 program on the 4D-Nucleofector system (Lonza). Cell were then cultured in StemSpan SFEM II (StemCell Technologies) supplemented with 50

ng/ml SCF and FLT3L, 7.5 ng/mL TPO, 10 ng/mL IL-3 and IL-6, 1 μM UM729, 1 μM SR1 (StemCell Technologies) and 0.1% PVA (Sigma-Aldrich). Within 15 minutes, corresponding AAV virus was added to cells at an MOI of 50,000-100,000. Within a week of nucleofection, mScarlet^{+} cells were sorted and cultured for 24 hours. Following culture, cells were electroporated using the Neon Transfection system (ThermoFisher) to introduce the second mutation. Conditions were 1600V, 10ms, 3 pulses. After 48 hours, cells were plated in MethoCult Enriched H4435 (StemCell Technologies). Colonies were counted after 12 days. For secondary replating assays, colonies were dissociated, and equal numbers of cells were replated in MethoCult. For IDH2 overexpression, CD34^{+} cord blood cells were infected using lentivirus, 12 ug/mL polybrene (AmericanBio), 30 μL of 1 M HEPES (Thermo) and media conditions as above. Individual infections were transferred to a single well of a 6-well plate and cells were centrifuged at 800 rcf for 1 hour at 32°C. The next day, cells were electroporated to introduce the second mutation as described above. Expression of cell surface markers was assessed by flow cytometry after 10 days.

2-HG measurement

Cell pellets were extracted with 1000 μL ice-cold 80:20 methanol:water containing 4 uM deuterated 2-hydroxyglutarate (D,L-2-hydroxyglutaric acid-d3 disodium salt, Toronto Research chemical) as an internal standard. After overnight incubation at -80° C, extracts were centrifuged at 21,000 *g* for 20 min at 4°C to precipitate protein and 800 μL dried in an evaporator (Genevac EZ-2 Elite). Samples were the derivatized with 100 μl of freshly prepared 50 mg/ml (+)-diacetyl-L-tartaric anhydride (DATAN, Sigma)

in dichloromethane-acetic acid (v/v=4:1) at 75° C for 30 min. After cooling to room temperature, derivatized samples were dried under nitrogen at room temperature and resuspended in 100 ul of water. LC-MS/MS analysis was performed using a Thermo Vantage triple-quadrupole mass spectrometer operating in MRM and negative ionization modes. LC separation was using an Acquity UPLC HSS T3 analytical column (2.1 x 100 mm, 1.8 μm, Waters) and an Agilent 1260 infinity binary pump. Mobile phase A was 125 mg/L ammonium formate in water, adjusted to pH 3.5 with formic acid, and mobile phase B was methanol; flow rate was 0.3 mL/min. Initial conditions were 3% B for 5 min, increasing to 97% B at 5.5 min and held for a further 2.5 min. 7 min of re-equilibration time was used to ensure retention time stability. The column temperature was held at 40° C. Samples were kept at 4° C and the injection volume was 10 μL. MS source parameters were: spray voltage 2500 V; capillary temperature 300° C; vaporizer temperature 250° C; sheath gas pressure 50; aux gas pressure 40; S-lens 37 V. Individual reactions monitored and collision energies (CE) were: 2HG *m/z* 363.0 → 147.1 (CE: 12 V)*, 129.1 (CE: 27 V); D3-2HG *m/z* 366.0 → 150.1 (CE: 12 V)*, 132.0 (CE: 27 V), with * indicating the primary transition used to quantify each metabolite. Pure standards of L-2HG, D-2HG were derivatized and analyzed in parallel for each chiral determination experiment and identity of 2-HG enantiomers were determined by comparing to the retention times of the derivatized pure standards. Data was acquired and processed with TraceFinder 4.1 software (ThermoFisher).

Histology staining and immunohistochemistry, photography

Spleen and tibia samples were fixed (4% paraformaldehyde) for >24 hours and embedded in paraffin. Sections were cut using microtome (Mikrom International AG), mounted on slides, and dried at 37°C overnight. Hematoxylin and eosin (H&E) staining was performed on a COT20 stainer (Medite). All sample handling and preparation was performed by the Tri-Institutional Laboratory of Comparative Pathology (LCP) facility. Pictures were taken at 400X magnification using an Olympus microscope. Tissue sections were formally evaluated by a hematopathologist (W. Xiao).

Quantitative real-time PCR

RNA was extracted using the Direct-zol RNA Microprep Kit (Zymo) following the manufacturer's protocol. Complementary DNA (cDNA) was then reverse transcribed using ProtoScript II First Strand cDNA synthesis kit (New England Biolabs) per manufacturer's protocol. *KDM3B* expression was evaluated by quantitative reverse-transcription (qRT) PCR using Taqman probes (Hs00382671, Hs00213240, Mm00804683, and Mm01150330, Thermo) on the QuantStudio 7 Flex System (Applied Biosystems). The quantity of cDNA was normalized according to the expression of ACTIN and GADPH (Hs01060665, Hs02786624, Mm04394036, and Mm99999915, Thermo). Data were analyzed by the delta delta Ct ratio technique using housekeeping genes.

CRISPR cut site sequencing

For assessment of variant allele frequencies, genomic DNA was extracted from targeted cells and PCR amplicons of the targeted site was generated. Sequencing libraries

were prepared from amplicons using the KAPA Hyper Library Preparation Kit (Kapa Biosystems) according to the manufacturer's instructions using 8 cycles of PCR. Barcoded libraries were pooled equivolume and run on a MiSeq or NovaSeq 6000 (Illumina). The CRISPResso2 package was used to filter low quality reads, trim adapters, align reads to the reference amplicon, and quantify editing frequency in the amplicon[230].

RNA sequencing and data analysis

For RNA sequencing, RNA was isolated using the Direct-zol RNA Microprep Kit (Zymo) from FACS purified live cells and quantified using the High Sensitivity RNA Screentape (Agilent) on an Agilent 2200 TapeStation. cDNA was generated with the SMART-Seq HT Kit (Takara), and RNA-sequencing libraries were prepared with the Nextera XT (Illumina) Kit following manufacturers' protocols. cDNA and tagmented libraries were quantified using High Sensitivity D5000 ScreenTape (Agilent) and High Sensitivity D1000 ScreenTape (Agilent) respectively. Libraries were sequenced on a NovaSeq at the Integrated Genomics Operation (IGO) at MSKCC. FASTQ files were demultiplexed using a java script from Takara. FASTQ files were mapped, and transcript counts were enumerated using STAR. Counts were input into R and RNA-sequencing analysis was completed using DESeq2. Differentially expressed genes were identified with an adjusted p-value of 0.05. Gene set enrichment analysis was performed using the fgsea package with genesets extracted from the msigdbr package. Single sample gene set enrichment analysis was performed using normalized expression values of genes in the indicated gene set.

ATAC sequencing and data analysis

For ATAC sequencing, FACS purified live cells were sent to MSKCC's Epigenetics Research Innovation Lab for processing. ATAC was performed as previously described using the Tagment DNA TDE1 Enzyme (Illumina)[231]. Sequencing libraries were prepared using the ThruPLEX DNA-Seq Kit (Takarabio) and sent to the MSKCC Integrated Genomics Operation core facility for sequencing on a NovaSeq 6000. Raw sequencing reads were trimmed and filtered for quality (Q>15) and adapter content using version 0.4.5 of TrimGalore and running version 1.15 of cutadapt and version 0.11.5 of FastQC. Version 2.3.4.1 of bowtie2 was employed to align reads to mouse assembly mm10 and alignments were deduplicated using MarkDuplicates in Picard Tools v2.16.0. Enriched regions were discovered using MACS2 with a p-value setting of 0.001, filtered for blacklisted regions, and a peak atlas was created using +/- 250 bp around peak summits. The BEDTools suite was used to create normalized bigwig files. Version 1.6.1 of featureCounts was used to build a raw counts matrix and DESeq2 was employed to calculate differential enrichment for all pairwise contrasts. Peak-gene associations were created by assigning all intragenic peaks to that gene, while intergenic peaks were assigned using linear genomic distance to transcription start sites (TSS).

Data analysis for CRISPR screens

Sequencing reads were aligned to the screened library and counts were obtained for each sgRNA. Enrichment and depletion of genes in wild-type cells were analyzed using the MAGeCK package by comparing read counts at the final timepoint with counts from the initial timepoint[192]. The MAGeCK-MLE package was used to compute

normalized dependency scores for each gene across each genotype. An FDR cutoff of 0.25 was used for all analyses.

Processing of TCGA and BEAT-AML data

We used RNA-sequencing datasets of TCGA (acute myeloid leukemia, NEJM 2013) and BEAT-AML (acute myeloid leukemia, Cancer Cell 2022) patients, which were available from the cBioPortal for cancer genomics[232,233]. Data for the presence of mutations in *TET2* and *IDH2* and expression of *CSF2RB* and *MPL* was downloaded. For each individual dataset, we stratified patients based on the presence of mutations in *TET2* and/or *IDH2* and plotted expression scores across these subsets.

Statistical analyses

Statistical analyses were performed using Student's t-test using GraphPad Prism (GraphPad Software, San Diego, CA) unless otherwise noted. $P < 0.05$ was considered statistically significant. The number of animals and experimental replications can be found in the respective figure legends.

CHAPTER FOUR

CONCLUDING REMARKS

This thesis provides a platform to the field that enables rapid *ex vivo* genetic and chemical perturbation studies, including in the application of unbiased high-throughput screens, in primary genetically defined HSPCs. Of note, other chemical and/or co-culture systems that enable the *ex vivo* expansion of HSPCs have also recently been described[169,234]. While these systems have yet to be applied in the context of CH, it is likely that additional studies using these platforms in this application will soon follow. Here, we demonstrate that co-culture of HSPCs with BMECs allows for the long-term *ex vivo* maintenance of CH-mutant HSPCs and yields rapid *ex vivo* phenotypes. We show that these phenotypes are largely consistent with months-long *in vivo* readouts and so we anticipate this platform will be of use for obtaining rapid results for hypothesis-driven functional experiments. Of course, small scale hypothesis-driven experiments can, despite the long timeframe, typically be performed *in vivo* and we believe the critical utility in the platform we describe is in its application in unbiased screening. As a proof of concept, we used this system to perform a CRISPR/Cas9 screen in primary wild-type

HSPCs and identified a set of critical epigenetic regulators important for HSPCs. While other studies have nominated genes believed to be important for HSPC self-renewal and/or differentiation, our work provides the first systematic, unbiased approach to map the key chromatin regulators in HSPCs. Additionally, our results in wild-type HSPCs may have implications for potential leukemia therapies in informing the potential toxicities associated with targets that are also dependencies in native hematopoiesis.

Our study enabled a thorough dependency map of genetic vulnerabilities in HSPCs harboring four of the most recurrent mutations in CH. While we chose to focus on the *KDM3* family members, we anticipate that future studies will further investigate the other dependencies we identified in our study. Additionally, our screen was also able to identify a number of positive regulators of HSPCs whose loss cooperated with CH-associated mutations to cause expansion; further investigation of these genes is also warranted. Notably, we chose to focus our screen on potential synthetic lethal dependencies encoding chromatin modifiers given the biological role of the genes recurrently mutated in CH. However, it is very likely that CH-associated mutations will also confer dependencies to additional regulators encoded by other classes of genes, such as kinases or inflammation-related proteins. Our study provides a roadmap for additional screens to search this genetic space.

As the central finding of this work, we demonstrate that a common subset of CH marked by mutations in *TET2* or *IDH2* is dependent on the activity of the *KDM3* family of histone demethylases, particularly *KDM3B*. Our finding that *KDM3B* is a dependency in both *TET2*- and *IDH2*-mutant HSPCs fits well with prior data demonstrating overlapping mechanisms of pathogenesis of these mutations in CH and AML[132].

Interestingly, mutations in *IDH2* are believed to contribute to disease through inhibition of both TET and KDM enzymes, as well as through inhibition of other α-KG-dependent enzymes[134]. Other work has demonstrated that inhibition of KDM5 family members mediated by the *IDH2* mutation enhances leukemic cell fitness[235]. As such, our results suggest that *IDH2* mutation-mediated inhibition of KDM family members may have both positive and negative consequences for mutant cell fitness. In line with this, we demonstrated that *IDH2*-mutant cells are unable to tolerate further treatment with cell-permeable 2-HG. Additionally, we demonstrate in multiple models through transcriptomic and epigenomic studies that the *IDH2* mutation and *KDM3B* cause additive changes in chromatin accessibility and transcription at an overlapping gene set. Taken together, our data suggests that there may be a critical threshold for *IDH2*-mutant mediated inhibition of α-KG-dependent enzymes that supports leukemogenesis.

Although our work nominates the KDM3 family of enzymes as a potential therapeutic target in CH, several challenges in bringing a therapy to the clinic remain. First, small molecules with high specificity and potency against the KDM3 family have not been described. While a handful of KDM3 inhibitors have been reported, they also target other KDM proteins at similar potencies[236,237]. Critically, since it is believed that inhibition of other KDM enzymes, including the KDM5 family, is oncogenic, small molecules that are not sufficiently specific enough for the KDM3 family are not predicted to show efficacy. However, our work does demonstrate that all three KDM3 family members, KDM3A, KDM3B, and JMJD1C, are dependencies in this context and so small molecules may not need be specific for any individual family member. Second, the appropriate patient population for a potential KDM3 targeted therapy has yet to be

defined. *TET2* is very frequently mutated in the general population and the vast majority of individuals with *TET2*-mutant CH do not develop a hematologic malignancy. *IDH2*-mutant CH is characterized by a high risk of malignant transformation but is infrequently observed; however, this patient population may nevertheless present an opportunity for a clinical trial as has been reported previously with IDH2 inhibitors. Importantly, our work falls short of definitely answering whether the KDM3 family is a dependency in myeloid malignancies, including MDS and AML. Further work is needed to delineate the role of the KDM3 family in these diseases and it is possible that the malignant context may represent a more tractable intervention opportunity for initial trials of KDM3 targeted therapies. Finally, our work also leaves open the question of whether KDM3 inhibition would cause clonal collapse or rather restrain further clonal outgrowth. While we demonstrated in multiple models that KDM3 family members are targets to prevent further clonal expansion, it is unclear through our results whether KDM3 inhibition has the capacity to completely eliminate already established mutant clones. This is an important question that needs further investigation as the answer will guide possible dosing requirements involving KDM3 inhibition and/or the requirement for additional targets/therapies to enable elimination of mutant clones.

Collectively, this thesis describes an approach toward the identification of potential therapeutic targets in CH and nominates an epigenetic regulator and an epigenetically regulated signaling pathway as tractable dependencies in a subset of CH. We envision that future work will utilize our approach to expand the set of potential therapeutic targets in CH and AML.

BIBLIOGRAPHY

1 Coombs, C. C., Zehir, A., Devlin, S. M., Kishtagari, A., Syed, A., Jonsson, P. *et al.* Therapy-Related Clonal Hematopoiesis in Patients with Non-hematologic Cancers Is Common and Associated with Adverse Clinical Outcomes. *Cell Stem Cell* **21**, 374-382 e374 (2017). https://doi.org:10.1016/j.stem.2017.07.010

2 Buscarlet, M., Provost, S., Zada, Y. F., Barhdadi, A., Bourgoin, V., Lepine, G. *et al.* DNMT3A and TET2 dominate clonal hematopoiesis and demonstrate benign phenotypes and different genetic predispositions. *Blood* **130**, 753-762 (2017). https://doi.org:10.1182/blood-2017-04-777029

3 McKerrell, T., Park, N., Moreno, T., Grove, C. S., Ponstingl, H., Stephens, J. *et al.* Leukemia-associated somatic mutations drive distinct patterns of age-related clonal hemopoiesis. *Cell Rep* **10**, 1239-1245 (2015). https://doi.org:10.1016/j.celrep.2015.02.005

4 Papaemmanuil, E., Gerstung, M., Bullinger, L., Gaidzik, V. I., Paschka, P., Roberts, N. D. *et al.* Genomic Classification and Prognosis in Acute Myeloid Leukemia. *N Engl J Med* **374**, 2209-2221 (2016). https://doi.org:10.1056/NEJMoa1516192

5 Moran-Crusio, K., Reavie, L., Shih, A., Abdel-Wahab, O., Ndiaye-Lobry, D., Lobry, C. *et al.* Tet2 loss leads to increased hematopoietic stem cell self-renewal and myeloid transformation. *Cancer Cell* **20**, 11-24 (2011). https://doi.org:10.1016/j.ccr.2011.06.001

6 Guryanova, O. A., Lieu, Y. K., Garrett-Bakelman, F. E., Spitzer, B., Glass, J. L., Shank, K. *et al.* Dnmt3a regulates myeloproliferation and liver-specific expansion of hematopoietic stem and progenitor cells. *Leukemia* **30**, 1133-1142 (2016). https://doi.org:10.1038/leu.2015.358

7 Abdel-Wahab, O., Adli, M., LaFave, L. M., Gao, J., Hricik, T., Shih, A. H. *et al.* ASXL1 mutations promote myeloid transformation through loss of PRC2-mediated gene repression. *Cancer Cell* **22**, 180-193 (2012). https://doi.org:10.1016/j.ccr.2012.06.032

8 Abdel-Wahab, O., Gao, J., Adli, M., Dey, A., Trimarchi, T., Chung, Y. R. *et al.* Deletion of Asxl1 results in myelodysplasia and severe developmental defects in vivo. *J Exp Med* **210**, 2641-2659 (2013). https://doi.org:10.1084/jem.20131141

9 Shih, A. H., Meydan, C., Shank, K., Garrett-Bakelman, F. E., Ward, P. S., Intlekofer, A. M. *et al.* Combination Targeted Therapy to Disrupt Aberrant Oncogenic Signaling and Reverse Epigenetic Dysfunction in IDH2- and TET2-Mutant Acute Myeloid Leukemia. *Cancer Discov* **7**, 494-505 (2017). https://doi.org:10.1158/2159-8290.CD-16-1049

10 Miles, L. A., Bowman, R. L., Merlinsky, T. R., Csete, I. S., Ooi, A. T., Durruthy-Durruthy, R. *et al.* Single-cell mutation analysis of clonal evolution in myeloid malignancies. *Nature* **587**, 477-482 (2020). https://doi.org:10.1038/s41586-020-2864-x

11 McMurry, H., Fletcher, L. & Traer, E. IDH Inhibitors in AML-Promise and Pitfalls. *Curr Hematol Malig Rep* **16**, 207-217 (2021). https://doi.org:10.1007/s11899-021-00619-3

12 Poulos, M. G., Crowley, M. J. P., Gutkin, M. C., Ramalingam, P., Schachterle, W., Thomas, J. L. *et al.* Vascular Platform to Define Hematopoietic Stem Cell Factors and Enhance Regenerative Hematopoiesis. *Stem Cell Reports* **5**, 881-894 (2015). https://doi.org:10.1016/j.stemcr.2015.08.018

13 Levy, S. E. & Myers, R. M. Advancements in Next-Generation Sequencing. *Annu Rev Genomics Hum Genet* **17**, 95-115 (2016). https://doi.org:10.1146/annurev-genom-083115-022413

14 Tomczak, K., Czerwinska, P. & Wiznerowicz, M. The Cancer Genome Atlas (TCGA): an immeasurable source of knowledge. *Contemp Oncol (Pozn)* **19**, A68-77 (2015). https://doi.org:10.5114/wo.2014.47136

15 Cheng, D. T., Mitchell, T. N., Zehir, A., Shah, R. H., Benayed, R., Syed, A. *et al.* Memorial Sloan Kettering-Integrated Mutation Profiling of Actionable Cancer Targets (MSK-IMPACT): A Hybridization Capture-Based Next-Generation Sequencing Clinical Assay for Solid Tumor Molecular Oncology. *J Mol Diagn* **17**, 251-264 (2015). https://doi.org:10.1016/j.jmoldx.2014.12.006

16 Nagahashi, M., Shimada, Y., Ichikawa, H., Kameyama, H., Takabe, K., Okuda, S. *et al.* Next generation sequencing-based gene panel tests for the management of solid tumors. *Cancer Sci* **110**, 6-15 (2019). https://doi.org:10.1111/cas.13837

17 Roskoski, R., Jr. Classification of small molecule protein kinase inhibitors based upon the structures of their drug-enzyme complexes. *Pharmacol Res* **103**, 26-48 (2016). https://doi.org:10.1016/j.phrs.2015.10.021

18 Zhang, J., Yang, P. L. & Gray, N. S. Targeting cancer with small molecule kinase inhibitors. *Nat Rev Cancer* **9**, 28-39 (2009). https://doi.org:10.1038/nrc2559

19 Scott, A. M., Allison, J. P. & Wolchok, J. D. Monoclonal antibodies in cancer therapy. *Cancer Immun* **12**, 14 (2012).

20 Weiner, L. M., Surana, R. & Wang, S. Monoclonal antibodies: versatile platforms for cancer immunotherapy. *Nat Rev Immunol* **10**, 317-327 (2010). https://doi.org:10.1038/nri2744

21 Kurzrock, R., Gutterman, J. U. & Talpaz, M. The molecular genetics of Philadelphia chromosome-positive leukemias. *N Engl J Med* **319**, 990-998 (1988). https://doi.org:10.1056/NEJM198810133191506

22 Daley, G. Q., Van Etten, R. A. & Baltimore, D. Induction of chronic myelogenous leukemia in mice by the P210bcr/abl gene of the Philadelphia chromosome. *Science* **247**, 824-830 (1990). https://doi.org:10.1126/science.2406902

23 Sattler, M. & Griffin, J. D. Molecular mechanisms of transformation by the BCR-ABL oncogene. *Semin Hematol* **40**, 4-10 (2003). https://doi.org:10.1053/shem.2003.50034

24 Kantarjian, H., Sawyers, C., Hochhaus, A., Guilhot, F., Schiffer, C., Gambacorti-Passerini, C. *et al.* Hematologic and cytogenetic responses to imatinib mesylate in chronic myelogenous leukemia. *N Engl J Med* **346**, 645-652 (2002). https://doi.org:10.1056/NEJMoa011573

25 Hochhaus, A., Larson, R. A., Guilhot, F., Radich, J. P., Branford, S., Hughes, T. P. *et al.* Long-Term Outcomes of Imatinib Treatment for Chronic Myeloid Leukemia. *N Engl J Med* **376**, 917-927 (2017). https://doi.org:10.1056/NEJMoa1609324

26 Gambacorti-Passerini, C. B., Gunby, R. H., Piazza, R., Galietta, A., Rostagno, R. & Scapozza, L. Molecular mechanisms of resistance to imatinib in Philadelphia-chromosome-positive leukaemias. *Lancet Oncol* **4**, 75-85 (2003). https://doi.org:10.1016/s1470-2045(03)00979-3

27 von Bubnoff, N., Schneller, F., Peschel, C. & Duyster, J. BCR-ABL gene mutations in relation to clinical resistance of Philadelphia-chromosome-positive leukaemia to STI571: a prospective study. *Lancet* **359**, 487-491 (2002). https://doi.org:10.1016/S0140-6736(02)07679-1

28 Gorre, M. E., Mohammed, M., Ellwood, K., Hsu, N., Paquette, R., Rao, P. N. *et al.* Clinical resistance to STI-571 cancer therapy caused by BCR-ABL gene mutation or amplification. *Science* **293**, 876-880 (2001). https://doi.org:10.1126/science.1062538

29 Roche-Lestienne, C., Soenen-Cornu, V., Grardel-Duflos, N., Lai, J. L., Philippe, N., Facon, T. *et al.* Several types of mutations of the Abl gene can be found in chronic myeloid leukemia patients resistant to STI571, and they can pre-exist to the onset of treatment. *Blood* **100**, 1014-1018 (2002). https://doi.org:10.1182/blood.v100.3.1014

30 Saglio, G., Kim, D. W., Issaragrisil, S., le Coutre, P., Etienne, G., Lobo, C. *et al.* Nilotinib versus imatinib for newly diagnosed chronic myeloid leukemia. *N Engl J Med* **362**, 2251-2259 (2010). https://doi.org:10.1056/NEJMoa0912614

31 Kantarjian, H., Shah, N. P., Hochhaus, A., Cortes, J., Shah, S., Ayala, M. *et al.* Dasatinib versus imatinib in newly diagnosed chronic-phase chronic myeloid leukemia. *N Engl J Med* **362**, 2260-2270 (2010). https://doi.org:10.1056/NEJMoa1002315

32 Cortes, J. E., Kim, D. W., Kantarjian, H. M., Brummendorf, T. H., Dyagil, I., Griskevicius, L. *et al.* Bosutinib versus imatinib in newly diagnosed chronic-phase chronic myeloid leukemia: results from the BELA trial. *J Clin Oncol* **30**, 3486-3492 (2012). https://doi.org:10.1200/JCO.2011.38.7522

33 Cortes, J. E., Kantarjian, H., Shah, N. P., Bixby, D., Mauro, M. J., Flinn, I. *et al.* Ponatinib in refractory Philadelphia chromosome-positive leukemias. *N Engl J Med* **367**, 2075-2088 (2012). https://doi.org:10.1056/NEJMoa1205127

34 Rea, D., Mauro, M. J., Boquimpani, C., Minami, Y., Lomaia, E., Voloshin, S. *et al.* A phase 3, open-label, randomized study of asciminib, a STAMP inhibitor, vs bosutinib in CML after 2 or more prior TKIs. *Blood* **138**, 2031-2041 (2021). https://doi.org:10.1182/blood.2020009984

35 Schoepfer, J., Jahnke, W., Berellini, G., Buonamici, S., Cotesta, S., Cowan-Jacob, S. W. *et al.* Discovery of Asciminib (ABL001), an Allosteric Inhibitor of the Tyrosine Kinase Activity of BCR-ABL1. *J Med Chem* **61**, 8120-8135 (2018). https://doi.org:10.1021/acs.jmedchem.8b01040

36 Eide, C. A., Zabriskie, M. S., Savage Stevens, S. L., Antelope, O., Vellore, N. A., Than, H. *et al.* Combining the Allosteric Inhibitor Asciminib with Ponatinib Suppresses Emergence of and Restores Efficacy against Highly Resistant BCR-ABL1 Mutants. *Cancer Cell* **36**, 431-443 e435 (2019). https://doi.org:10.1016/j.ccell.2019.08.004

37 Rousselot, P., Huguet, F., Rea, D., Legros, L., Cayuela, J. M., Maarek, O. *et al.* Imatinib mesylate discontinuation in patients with chronic myelogenous leukemia in complete molecular remission for more than 2 years. *Blood* **109**, 58-60 (2007). https://doi.org:10.1182/blood-2006-03-011239

38 Moasser, M. M. The oncogene HER2: its signaling and transforming functions and its role in human cancer pathogenesis. *Oncogene* **26**, 6469-6487 (2007). https://doi.org:10.1038/sj.onc.1210477

39 Wang, J. & Xu, B. Targeted therapeutic options and future perspectives for HER2-positive breast cancer. *Signal Transduct Target Ther* **4**, 34 (2019). https://doi.org:10.1038/s41392-019-0069-2

40 Kris, M. G., Natale, R. B., Herbst, R. S., Lynch, T. J., Jr., Prager, D., Belani, C. P. *et al.* Efficacy of gefitinib, an inhibitor of the epidermal growth factor receptor tyrosine kinase, in symptomatic patients with non-small cell lung cancer: a randomized trial. *JAMA* **290**, 2149-2158 (2003). https://doi.org:10.1001/jama.290.16.2149

41 Sequist, L. V., Bell, D. W., Lynch, T. J. & Haber, D. A. Molecular predictors of response to epidermal growth factor receptor antagonists in non-small-cell lung cancer. *J Clin Oncol* **25**, 587-595 (2007). https://doi.org:10.1200/JCO.2006.07.3585

42 Sequist, L. V., Yang, J. C., Yamamoto, N., O'Byrne, K., Hirsh, V., Mok, T. *et al.* Phase III study of afatinib or cisplatin plus pemetrexed in patients with metastatic lung adenocarcinoma with EGFR mutations. *J Clin Oncol* **31**, 3327-3334 (2013). https://doi.org:10.1200/JCO.2012.44.2806

43 Wu, Y. L., Cheng, Y., Zhou, X., Lee, K. H., Nakagawa, K., Niho, S. *et al.* Dacomitinib versus gefitinib as first-line treatment for patients with EGFR-mutation-positive non-small-cell lung cancer (ARCHER 1050): a randomised, open-label, phase 3 trial. *Lancet Oncol* **18**, 1454-1466 (2017). https://doi.org:10.1016/S1470-2045(17)30608-3

44 Soria, J. C., Ohe, Y., Vansteenkiste, J., Reungwetwattana, T., Chewaskulyong, B., Lee, K. H. *et al.* Osimertinib in Untreated EGFR-Mutated Advanced Non-Small-Cell Lung Cancer. *N Engl J Med* **378**, 113-125 (2018). https://doi.org:10.1056/NEJMoa1713137

45 Ramalingam, S. S., Vansteenkiste, J., Planchard, D., Cho, B. C., Gray, J. E., Ohe, Y. *et al.* Overall Survival with Osimertinib in Untreated, EGFR-Mutated Advanced NSCLC. *N Engl J Med* **382**, 41-50 (2020). https://doi.org:10.1056/NEJMoa1913662

46 Mok, T. S., Wu, Y. L., Ahn, M. J., Garassino, M. C., Kim, H. R., Ramalingam, S. S. *et al.* Osimertinib or Platinum-Pemetrexed in EGFR T790M-Positive Lung Cancer. *N Engl J Med* **376**, 629-640 (2017). https://doi.org:10.1056/NEJMoa1612674

47 Yang, Z., Yang, N., Ou, Q., Xiang, Y., Jiang, T., Wu, X. *et al.* Investigating Novel Resistance Mechanisms to Third-Generation EGFR Tyrosine Kinase Inhibitor Osimertinib in Non-Small Cell Lung Cancer Patients. *Clin Cancer Res* **24**, 3097-3107 (2018). https://doi.org:10.1158/1078-0432.CCR-17-2310

48 Slamon, D., Eiermann, W., Robert, N., Pienkowski, T., Martin, M., Press, M. *et al.* Adjuvant trastuzumab in HER2-positive breast cancer. *N Engl J Med* **365**, 1273-1283 (2011). https://doi.org:10.1056/NEJMoa0910383

49 Adams, C. W., Allison, D. E., Flagella, K., Presta, L., Clarke, J., Dybdal, N. *et al.* Humanization of a recombinant monoclonal antibody to produce a therapeutic HER dimerization inhibitor, pertuzumab. *Cancer Immunol Immunother* **55**, 717-727 (2006). https://doi.org:10.1007/s00262-005-0058-x

50 Baselga, J., Cortes, J., Kim, S. B., Im, S. A., Hegg, R., Im, Y. H. *et al.* Pertuzumab plus trastuzumab plus docetaxel for metastatic breast cancer. *N Engl J Med* **366**, 109-119 (2012). https://doi.org:10.1056/NEJMoa1113216

51 Rugo, H. S., Im, S. A., Cardoso, F., Cortes, J., Curigliano, G., Musolino, A. *et al.* Efficacy of Margetuximab vs Trastuzumab in Patients With Pretreated ERBB2-Positive Advanced Breast Cancer: A Phase 3 Randomized Clinical Trial. *JAMA Oncol* **7**, 573-584 (2021). https://doi.org:10.1001/jamaoncol.2020.7932

52 Lambert, J. M. & Berkenblit, A. Antibody-Drug Conjugates for Cancer Treatment. *Annu Rev Med* **69**, 191-207 (2018). https://doi.org:10.1146/annurev-med-061516-121357

53 Rinnerthaler, G., Gampenrieder, S. P. & Greil, R. HER2 Directed Antibody-Drug-Conjugates beyond T-DM1 in Breast Cancer. *Int J Mol Sci* **20** (2019). https://doi.org:10.3390/ijms20051115

54 Park, K., Haura, E. B., Leighl, N. B., Mitchell, P., Shu, C. A., Girard, N. *et al.* Amivantamab in EGFR Exon 20 Insertion-Mutated Non-Small-Cell Lung Cancer Progressing on Platinum Chemotherapy: Initial Results From the CHRYSALIS Phase I Study. *J Clin Oncol* **39**, 3391-3402 (2021). https://doi.org:10.1200/JCO.21.00662

55 Scaltriti, M., Rojo, F., Ocana, A., Anido, J., Guzman, M., Cortes, J. *et al.* Expression of p95HER2, a truncated form of the HER2 receptor, and response to anti-HER2 therapies in breast cancer. *J Natl Cancer Inst* **99**, 628-638 (2007). https://doi.org:10.1093/jnci/djk134

56 Nagata, Y., Lan, K. H., Zhou, X., Tan, M., Esteva, F. J., Sahin, A. A. *et al.* PTEN activation contributes to tumor inhibition by trastuzumab, and loss of PTEN predicts trastuzumab resistance in patients. *Cancer Cell* **6**, 117-127 (2004). https://doi.org:10.1016/j.ccr.2004.06.022

57 Musolino, A., Naldi, N., Bortesi, B., Pezzuolo, D., Capelletti, M., Missale, G. *et al.* Immunoglobulin G fragment C receptor polymorphisms and clinical efficacy of trastuzumab-based therapy in patients with HER-2/neu-positive metastatic breast cancer. *J Clin Oncol* **26**, 1789-1796 (2008). https://doi.org:10.1200/JCO.2007.14.8957

58 Pohlmann, P. R., Mayer, I. A. & Mernaugh, R. Resistance to Trastuzumab in Breast Cancer. *Clin Cancer Res* **15**, 7479-7491 (2009). https://doi.org:10.1158/1078-0432.CCR-09-0636

59 Zhao, Y. & Adjei, A. A. Targeting Angiogenesis in Cancer Therapy: Moving Beyond Vascular Endothelial Growth Factor. *Oncologist* **20**, 660-673 (2015). https://doi.org:10.1634/theoncologist.2014-0465

60 Touat, M., Ileana, E., Postel-Vinay, S., Andre, F. & Soria, J. C. Targeting FGFR Signaling in Cancer. *Clin Cancer Res* **21**, 2684-2694 (2015). https://doi.org:10.1158/1078-0432.CCR-14-2329

61 Loriot, Y., Necchi, A., Park, S. H., Garcia-Donas, J., Huddart, R., Burgess, E. *et al.* Erdafitinib in Locally Advanced or Metastatic Urothelial Carcinoma. *N Engl J Med* **381**, 338-348 (2019). https://doi.org:10.1056/NEJMoa1817323

62 Makawita, S., G, K. A.-A., Roychowdhury, S., Sadeghi, S., Borbath, I., Goyal, L. *et al.* Infigratinib in patients with advanced cholangiocarcinoma with FGFR2 gene fusions/translocations: the PROOF 301 trial. *Future Oncol* **16**, 2375-2384 (2020). https://doi.org:10.2217/fon-2020-0299

63 Abou-Alfa, G. K., Sahai, V., Hollebecque, A., Vaccaro, G., Melisi, D., Al-Rajabi, R. *et al.* Pemigatinib for previously treated, locally advanced or metastatic cholangiocarcinoma: a multicentre, open-label, phase 2 study. *Lancet Oncol* **21**, 671-684 (2020). https://doi.org:10.1016/S1470-2045(20)30109-1

64 Wynes, M. W., Hinz, T. K., Gao, D., Martini, M., Marek, L. A., Ware, K. E. *et al.* FGFR1 mRNA and protein expression, not gene copy number, predict FGFR TKI sensitivity across all lung cancer histologies. *Clin Cancer Res* **20**, 3299-3309 (2014). https://doi.org:10.1158/1078-0432.CCR-13-3060

65 Kotani, H., Ebi, H., Kitai, H., Nanjo, S., Kita, K., Huynh, T. G. *et al.* Co-active receptor tyrosine kinases mitigate the effect of FGFR inhibitors in FGFR1-amplified lung cancers with low FGFR1 protein expression. *Oncogene* **35**, 3587-3597 (2016). https://doi.org:10.1038/onc.2015.426

66 Braicu, C., Buse, M., Busuioc, C., Drula, R., Gulei, D., Raduly, L. *et al.* A Comprehensive Review on MAPK: A Promising Therapeutic Target in Cancer. *Cancers (Basel)* **11** (2019). https://doi.org:10.3390/cancers11101618

67 Pratilas, C. A., Taylor, B. S., Ye, Q., Viale, A., Sander, C., Solit, D. B. *et al.* (V600E)BRAF is associated with disabled feedback inhibition of RAF-MEK signaling and elevated transcriptional output of the pathway. *Proc Natl Acad Sci U S A* **106**, 4519-4524 (2009). https://doi.org:10.1073/pnas.0900780106

68 Hauschild, A., Agarwala, S. S., Trefzer, U., Hogg, D., Robert, C., Hersey, P. *et al.* Results of a phase III, randomized, placebo-controlled study of sorafenib in combination with carboplatin and paclitaxel as second-line treatment in patients with unresectable stage III or stage IV melanoma. *J Clin Oncol* **27**, 2823-2830 (2009). https://doi.org:10.1200/JCO.2007.15.7636

69 Eisen, T., Ahmad, T., Flaherty, K. T., Gore, M., Kaye, S., Marais, R. *et al.* Sorafenib in advanced melanoma: a Phase II randomised discontinuation trial analysis. *Br J Cancer* **95**, 581-586 (2006). https://doi.org:10.1038/sj.bjc.6603291

70 Chapman, P. B., Hauschild, A., Robert, C., Haanen, J. B., Ascierto, P., Larkin, J. *et al.* Improved survival with vemurafenib in melanoma with BRAF V600E mutation. *N Engl J Med* **364**, 2507-2516 (2011). https://doi.org:10.1056/NEJMoa1103782

71 Hauschild, A., Grob, J. J., Demidov, L. V., Jouary, T., Gutzmer, R., Millward, M. *et al.* Dabrafenib in BRAF-mutated metastatic melanoma: a multicentre, open-label, phase 3 randomised controlled trial. *Lancet* **380**, 358-365 (2012). https://doi.org:10.1016/S0140-6736(12)60868-X

72 Dummer, R., Ascierto, P. A., Gogas, H. J., Arance, A., Mandala, M., Liszkay, G. *et al.* Encorafenib plus binimetinib versus vemurafenib or encorafenib in patients with BRAF-mutant melanoma (COLUMBUS): a multicentre, open-label, randomised phase 3 trial. *Lancet Oncol* **19**, 603-615 (2018). https://doi.org:10.1016/S1470-2045(18)30142-6

73 Hatzivassiliou, G., Song, K., Yen, I., Brandhuber, B. J., Anderson, D. J., Alvarado, R. *et al.* RAF inhibitors prime wild-type RAF to activate the MAPK pathway and enhance growth. *Nature* **464**, 431-435 (2010). https://doi.org:10.1038/nature08833

74 Su, F., Viros, A., Milagre, C., Trunzer, K., Bollag, G., Spleiss, O. *et al.* RAS mutations in cutaneous squamous-cell carcinomas in patients treated with BRAF inhibitors. *N Engl J Med* **366**, 207-215 (2012). https://doi.org:10.1056/NEJMoa1105358

75 Lacouture, M. E., Duvic, M., Hauschild, A., Prieto, V. G., Robert, C., Schadendorf, D. *et al.* Analysis of dermatologic events in vemurafenib-treated patients with melanoma. *Oncologist* **18**, 314-322 (2013). https://doi.org:10.1634/theoncologist.2012-0333

76 Robert, C., Karaszewska, B., Schachter, J., Rutkowski, P., Mackiewicz, A., Stroiakovski, D. *et al.* Improved overall survival in melanoma with combined dabrafenib and trametinib. *N Engl J Med* **372**, 30-39 (2015). https://doi.org:10.1056/NEJMoa1412690

77 Larkin, J., Ascierto, P. A., Dreno, B., Atkinson, V., Liszkay, G., Maio, M. *et al.* Combined vemurafenib and cobimetinib in BRAF-mutated melanoma. *N Engl J Med* **371**, 1867-1876 (2014). https://doi.org:10.1056/NEJMoa1408868

78 Kopetz, S., Grothey, A., Yaeger, R., Van Cutsem, E., Desai, J., Yoshino, T. *et al.* Encorafenib, Binimetinib, and Cetuximab in BRAF V600E-Mutated Colorectal Cancer. *N Engl J Med* **381**, 1632-1643 (2019). https://doi.org:10.1056/NEJMoa1908075

79 Long, G. V., Fung, C., Menzies, A. M., Pupo, G. M., Carlino, M. S., Hyman, J. *et al.* Increased MAPK reactivation in early resistance to dabrafenib/trametinib combination therapy of BRAF-mutant metastatic melanoma. *Nat Commun* **5**, 5694 (2014). https://doi.org:10.1038/ncomms6694

80 Gao, Y., Chang, M. T., McKay, D., Na, N., Zhou, B., Yaeger, R. *et al.* Allele-Specific Mechanisms of Activation of MEK1 Mutants Determine Their

Properties. *Cancer Discov* **8**, 648-661 (2018). https://doi.org:10.1158/2159-8290.CD-17-1452

81 Taparowsky, E., Shimizu, K., Goldfarb, M. & Wigler, M. Structure and activation of the human N-ras gene. *Cell* **34**, 581-586 (1983). https://doi.org:10.1016/0092-8674(83)90390-2

82 Bonfini, L., Karlovich, C. A., Dasgupta, C. & Banerjee, U. The Son of sevenless gene product: a putative activator of Ras. *Science* **255**, 603-606 (1992). https://doi.org:10.1126/science.1736363

83 Whyte, D. B., Kirschmeier, P., Hockenberry, T. N., Nunez-Oliva, I., James, L., Catino, J. J. *et al.* K- and N-Ras are geranylgeranylated in cells treated with farnesyl protein transferase inhibitors. *J Biol Chem* **272**, 14459-14464 (1997). https://doi.org:10.1074/jbc.272.22.14459

84 Sebti, S. M. & Hamilton, A. D. Farnesyltransferase and geranylgeranyltransferase I inhibitors and cancer therapy: lessons from mechanism and bench-to-bedside translational studies. *Oncogene* **19**, 6584-6593 (2000). https://doi.org:10.1038/sj.onc.1204146

85 Ho, A. L., Brana, I., Haddad, R., Bauman, J., Bible, K., Oosting, S. *et al.* Tipifarnib in Head and Neck Squamous Cell Carcinoma With HRAS Mutations. *J Clin Oncol* **39**, 1856-1864 (2021). https://doi.org:10.1200/JCO.20.02903

86 Hunter, J. C., Manandhar, A., Carrasco, M. A., Gurbani, D., Gondi, S. & Westover, K. D. Biochemical and Structural Analysis of Common Cancer-Associated KRAS Mutations. *Mol Cancer Res* **13**, 1325-1335 (2015). https://doi.org:10.1158/1541-7786.MCR-15-0203

87 Gehringer, M. & Laufer, S. A. Emerging and Re-Emerging Warheads for Targeted Covalent Inhibitors: Applications in Medicinal Chemistry and Chemical Biology. *J Med Chem* **62**, 5673-5724 (2019). https://doi.org:10.1021/acs.jmedchem.8b01153

88 Hong, D. S., Fakih, M. G., Strickler, J. H., Desai, J., Durm, G. A., Shapiro, G. I. *et al.* KRAS(G12C) Inhibition with Sotorasib in Advanced Solid Tumors. *N Engl J Med* **383**, 1207-1217 (2020). https://doi.org:10.1056/NEJMoa1917239

89 Ostrem, J. M., Peters, U., Sos, M. L., Wells, J. A. & Shokat, K. M. K-Ras(G12C) inhibitors allosterically control GTP affinity and effector interactions. *Nature* **503**, 548-551 (2013). https://doi.org:10.1038/nature12796

90 Hallin, J., Engstrom, L. D., Hargis, L., Calinisan, A., Aranda, R., Briere, D. M. *et al.* The KRAS(G12C) Inhibitor MRTX849 Provides Insight toward Therapeutic Susceptibility of KRAS-Mutant Cancers in Mouse Models and Patients. *Cancer Discov* **10**, 54-71 (2020). https://doi.org:10.1158/2159-8290.CD-19-1167

91 Dunnett-Kane, V., Nicola, P., Blackhall, F. & Lindsay, C. Mechanisms of Resistance to KRAS(G12C) Inhibitors. *Cancers (Basel)* **13** (2021). https://doi.org:10.3390/cancers13010151

92 Welsch, M. E., Kaplan, A., Chambers, J. M., Stokes, M. E., Bos, P. H., Zask, A. *et al.* Multivalent Small-Molecule Pan-RAS Inhibitors. *Cell* **168**, 878-889 e829 (2017). https://doi.org:10.1016/j.cell.2017.02.006

93 Fresno Vara, J. A., Casado, E., de Castro, J., Cejas, P., Belda-Iniesta, C. & Gonzalez-Baron, M. PI3K/Akt signalling pathway and cancer. *Cancer Treat Rev* **30**, 193-204 (2004). https://doi.org:10.1016/j.ctrv.2003.07.007

94 Furman, R. R., Sharman, J. P., Coutre, S. E., Cheson, B. D., Pagel, J. M., Hillmen, P. *et al.* Idelalisib and rituximab in relapsed chronic lymphocytic leukemia. *N Engl J Med* **370**, 997-1007 (2014). https://doi.org:10.1056/NEJMoa1315226

95 Dreyling, M., Morschhauser, F., Bouabdallah, K., Bron, D., Cunningham, D., Assouline, S. E. *et al.* Phase II study of copanlisib, a PI3K inhibitor, in relapsed or refractory, indolent or aggressive lymphoma. *Ann Oncol* **28**, 2169-2178 (2017). https://doi.org:10.1093/annonc/mdx289

96 Flinn, I. W., Hillmen, P., Montillo, M., Nagy, Z., Illes, A., Etienne, G. *et al.* The phase 3 DUO trial: duvelisib vs ofatumumab in relapsed and refractory CLL/SLL. *Blood* **132**, 2446-2455 (2018). https://doi.org:10.1182/blood-2018-05-850461

97 Burris, H. A., 3rd, Flinn, I. W., Patel, M. R., Fenske, T. S., Deng, C., Brander, D. M. *et al.* Umbralisib, a novel PI3Kdelta and casein kinase-1epsilon inhibitor, in relapsed or refractory chronic lymphocytic leukaemia and lymphoma: an open-label, phase 1, dose-escalation, first-in-human study. *Lancet Oncol* **19**, 486-496 (2018). https://doi.org:10.1016/S1470-2045(18)30082-2

98 Andre, F., Ciruelos, E., Rubovszky, G., Campone, M., Loibl, S., Rugo, H. S. *et al.* Alpelisib for PIK3CA-Mutated, Hormone Receptor-Positive Advanced Breast Cancer. *N Engl J Med* **380**, 1929-1940 (2019). https://doi.org:10.1056/NEJMoa1813904

99 Yang, J., Nie, J., Ma, X., Wei, Y., Peng, Y. & Wei, X. Targeting PI3K in cancer: mechanisms and advances in clinical trials. *Mol Cancer* **18**, 26 (2019). https://doi.org:10.1186/s12943-019-0954-x

100 Jones, R. H., Casbard, A., Carucci, M., Cox, C., Butler, R., Alchami, F. *et al.* Fulvestrant plus capivasertib versus placebo after relapse or progression on an aromatase inhibitor in metastatic, oestrogen receptor-positive breast cancer (FAKTION): a multicentre, randomised, controlled, phase 2 trial. *Lancet Oncol* **21**, 345-357 (2020). https://doi.org:10.1016/S1470-2045(19)30817-4

101 Hua, H., Kong, Q., Zhang, H., Wang, J., Luo, T. & Jiang, Y. Targeting mTOR for cancer therapy. *J Hematol Oncol* **12**, 71 (2019). https://doi.org:10.1186/s13045-019-0754-1

102 Hortobagyi, G. N., Chen, D., Piccart, M., Rugo, H. S., Burris, H. A., 3rd, Pritchard, K. I. *et al.* Correlative Analysis of Genetic Alterations and Everolimus Benefit in Hormone Receptor-Positive, Human Epidermal Growth Factor Receptor 2-Negative Advanced Breast Cancer: Results From BOLERO-2. *J Clin Oncol* **34**, 419-426 (2016). https://doi.org:10.1200/JCO.2014.60.1971

103 Yang, L., Clarke, M. J., Carlson, B. L., Mladek, A. C., Schroeder, M. A., Decker, P. *et al.* PTEN loss does not predict for response to RAD001 (Everolimus) in a glioblastoma orthotopic xenograft test panel. *Clin Cancer Res* **14**, 3993-4001 (2008). https://doi.org:10.1158/1078-0432.CCR-07-4152

104 Roy, R., Chun, J. & Powell, S. N. BRCA1 and BRCA2: different roles in a common pathway of genome protection. *Nat Rev Cancer* **12**, 68-78 (2011). https://doi.org:10.1038/nrc3181

105 Lee, J. M., Ledermann, J. A. & Kohn, E. C. PARP Inhibitors for BRCA1/2 mutation-associated and BRCA-like malignancies. *Ann Oncol* **25**, 32-40 (2014). https://doi.org:10.1093/annonc/mdt384

106 Robson, M., Im, S. A., Senkus, E., Xu, B., Domchek, S. M., Masuda, N. *et al.* Olaparib for Metastatic Breast Cancer in Patients with a Germline BRCA Mutation. *N Engl J Med* **377**, 523-533 (2017). https://doi.org:10.1056/NEJMoa1706450

107 Mirza, M. R., Monk, B. J., Herrstedt, J., Oza, A. M., Mahner, S., Redondo, A. *et al.* Niraparib Maintenance Therapy in Platinum-Sensitive, Recurrent Ovarian Cancer. *N Engl J Med* **375**, 2154-2164 (2016). https://doi.org:10.1056/NEJMoa1611310

108 Coleman, R. L., Oza, A. M., Lorusso, D., Aghajanian, C., Oaknin, A., Dean, A. *et al.* Rucaparib maintenance treatment for recurrent ovarian carcinoma after response to platinum therapy (ARIEL3): a randomised, double-blind, placebo-controlled, phase 3 trial. *Lancet* **390**, 1949-1961 (2017). https://doi.org:10.1016/S0140-6736(17)32440-6

109 Litton, J. K., Rugo, H. S., Ettl, J., Hurvitz, S. A., Goncalves, A., Lee, K. H. *et al.* Talazoparib in Patients with Advanced Breast Cancer and a Germline BRCA Mutation. *N Engl J Med* **379**, 753-763 (2018). https://doi.org:10.1056/NEJMoa1802905

110 Coleman, R. L., Fleming, G. F., Brady, M. F., Swisher, E. M., Steffensen, K. D., Friedlander, M. *et al.* Veliparib with First-Line Chemotherapy and as Maintenance Therapy in Ovarian Cancer. *N Engl J Med* **381**, 2403-2415 (2019). https://doi.org:10.1056/NEJMoa1909707

111 Murai, J., Huang, S. Y., Das, B. B., Renaud, A., Zhang, Y., Doroshow, J. H. *et al.* Trapping of PARP1 and PARP2 by Clinical PARP Inhibitors. *Cancer Res* **72**, 5588-5599 (2012). https://doi.org:10.1158/0008-5472.CAN-12-2753

112 Murai, J., Huang, S. Y., Renaud, A., Zhang, Y., Ji, J., Takeda, S. *et al.* Stereospecific PARP trapping by BMN 673 and comparison with olaparib and rucaparib. *Mol Cancer Ther* **13**, 433-443 (2014). https://doi.org:10.1158/1535-7163.MCT-13-0803

113 Hodgson, D. R., Dougherty, B. A., Lai, Z., Fielding, A., Grinsted, L., Spencer, S. *et al.* Candidate biomarkers of PARP inhibitor sensitivity in ovarian cancer beyond the BRCA genes. *Br J Cancer* **119**, 1401-1409 (2018). https://doi.org:10.1038/s41416-018-0274-8

114 Polak, P., Kim, J., Braunstein, L. Z., Karlic, R., Haradhavala, N. J., Tiao, G. *et al.* A mutational signature reveals alterations underlying deficient homologous recombination repair in breast cancer. *Nat Genet* **49**, 1476-1486 (2017). https://doi.org:10.1038/ng.3934

115 Criscuolo, D., Morra, F., Giannella, R., Cerrato, A. & Celetti, A. Identification of Novel Biomarkers of Homologous Recombination Defect in DNA Repair to Predict Sensitivity of Prostate Cancer Cells to PARP-Inhibitors. *Int J Mol Sci* **20** (2019). https://doi.org:10.3390/ijms20123100

116 Ford, L., Wolford, J. E., Brown, S. M. & Randall, L. M. A profile on the FoundationFocus CDxBRCA tests. *Expert Rev Mol Diagn* **20**, 285-292 (2020). https://doi.org:10.1080/14737159.2020.1701438

117 Morice, P. M., Coquan, E., Weiswald, L. B., Lambert, B., Vaur, D. & Poulain, L. Identifying patients eligible for PARP inhibitor treatment: from NGS-based tests

to 3D functional assays. *Br J Cancer* **125**, 7-14 (2021). https://doi.org:10.1038/s41416-021-01295-z

118 Dias, M. P., Moser, S. C., Ganesan, S. & Jonkers, J. Understanding and overcoming resistance to PARP inhibitors in cancer therapy. *Nat Rev Clin Oncol* **18**, 773-791 (2021). https://doi.org:10.1038/s41571-021-00532-x

119 Pettitt, S. J., Krastev, D. B., Brandsma, I., Drean, A., Song, F., Aleksandrov, R. *et al.* Genome-wide and high-density CRISPR-Cas9 screens identify point mutations in PARP1 causing PARP inhibitor resistance. *Nat Commun* **9**, 1849 (2018). https://doi.org:10.1038/s41467-018-03917-2

120 Ray Chaudhuri, A., Callen, E., Ding, X., Gogola, E., Duarte, A. A., Lee, J. E. *et al.* Replication fork stability confers chemoresistance in BRCA-deficient cells. *Nature* **535**, 382-387 (2016). https://doi.org:10.1038/nature18325

121 Bunting, S. F., Callen, E., Wong, N., Chen, H. T., Polato, F., Gunn, A. *et al.* 53BP1 inhibits homologous recombination in Brca1-deficient cells by blocking resection of DNA breaks. *Cell* **141**, 243-254 (2010). https://doi.org:10.1016/j.cell.2010.03.012

122 Petitjean, A., Achatz, M. I., Borresen-Dale, A. L., Hainaut, P. & Olivier, M. TP53 mutations in human cancers: functional selection and impact on cancer prognosis and outcomes. *Oncogene* **26**, 2157-2165 (2007). https://doi.org:10.1038/sj.onc.1210302

123 Foster, B. A., Coffey, H. A., Morin, M. J. & Rastinejad, F. Pharmacological rescue of mutant p53 conformation and function. *Science* **286**, 2507-2510 (1999). https://doi.org:10.1126/science.286.5449.2507

124 Rippin, T. M., Bykov, V. J., Freund, S. M., Selivanova, G., Wiman, K. G. & Fersht, A. R. Characterization of the p53-rescue drug CP-31398 in vitro and in living cells. *Oncogene* **21**, 2119-2129 (2002). https://doi.org:10.1038/sj.onc.1205362

125 Bykov, V. J., Issaeva, N., Shilov, A., Hultcrantz, M., Pugacheva, E., Chumakov, P. *et al.* Restoration of the tumor suppressor function to mutant p53 by a low-molecular-weight compound. *Nat Med* **8**, 282-288 (2002). https://doi.org:10.1038/nm0302-282

126 Zache, N., Lambert, J. M., Wiman, K. G. & Bykov, V. J. PRIMA-1MET inhibits growth of mouse tumors carrying mutant p53. *Cell Oncol* **30**, 411-418 (2008). https://doi.org:10.3233/clo-2008-0440

127 Sallman, D. A., DeZern, A. E., Garcia-Manero, G., Steensma, D. P., Roboz, G. J., Sekeres, M. A. *et al.* Eprenetapopt (APR-246) and Azacitidine in TP53-Mutant Myelodysplastic Syndromes. *J Clin Oncol* **39**, 1584-1594 (2021). https://doi.org:10.1200/JCO.20.02341

128 Zandi, R., Selivanova, G., Christensen, C. L., Gerds, T. A., Willumsen, B. M. & Poulsen, H. S. PRIMA-1Met/APR-246 induces apoptosis and tumor growth delay in small cell lung cancer expressing mutant p53. *Clin Cancer Res* **17**, 2830-2841 (2011). https://doi.org:10.1158/1078-0432.CCR-10-3168

129 Bykov, V. J. N., Eriksson, S. E., Bianchi, J. & Wiman, K. G. Targeting mutant p53 for efficient cancer therapy. *Nat Rev Cancer* **18**, 89-102 (2018). https://doi.org:10.1038/nrc.2017.109

130 Dang, L., White, D. W., Gross, S., Bennett, B. D., Bittinger, M. A., Driggers, E. M. *et al.* Cancer-associated IDH1 mutations produce 2-hydroxyglutarate. *Nature* **462**, 739-744 (2009). https://doi.org:10.1038/nature08617

131 Zhao, S., Lin, Y., Xu, W., Jiang, W., Zha, Z., Wang, P. *et al.* Glioma-derived mutations in IDH1 dominantly inhibit IDH1 catalytic activity and induce HIF-1alpha. *Science* **324**, 261-265 (2009). https://doi.org:10.1126/science.1170944

132 Figueroa, M. E., Abdel-Wahab, O., Lu, C., Ward, P. S., Patel, J., Shih, A. *et al.* Leukemic IDH1 and IDH2 mutations result in a hypermethylation phenotype, disrupt TET2 function, and impair hematopoietic differentiation. *Cancer Cell* **18**, 553-567 (2010). https://doi.org:10.1016/j.ccr.2010.11.015

133 Hartmann, C., Meyer, J., Balss, J., Capper, D., Mueller, W., Christians, A. *et al.* Type and frequency of IDH1 and IDH2 mutations are related to astrocytic and oligodendroglial differentiation and age: a study of 1,010 diffuse gliomas. *Acta Neuropathol* **118**, 469-474 (2009). https://doi.org:10.1007/s00401-009-0561-9

134 Xu, W., Yang, H., Liu, Y., Yang, Y., Wang, P., Kim, S. H. *et al.* Oncometabolite 2-hydroxyglutarate is a competitive inhibitor of alpha-ketoglutarate-dependent dioxygenases. *Cancer Cell* **19**, 17-30 (2011). https://doi.org:10.1016/j.ccr.2010.12.014

135 Popovici-Muller, J., Lemieux, R. M., Artin, E., Saunders, J. O., Salituro, F. G., Travins, J. *et al.* Discovery of AG-120 (Ivosidenib): A First-in-Class Mutant IDH1 Inhibitor for the Treatment of IDH1 Mutant Cancers. *ACS Med Chem Lett* **9**, 300-305 (2018). https://doi.org:10.1021/acsmedchemlett.7b00421

136 Yen, K., Travins, J., Wang, F., David, M. D., Artin, E., Straley, K. *et al.* AG-221, a First-in-Class Therapy Targeting Acute Myeloid Leukemia Harboring Oncogenic IDH2 Mutations. *Cancer Discov* **7**, 478-493 (2017). https://doi.org:10.1158/2159-8290.CD-16-1034

137 Wang, F., Travins, J., DeLaBarre, B., Penard-Lacronique, V., Schalm, S., Hansen, E. *et al.* Targeted inhibition of mutant IDH2 in leukemia cells induces cellular differentiation. *Science* **340**, 622-626 (2013). https://doi.org:10.1126/science.1234769

138 DiNardo, C. D., Stein, E. M., de Botton, S., Roboz, G. J., Altman, J. K., Mims, A. S. *et al.* Durable Remissions with Ivosidenib in IDH1-Mutated Relapsed or Refractory AML. *N Engl J Med* **378**, 2386-2398 (2018). https://doi.org:10.1056/NEJMoa1716984

139 Stein, E. M. Enasidenib, a targeted inhibitor of mutant IDH2 proteins for treatment of relapsed or refractory acute myeloid leukemia. *Future Oncol* **14**, 23-40 (2018). https://doi.org:10.2217/fon-2017-0392

140 Intlekofer, A. M., Shih, A. H., Wang, B., Nazir, A., Rustenburg, A. S., Albanese, S. K. *et al.* Acquired resistance to IDH inhibition through trans or cis dimer-interface mutations. *Nature* **559**, 125-129 (2018). https://doi.org:10.1038/s41586-018-0251-7

141 Harding, J. J., Lowery, M. A., Shih, A. H., Schvartzman, J. M., Hou, S., Famulare, C. *et al.* Isoform Switching as a Mechanism of Acquired Resistance to Mutant Isocitrate Dehydrogenase Inhibition. *Cancer Discov* **8**, 1540-1547 (2018). https://doi.org:10.1158/2159-8290.CD-18-0877

142 Johannessen, T. A., Mukherjee, J., Viswanath, P., Ohba, S., Ronen, S. M., Bjerkvig, R. *et al.* Rapid Conversion of Mutant IDH1 from Driver to Passenger in a Model of Human Gliomagenesis. *Mol Cancer Res* **14**, 976-983 (2016). https://doi.org:10.1158/1541-7786.MCR-16-0141

143 Konteatis, Z., Artin, E., Nicolay, B., Straley, K., Padyana, A. K., Jin, L. *et al.* Vorasidenib (AG-881): A First-in-Class, Brain-Penetrant Dual Inhibitor of Mutant IDH1 and 2 for Treatment of Glioma. *ACS Med Chem Lett* **11**, 101-107 (2020). https://doi.org:10.1021/acsmedchemlett.9b00509

144 Bodor, C., O'Riain, C., Wrench, D., Matthews, J., Iyengar, S., Tayyib, H. *et al.* EZH2 Y641 mutations in follicular lymphoma. *Leukemia* **25**, 726-729 (2011). https://doi.org:10.1038/leu.2010.311

145 Beguelin, W., Popovic, R., Teater, M., Jiang, Y., Bunting, K. L., Rosen, M. *et al.* EZH2 is required for germinal center formation and somatic EZH2 mutations promote lymphoid transformation. *Cancer Cell* **23**, 677-692 (2013). https://doi.org:10.1016/j.ccr.2013.04.011

146 Yap, D. B., Chu, J., Berg, T., Schapira, M., Cheng, S. W., Moradian, A. *et al.* Somatic mutations at EZH2 Y641 act dominantly through a mechanism of selectively altered PRC2 catalytic activity, to increase H3K27 trimethylation. *Blood* **117**, 2451-2459 (2011). https://doi.org:10.1182/blood-2010-11-321208

147 Knutson, S. K., Warholic, N. M., Wigle, T. J., Klaus, C. R., Allain, C. J., Raimondi, A. *et al.* Durable tumor regression in genetically altered malignant rhabdoid tumors by inhibition of methyltransferase EZH2. *Proc Natl Acad Sci U S A* **110**, 7922-7927 (2013). https://doi.org:10.1073/pnas.1303800110

148 Knutson, S. K., Kawano, S., Minoshima, Y., Warholic, N. M., Huang, K. C., Xiao, Y. *et al.* Selective inhibition of EZH2 by EPZ-6438 leads to potent antitumor activity in EZH2-mutant non-Hodgkin lymphoma. *Mol Cancer Ther* **13**, 842-854 (2014). https://doi.org:10.1158/1535-7163.MCT-13-0773

149 Morschhauser, F., Tilly, H., Chaidos, A., McKay, P., Phillips, T., Assouline, S. *et al.* Tazemetostat for patients with relapsed or refractory follicular lymphoma: an open-label, single-arm, multicentre, phase 2 trial. *Lancet Oncol* **21**, 1433-1442 (2020). https://doi.org:10.1016/S1470-2045(20)30441-1

150 Beguelin, W., Teater, M., Meydan, C., Hoehn, K. B., Phillip, J. M., Soshnev, A. A. *et al.* Mutant EZH2 Induces a Pre-malignant Lymphoma Niche by Reprogramming the Immune Response. *Cancer Cell* **37**, 655-673 e611 (2020). https://doi.org:10.1016/j.ccell.2020.04.004

151 Toure, M. & Crews, C. M. Small-Molecule PROTACS: New Approaches to Protein Degradation. *Angew Chem Int Ed Engl* **55**, 1966-1973 (2016). https://doi.org:10.1002/anie.201507978

152 Nowak, R. P., DeAngelo, S. L., Buckley, D., He, Z., Donovan, K. A., An, J. *et al.* Plasticity in binding confers selectivity in ligand-induced protein degradation. *Nat Chem Biol* **14**, 706-714 (2018). https://doi.org:10.1038/s41589-018-0055-y

153 Saxena, M., van der Burg, S. H., Melief, C. J. M. & Bhardwaj, N. Therapeutic cancer vaccines. *Nat Rev Cancer* **21**, 360-378 (2021). https://doi.org:10.1038/s41568-021-00346-0

154 Jaiswal, S., Fontanillas, P., Flannick, J., Manning, A., Grauman, P. V., Mar, B. G. *et al.* Age-related clonal hematopoiesis associated with adverse outcomes. *N Engl J Med* **371**, 2488-2498 (2014). https://doi.org:10.1056/NEJMoa1408617
155 Genovese, G., Kahler, A. K., Handsaker, R. E., Lindberg, J., Rose, S. A., Bakhoum, S. F. *et al.* Clonal hematopoiesis and blood-cancer risk inferred from blood DNA sequence. *N Engl J Med* **371**, 2477-2487 (2014). https://doi.org:10.1056/NEJMoa1409405
156 Fearon, E. R. & Vogelstein, B. A genetic model for colorectal tumorigenesis. *Cell* **61**, 759-767 (1990). https://doi.org:10.1016/0092-8674(90)90186-i
157 Martincorena, I., Roshan, A., Gerstung, M., Ellis, P., Van Loo, P., McLaren, S. *et al.* Tumor evolution. High burden and pervasive positive selection of somatic mutations in normal human skin. *Science* **348**, 880-886 (2015). https://doi.org:10.1126/science.aaa6806
158 Martincorena, I., Fowler, J. C., Wabik, A., Lawson, A. R. J., Abascal, F., Hall, M. W. J. *et al.* Somatic mutant clones colonize the human esophagus with age. *Science* **362**, 911-917 (2018). https://doi.org:10.1126/science.aau3879
159 Yokoyama, A., Kakiuchi, N., Yoshizato, T., Nannya, Y., Suzuki, H., Takeuchi, Y. *et al.* Age-related remodelling of oesophageal epithelia by mutated cancer drivers. *Nature* **565**, 312-317 (2019). https://doi.org:10.1038/s41586-018-0811-x
160 Xie, M., Lu, C., Wang, J., McLellan, M. D., Johnson, K. J., Wendl, M. C. *et al.* Age-related mutations associated with clonal hematopoietic expansion and malignancies. *Nat Med* **20**, 1472-1478 (2014). https://doi.org:10.1038/nm.3733
161 Jaiswal, S., Natarajan, P., Silver, A. J., Gibson, C. J., Bick, A. G., Shvartz, E. *et al.* Clonal Hematopoiesis and Risk of Atherosclerotic Cardiovascular Disease. *N Engl J Med* **377**, 111-121 (2017). https://doi.org:10.1056/NEJMoa1701719
162 Jaiswal, S. & Ebert, B. L. Clonal hematopoiesis in human aging and disease. *Science* **366** (2019). https://doi.org:10.1126/science.aan4673
163 Bondar, T. & Medzhitov, R. p53-mediated hematopoietic stem and progenitor cell competition. *Cell Stem Cell* **6**, 309-322 (2010). https://doi.org:10.1016/j.stem.2010.03.002
164 Kahn, J. D., Miller, P. G., Silver, A. J., Sellar, R. S., Bhatt, S., Gibson, C. *et al.* PPM1D-truncating mutations confer resistance to chemotherapy and sensitivity to PPM1D inhibition in hematopoietic cells. *Blood* **132**, 1095-1105 (2018). https://doi.org:10.1182/blood-2018-05-850339
165 Hsu, J. I., Dayaram, T., Tovy, A., De Braekeleer, E., Jeong, M., Wang, F. *et al.* PPM1D Mutations Drive Clonal Hematopoiesis in Response to Cytotoxic Chemotherapy. *Cell Stem Cell* **23**, 700-713 e706 (2018). https://doi.org:10.1016/j.stem.2018.10.004
166 Challen, G. A., Sun, D., Jeong, M., Luo, M., Jelinek, J., Berg, J. S. *et al.* Dnmt3a is essential for hematopoietic stem cell differentiation. *Nat Genet* **44**, 23-31 (2011). https://doi.org:10.1038/ng.1009
167 Stein, E. M., DiNardo, C. D., Pollyea, D. A., Fathi, A. T., Roboz, G. J., Altman, J. K. *et al.* Enasidenib in mutant IDH2 relapsed or refractory acute myeloid leukemia. *Blood* **130**, 722-731 (2017). https://doi.org:10.1182/blood-2017-04-779405

168 Zhuoer Xie, K. M., Terra L. Lasho, Jenna A. Fernandez, Christy M Finke4, Michelle Renee Amundson, Betsy LaPlant, Abhishek Mangaokar, Naseema Gangat, Kaaren K. Reichard, Michelle Ann Elliott, Thomas E. Witzig, Mrinal M. Patnaik. Phase II Study Assessing Safety and Preliminary Efficacy of High Dose Intravenous Ascorbic Acid in Patients with TET2 Mutant Clonal Cytopenias. *Blood* **142** (2023).

169 Wilkinson, A. C., Ishida, R., Kikuchi, M., Sudo, K., Morita, M., Crisostomo, R. V. *et al.* Long-term ex vivo haematopoietic-stem-cell expansion allows nonconditioned transplantation. *Nature* **571**, 117-121 (2019). https://doi.org:10.1038/s41586-019-1244-x

170 Butler, J. M., Nolan, D. J., Vertes, E. L., Varnum-Finney, B., Kobayashi, H., Hooper, A. T. *et al.* Endothelial cells are essential for the self-renewal and repopulation of Notch-dependent hematopoietic stem cells. *Cell Stem Cell* **6**, 251-264 (2010). https://doi.org:10.1016/j.stem.2010.02.001

171 Bejar, R., Lord, A., Stevenson, K., Bar-Natan, M., Perez-Ladaga, A., Zaneveld, J. *et al.* TET2 mutations predict response to hypomethylating agents in myelodysplastic syndrome patients. *Blood* **124**, 2705-2712 (2014). https://doi.org:10.1182/blood-2014-06-582809

172 Shi, J., Wang, E., Milazzo, J. P., Wang, Z., Kinney, J. B. & Vakoc, C. R. Discovery of cancer drug targets by CRISPR-Cas9 screening of protein domains. *Nat Biotechnol* **33**, 661-667 (2015). https://doi.org:10.1038/nbt.3235

173 Liu, F., Cheng, G., Hamard, P. J., Greenblatt, S., Wang, L., Man, N. *et al.* Arginine methyltransferase PRMT5 is essential for sustaining normal adult hematopoiesis. *J Clin Invest* **125**, 3532-3544 (2015). https://doi.org:10.1172/JCI81749

174 Valerio, D. G., Xu, H., Eisold, M. E., Woolthuis, C. M., Pandita, T. K. & Armstrong, S. A. Histone acetyltransferase activity of MOF is required for adult but not early fetal hematopoiesis in mice. *Blood* **129**, 48-59 (2017). https://doi.org:10.1182/blood-2016-05-714568

175 Yang, Y., Kueh, A. J., Grant, Z. L., Abeysekera, W., Garnham, A. L., Wilcox, S. *et al.* The histone lysine acetyltransferase HBO1 (KAT7) regulates hematopoietic stem cell quiescence and self-renewal. *Blood* **139**, 845-858 (2022). https://doi.org:10.1182/blood.2021013954

176 Kerenyi, M. A., Shao, Z., Hsu, Y. J., Guo, G., Luc, S., O'Brien, K. *et al.* Histone demethylase Lsd1 represses hematopoietic stem and progenitor cell signatures during blood cell maturation. *Elife* **2**, e00633 (2013). https://doi.org:10.7554/eLife.00633

177 Kinkel, S. A., Galeev, R., Flensburg, C., Keniry, A., Breslin, K., Gilan, O. *et al.* Jarid2 regulates hematopoietic stem cell function by acting with polycomb repressive complex 2. *Blood* **125**, 1890-1900 (2015). https://doi.org:10.1182/blood-2014-10-603969

178 Zhang, Y., Wong, J., Klinger, M., Tran, M. T., Shannon, K. M. & Killeen, N. MLL5 contributes to hematopoietic stem cell fitness and homeostasis. *Blood* **113**, 1455-1463 (2009). https://doi.org:10.1182/blood-2008-05-159905

179 Zuber, J., Shi, J., Wang, E., Rappaport, A. R., Herrmann, H., Sison, E. A. *et al.* RNAi screen identifies Brd4 as a therapeutic target in acute myeloid leukaemia. *Nature* **478**, 524-528 (2011). https://doi.org:10.1038/nature10334
180 Dawson, M. A., Borthakur, G., Huntly, B. J. P., Karadimitris, A., Alegre, A., Chaidos, A. *et al.* A Phase I/II Open-Label Study of Molibresib for the Treatment of Relapsed/Refractory Hematologic Malignancies. *Clin Cancer Res* **29**, 711-722 (2023). https://doi.org:10.1158/1078-0432.CCR-22-1284
181 Jin, Y., Zhou, J., Xu, F., Jin, B., Cui, L., Wang, Y. *et al.* Targeting methyltransferase PRMT5 eliminates leukemia stem cells in chronic myelogenous leukemia. *J Clin Invest* **126**, 3961-3980 (2016). https://doi.org:10.1172/JCI85239
182 Patel, M. R., Monga, V., Jauhari, S., Stevens, D., Masarova, L., McKean, M. *et al.* A Phase 1 Dose Escalation Study of Protein Arginine Methyltransferase 5 (PRMT5) Inhibitor PRT543 in Patients with Myeloid Malignancies. *Blood* **138** (2021). https://doi.org:10.1182/blood-2021-150938
183 Daigle, S. R., Olhava, E. J., Therkelsen, C. A., Majer, C. R., Sneeringer, C. J., Song, J. *et al.* Selective killing of mixed lineage leukemia cells by a potent small-molecule DOT1L inhibitor. *Cancer Cell* **20**, 53-65 (2011). https://doi.org:10.1016/j.ccr.2011.06.009
184 Stein, E. M., Garcia-Manero, G., Rizzieri, D. A., Tibes, R., Berdeja, J. G., Savona, M. R. *et al.* The DOT1L inhibitor pinometostat reduces H3K79 methylation and has modest clinical activity in adult acute leukemia. *Blood* **131**, 2661-2669 (2018). https://doi.org:10.1182/blood-2017-12-818948
185 Shih, A. H., Jiang, Y., Meydan, C., Shank, K., Pandey, S., Barreyro, L. *et al.* Mutational cooperativity linked to combinatorial epigenetic gain of function in acute myeloid leukemia. *Cancer Cell* **27**, 502-515 (2015). https://doi.org:10.1016/j.ccell.2015.03.009
186 Stadtfeld, M. & Graf, T. Assessing the role of hematopoietic plasticity for endothelial and hepatocyte development by non-invasive lineage tracing. *Development* **132**, 203-213 (2005). https://doi.org:10.1242/dev.01558
187 Platt, R. J., Chen, S., Zhou, Y., Yim, M. J., Swiech, L., Kempton, H. R. *et al.* CRISPR-Cas9 knockin mice for genome editing and cancer modeling. *Cell* **159**, 440-455 (2014). https://doi.org:10.1016/j.cell.2014.09.014
188 Lee, B. H., Tothova, Z., Levine, R. L., Anderson, K., Buza-Vidas, N., Cullen, D. E. *et al.* FLT3 mutations confer enhanced proliferation and survival properties to multipotent progenitors in a murine model of chronic myelomonocytic leukemia. *Cancer Cell* **12**, 367-380 (2007). https://doi.org:10.1016/j.ccr.2007.08.031
189 Gothert, J. R., Gustin, S. E., Hall, M. A., Green, A. R., Gottgens, B., Izon, D. J. *et al.* In vivo fate-tracing studies using the Scl stem cell enhancer: embryonic hematopoietic stem cells significantly contribute to adult hematopoiesis. *Blood* **105**, 2724-2732 (2005). https://doi.org:10.1182/blood-2004-08-3037
190 Vassiliou, G. S., Cooper, J. L., Rad, R., Li, J., Rice, S., Uren, A. *et al.* Mutant nucleophosmin and cooperating pathways drive leukemia initiation and progression in mice. *Nat Genet* **43**, 470-475 (2011). https://doi.org:10.1038/ng.796
191 Madisen, L., Zwingman, T. A., Sunkin, S. M., Oh, S. W., Zariwala, H. A., Gu, H. *et al.* A robust and high-throughput Cre reporting and characterization system for

the whole mouse brain. *Nat Neurosci* **13**, 133-140 (2010). https://doi.org:10.1038/nn.2467

192 Li, W., Xu, H., Xiao, T., Cong, L., Love, M. I., Zhang, F. *et al.* MAGeCK enables robust identification of essential genes from genome-scale CRISPR/Cas9 knockout screens. *Genome Biol* **15**, 554 (2014). https://doi.org:10.1186/s13059-014-0554-4

193 Chen, M., Zhu, N., Liu, X., Laurent, B., Tang, Z., Eng, R. *et al.* JMJD1C is required for the survival of acute myeloid leukemia by functioning as a coactivator for key transcription factors. *Genes Dev* **29**, 2123-2139 (2015). https://doi.org:10.1101/gad.267278.115

194 Li, S., Ali, S., Duan, X., Liu, S., Du, J., Liu, C. *et al.* JMJD1B Demethylates H4R3me2s and H3K9me2 to Facilitate Gene Expression for Development of Hematopoietic Stem and Progenitor Cells. *Cell Rep* **23**, 389-403 (2018). https://doi.org:10.1016/j.celrep.2018.03.051

195 Izaguirre-Carbonell, J., Christiansen, L., Burns, R., Schmitz, J., Li, C., Mokry, R. L. *et al.* Critical role of Jumonji domain of JMJD1C in MLL-rearranged leukemia. *Blood Adv* **3**, 1499-1511 (2019). https://doi.org:10.1182/bloodadvances.2018026054

196 Zhu, N., Chen, M., Eng, R., DeJong, J., Sinha, A. U., Rahnamay, N. F. *et al.* MLL-AF9- and HOXA9-mediated acute myeloid leukemia stem cell self-renewal requires JMJD1C. *J Clin Invest* **126**, 997-1011 (2016). https://doi.org:10.1172/JCI82978

197 Sroczynska, P., Cruickshank, V. A., Bukowski, J. P., Miyagi, S., Bagger, F. O., Walfridsson, J. *et al.* shRNA screening identifies JMJD1C as being required for leukemia maintenance. *Blood* **123**, 1870-1882 (2014). https://doi.org:10.1182/blood-2013-08-522094

198 Staehle, H. F., Heinemann, J., Gruender, A., Omlor, A. M., Pahl, H. L. & Jutzi, J. S. Jmjd1c is dispensable for healthy adult hematopoiesis and Jak2V617F-driven myeloproliferative disease initiation in mice. *PLoS One* **15**, e0228362 (2020). https://doi.org:10.1371/journal.pone.0228362

199 Kim, J. Y., Kim, K. B., Eom, G. H., Choe, N., Kee, H. J., Son, H. J. *et al.* KDM3B is the H3K9 demethylase involved in transcriptional activation of lmo2 in leukemia. *Mol Cell Biol* **32**, 2917-2933 (2012). https://doi.org:10.1128/MCB.00133-12

200 Bowman, R. L. & Levine, R. L. TET2 in Normal and Malignant Hematopoiesis. *Cold Spring Harb Perspect Med* **7** (2017). https://doi.org:10.1101/cshperspect.a026518

201 Kats, L. M., Reschke, M., Taulli, R., Pozdnyakova, O., Burgess, K., Bhargava, P. *et al.* Proto-oncogenic role of mutant IDH2 in leukemia initiation and maintenance. *Cell Stem Cell* **14**, 329-341 (2014). https://doi.org:10.1016/j.stem.2013.12.016

202 Kim, S. M., Kim, J. Y., Choe, N. W., Cho, I. H., Kim, J. R., Kim, D. W. *et al.* Regulation of mouse steroidogenesis by WHISTLE and JMJD1C through histone methylation balance. *Nucleic Acids Res* **38**, 6389-6403 (2010). https://doi.org:10.1093/nar/gkq491

203 Lu, R., Czechowicz, A., Seita, J., Jiang, D. & Weissman, I. L. Clonal-level lineage commitment pathways of hematopoietic stem cells in vivo. *Proc Natl Acad Sci U S A* **116**, 1447-1456 (2019). https://doi.org:10.1073/pnas.1801480116
204 Ward, P. S., Patel, J., Wise, D. R., Abdel-Wahab, O., Bennett, B. D., Coller, H. A. *et al.* The common feature of leukemia-associated IDH1 and IDH2 mutations is a neomorphic enzyme activity converting alpha-ketoglutarate to 2-hydroxyglutarate. *Cancer Cell* **17**, 225-234 (2010). https://doi.org:10.1016/j.ccr.2010.01.020
205 Lu, C., Ward, P. S., Kapoor, G. S., Rohle, D., Turcan, S., Abdel-Wahab, O. *et al.* IDH mutation impairs histone demethylation and results in a block to cell differentiation. *Nature* **483**, 474-478 (2012). https://doi.org:10.1038/nature10860
206 Lyu, J., Liu, Y., Gong, L., Chen, M., Madanat, Y. F., Zhang, Y. *et al.* Disabling Uncompetitive Inhibition of Oncogenic IDH Mutations Drives Acquired Resistance. *Cancer Discov* **13**, 170-193 (2023). https://doi.org:10.1158/2159-8290.CD-21-1661
207 Brauchle, M., Yao, Z., Arora, R., Thigale, S., Clay, I., Inverardi, B. *et al.* Protein complex interactor analysis and differential activity of KDM3 subfamily members towards H3K9 methylation. *PLoS One* **8**, e60549 (2013). https://doi.org:10.1371/journal.pone.0060549
208 Barbie, D. A., Tamayo, P., Boehm, J. S., Kim, S. Y., Moody, S. E., Dunn, I. F. *et al.* Systematic RNA interference reveals that oncogenic KRAS-driven cancers require TBK1. *Nature* **462**, 108-112 (2009). https://doi.org:10.1038/nature08460
209 Kitamura, T., Tange, T., Terasawa, T., Chiba, S., Kuwaki, T., Miyagawa, K. *et al.* Establishment and characterization of a unique human cell line that proliferates dependently on GM-CSF, IL-3, or erythropoietin. *J Cell Physiol* **140**, 323-334 (1989). https://doi.org:10.1002/jcp.1041400219
210 Hamilton, J. A. & Achuthan, A. Colony stimulating factors and myeloid cell biology in health and disease. *Trends Immunol* **34**, 81-89 (2013). https://doi.org:10.1016/j.it.2012.08.006
211 Yoshihara, H., Arai, F., Hosokawa, K., Hagiwara, T., Takubo, K., Nakamura, Y. *et al.* Thrombopoietin/MPL signaling regulates hematopoietic stem cell quiescence and interaction with the osteoblastic niche. *Cell Stem Cell* **1**, 685-697 (2007). https://doi.org:10.1016/j.stem.2007.10.020
212 Robb, L., Drinkwater, C. C., Metcalf, D., Li, R., Kontgen, F., Nicola, N. A. *et al.* Hematopoietic and lung abnormalities in mice with a null mutation of the common beta subunit of the receptors for granulocyte-macrophage colony-stimulating factor and interleukins 3 and 5. *Proc Natl Acad Sci U S A* **92**, 9565-9569 (1995). https://doi.org:10.1073/pnas.92.21.9565
213 Regan-Komito, D., Swann, J. W., Demetriou, P., Cohen, E. S., Horwood, N. J., Sansom, S. N. *et al.* GM-CSF drives dysregulated hematopoietic stem cell activity and pathogenic extramedullary myelopoiesis in experimental spondyloarthritis. *Nat Commun* **11**, 155 (2020). https://doi.org:10.1038/s41467-019-13853-4
214 Zhao, Y., Li, X., Zhao, W., Wang, J., Yu, J., Wan, Z. *et al.* Single-cell transcriptomic landscape of nucleated cells in umbilical cord blood. *Gigascience* **8** (2019). https://doi.org:10.1093/gigascience/giz047

215 Drissen, R., Thongjuea, S., Theilgaard-Monch, K. & Nerlov, C. Identification of two distinct pathways of human myelopoiesis. *Sci Immunol* **4** (2019). https://doi.org:10.1126/sciimmunol.aau7148
216 Sitnicka, E., Lin, N., Priestley, G. V., Fox, N., Broudy, V. C., Wolf, N. S. *et al.* The effect of thrombopoietin on the proliferation and differentiation of murine hematopoietic stem cells. *Blood* **87**, 4998-5005 (1996).
217 Vainchenker, W. & Constantinescu, S. N. JAK/STAT signaling in hematological malignancies. *Oncogene* **32**, 2601-2613 (2013). https://doi.org:10.1038/onc.2012.347
218 Padeken, J., Methot, S. P. & Gasser, S. M. Establishment of H3K9-methylated heterochromatin and its functions in tissue differentiation and maintenance. *Nat Rev Mol Cell Biol* **23**, 623-640 (2022). https://doi.org:10.1038/s41580-022-00483-w
219 Binder, S., Luciano, M. & Horejs-Hoeck, J. The cytokine network in acute myeloid leukemia (AML): A focus on pro- and anti-inflammatory mediators. *Cytokine Growth Factor Rev* **43**, 8-15 (2018). https://doi.org:10.1016/j.cytogfr.2018.08.004
220 Hyde, R. K., Kamikubo, Y., Anderson, S., Kirby, M., Alemu, L., Zhao, L. *et al.* Cbfb/Runx1 repression-independent blockage of differentiation and accumulation of Csf2rb-expressing cells by Cbfb-MYH11. *Blood* **115**, 1433-1443 (2010). https://doi.org:10.1182/blood-2009-06-227413
221 Sunthankar, K. I., Jenkins, M. T., Cote, C. H., Patel, S. B., Welner, R. S. & Ferrell, P. B. Isocitrate dehydrogenase mutations are associated with altered IL-1beta responses in acute myeloid leukemia. *Leukemia* **36**, 923-934 (2022). https://doi.org:10.1038/s41375-021-01487-9
222 Cai, Z., Kotzin, J. J., Ramdas, B., Chen, S., Nelanuthala, S., Palam, L. R. *et al.* Inhibition of Inflammatory Signaling in Tet2 Mutant Preleukemic Cells Mitigates Stress-Induced Abnormalities and Clonal Hematopoiesis. *Cell Stem Cell* **23**, 833-849 e835 (2018). https://doi.org:10.1016/j.stem.2018.10.013
223 SanMiguel, J. M., Eudy, E., Loberg, M. A., Young, K. A., Mistry, J. J., Mujica, K. D. *et al.* Distinct Tumor Necrosis Factor Alpha Receptors Dictate Stem Cell Fitness versus Lineage Output in Dnmt3a-Mutant Clonal Hematopoiesis. *Cancer Discov* **12**, 2763-2773 (2022). https://doi.org:10.1158/2159-8290.CD-22-0086
224 Kan, W. L., Dhagat, U., Kaufmann, K. B., Hercus, T. R., Nero, T. L., Zeng, A. G. X. *et al.* Distinct Assemblies of Heterodimeric Cytokine Receptors Govern Stemness Programs in Leukemia. *Cancer Discov* **13**, 1922-1947 (2023). https://doi.org:10.1158/2159-8290.CD-22-1396
225 Wang, T., Lander, E. S. & Sabatini, D. M. Single Guide RNA Library Design and Construction. *Cold Spring Harb Protoc* **2016**, pdb prot090803 (2016). https://doi.org:10.1101/pdb.prot090803
226 Doench, J. G., Fusi, N., Sullender, M., Hegde, M., Vaimberg, E. W., Donovan, K. F. *et al.* Optimized sgRNA design to maximize activity and minimize off-target effects of CRISPR-Cas9. *Nat Biotechnol* **34**, 184-191 (2016). https://doi.org:10.1038/nbt.3437
227 Gundry, M. C., Brunetti, L., Lin, A., Mayle, A. E., Kitano, A., Wagner, D. *et al.* Highly Efficient Genome Editing of Murine and Human Hematopoietic

Progenitor Cells by CRISPR/Cas9. *Cell Rep* **17**, 1453-1461 (2016). https://doi.org:10.1016/j.celrep.2016.09.092

228 Kotini, A. G., Chang, C. J., Boussaad, I., Delrow, J. J., Dolezal, E. K., Nagulapally, A. B. *et al.* Functional analysis of a chromosomal deletion associated with myelodysplastic syndromes using isogenic human induced pluripotent stem cells. *Nat Biotechnol* **33**, 646-655 (2015). https://doi.org:10.1038/nbt.3178

229 Kotini, A. G., Chang, C. J., Chow, A., Yuan, H., Ho, T. C., Wang, T. *et al.* Stage-Specific Human Induced Pluripotent Stem Cells Map the Progression of Myeloid Transformation to Transplantable Leukemia. *Cell Stem Cell* **20**, 315-328 e317 (2017). https://doi.org:10.1016/j.stem.2017.01.009

230 Clement, K., Rees, H., Canver, M. C., Gehrke, J. M., Farouni, R., Hsu, J. Y. *et al.* CRISPResso2 provides accurate and rapid genome editing sequence analysis. *Nat Biotechnol* **37**, 224-226 (2019). https://doi.org:10.1038/s41587-019-0032-3

231 Corces, M. R., Trevino, A. E., Hamilton, E. G., Greenside, P. G., Sinnott-Armstrong, N. A., Vesuna, S. *et al.* An improved ATAC-seq protocol reduces background and enables interrogation of frozen tissues. *Nat Methods* **14**, 959-962 (2017). https://doi.org:10.1038/nmeth.4396

232 Bottomly, D., Long, N., Schultz, A. R., Kurtz, S. E., Tognon, C. E., Johnson, K. *et al.* Integrative analysis of drug response and clinical outcome in acute myeloid leukemia. *Cancer Cell* **40**, 850-864 e859 (2022). https://doi.org:10.1016/j.ccell.2022.07.002

233 Cancer Genome Atlas Research, N., Ley, T. J., Miller, C., Ding, L., Raphael, B. J., Mungall, A. J. *et al.* Genomic and epigenomic landscapes of adult de novo acute myeloid leukemia. *N Engl J Med* **368**, 2059-2074 (2013). https://doi.org:10.1056/NEJMoa1301689

234 Palikuqi, B., Nguyen, D. T., Li, G., Schreiner, R., Pellegata, A. F., Liu, Y. *et al.* Adaptable haemodynamic endothelial cells for organogenesis and tumorigenesis. *Nature* **585**, 426-432 (2020). https://doi.org:10.1038/s41586-020-2712-z

235 Gunn, K., Myllykoski, M., Cao, J. Z., Ahmed, M., Huang, B., Rouaisnel, B. *et al.* (R)-2-Hydroxyglutarate Inhibits KDM5 Histone Lysine Demethylases to Drive Transformation in IDH-Mutant Cancers. *Cancer Discov* **13**, 1478-1497 (2023). https://doi.org:10.1158/2159-8290.CD-22-0825

236 Kim, Y. Y., Gryder, B. E., Sinniah, R., Peach, M. L., Shern, J. F., Abdelmaksoud, A. *et al.* KDM3B inhibitors disrupt the oncogenic activity of PAX3-FOXO1 in fusion-positive rhabdomyosarcoma. *Nat Commun* **15**, 1703 (2024). https://doi.org:10.1038/s41467-024-45902-y

237 Schiller, R., Scozzafava, G., Tumber, A., Wickens, J. R., Bush, J. T., Rai, G. *et al.* A cell-permeable ester derivative of the JmjC histone demethylase inhibitor IOX1. *ChemMedChem* **9**, 566-571 (2014). https://doi.org:10.1002/cmdc.201300428